

## Sample Terminology Key

To aid the reader in understanding the terminology used throughout the text the table below has been produced.

<b>Sample Name</b>	<b>Intermediate Abbreviation</b>	<b>Ingredients (solids)</b>	<b>Process</b>	<b>Final Product Abbreviation</b>
Intermediate product 1	IP1	100 % native maize grits	Twin-screw extruded Directly Expanded Rotary Milled	FP1
Intermediate Product 2 40 %	IP2 40	100 % IP1	Twin-screw extruded at 40 % barrel water content Intermediate (not directly expanded)  Air dried	FP2 40
Intermediate Product 2 55 %	IP2 55	100 % IP1	Twin-screw extruded at 55 % barrel water content Intermediate (not directly expanded)  Air dried	FP2 55
Intermediate Product 3	IP3	100 % IP1	Single screw extruded at 40 % barrel water content Intermediate (not directly expanded)  Air dried	FP3
Intermediate Product 3 with Microcrystalline cellulose	IP3 + MCC	90 % IP1 10 % MCC	Single-screw extruded at 40 % barrel water content Intermediate (not directly expanded)  Air dried	FP3 + MCC
Intermediate Product 3 with Rice flour	IP3 + RF	90 % IP1 10 % RF	Single-screw extruded at 40 % barrel water content Intermediate (not directly expanded)  Air dried	FP3 + RF
Intermediate Product 3 with Potato Starch	IP3 + PS	90 % IP1 10 % PS	Single-screw extruded at 40 % barrel water content Intermediate (not directly expanded)  Air dried	FP3 + PS
Intermediate Product 4	IP4	100 % native maize grits	Twin-screw extruded at 40% barrel water content Intermediate (not directly expanded)  Air dried	FP4





The University of  
**Nottingham**



**PEPSICO**

UNITED KINGDOM · CHINA · MALAYSIA

## **Material science of in-directly expanded glucose $\alpha$ (1, 4) and (1, 6) linked polymers**

*By Suzanne L. Davies\* BSc (Hons) RSci*

***September 2017***

Project thesis submitted to The University of Nottingham in fulfilment of the requirements for the degree of Master of Philosophy in Food Sciences

**University Supervisor:** Prof. Tim Foster

**Industry Supervisor:** Dr. Bruce Linter

**Abstract word count:** 233

**Total word count:** 36,140

\*The University of Nottingham, School of Biosciences, Sutton Bonington Campus, Loughborough, Leicestershire, LE12 5RD, United Kingdom.

## Abstract

This research utilises twin-screw extruded directly expanded maize grits (IP1), into a secondary extrusion process, to create a homogenous intermediate product microstructure; that is later expanded into a final product using hot oil. The aim of this research is to begin to link ingredient processing to intermediate and final product microstructures and understand how this effects final product attributes.

The impact of two versus one extrusion process on final product microstructure was demonstrated with statistically significant differences in expansion ratio, viscoelastic properties of intermediates, and water release mechanisms during heating. To overcome limitations in standard analytical methods, high heating rates were used to replicate conditions more similar to that of frying.

Using a secondary single-screw extrusion process, intermediates were manufactured with the incorporation of semi-crystalline materials at 10 % (rice flour (RF), micro-crystalline cellulose (MCC) and potato starch (PS)) into the amorphous starch matrix to design an intermediate and final product microstructure. PS increased expansion ratio but decreased cell sizes and both MCC and RF were found to decrease expansion ratio. Initial sensory screening suggested 10 % semi-crystalline material can impact the textural attributes of final products, with MCC and RF being more effective. This work has delivered proof of principle of a design-led microstructure approach to final product attributes.

## Acknowledgements

Firstly, I wish to express my appreciation for the sponsorship of this Master of Philosophy by PepsiCo International and in particular Prof. Tim Ingmire for giving me the opportunity to continue my studies whilst working. Special thanks go to my industry supervisors Dr. Bruce Linter and Dr. Bhavnita Patel for providing valuable insight, support and patience throughout the project; enabling me to grow both professionally and personally.

I would like to offer special thanks to my university supervisor Prof. Tim Foster and sub-supervisor Prof. Sandra Hill for their support and guidance. Your patience and attention to detail in the final months of writing has pushed me to develop skills essential to pursue a career in research.

I owe huge thanks to the Beaumont Park analytical laboratory, specifically Amanda, Sam, Paul, Kiran and Jen for their continued support on routine analysis. Additionally, within the Nottingham Biomaterials laboratory, Ms Val Street, Dr Bill McNaughton and Mr Steven Johnson have been a huge support in training, method development and interpretation of results, of which I am hugely grateful for.

Camilla, Annika and Anne-Marie based at RISE Agrifood and Bioscience and Mrs Christine Grainger-Boulby based in the Nanoscale and Microscale Research Centre, have all provided valuable insight into method development for intermediate and final product microscopy and I must thank you for your valuable contribution to my results chapters.

## Table of Contents

<b>Chapter 1 Introduction.....</b>	<b>1</b>
1.1 <i>Project Background</i> .....	1
<b>Chapter 2 Literature Review .....</b>	<b>3</b>
2.1 <i>Maize grits</i> .....	3
2.2 <i>Semi-crystalline starch</i> .....	6
2.2.1 Amylose and Amylopectin .....	7
2.2.2 Starch gelatinisation (semi-crystalline to amorphous) .....	12
2.2.3 Melting .....	16
2.2.4 Starch conversion.....	17
2.2.5 Retrogradation .....	18
2.3 <i>Glass transition and aging of glasses</i> .....	19
2.3.1 Glass transition.....	19
2.3.2 Aging of glasses .....	21
2.4 <i>The manufacture of extruded snacks</i> .....	22
2.4.1 Hydration and pre-conditioning.....	22
2.4.2 Single and Twin-screw extrusion.....	23
2.4.3 Direct and in-direct expansion .....	24
2.5 <i>Structure creation of in-directly expanded snacks</i> .....	26
2.5.1 Intermediate-product microstructure .....	26
2.5.2 Intermediate-product to final-product expansion.....	28
2.5.3 Final product microstructure .....	34

2.6	<i>Business Focus for the future of snacks</i> .....	36
2.7	<i>Objectives</i> .....	37
<b>Chapter 3 Materials and Methods</b> .....		<b>39</b>
3.1	<i>Ingredients</i> .....	39
3.2	<i>Processing Methods</i> .....	40
3.2.1	Direct Expansion (IP1).....	40
3.2.2	Milling and Particle Separation .....	41
3.3	<i>Analytical Methods</i> .....	41
3.3.1	Expansion Ratio (ER) .....	41
3.3.2	Microscopy.....	42
3.3.3	Dry Particle Size Distribution (PSD).....	45
3.3.4	Thermogravimetric Analysis (TGA) .....	46
3.3.5	Rapid Visco Analyser (RVA) .....	47
3.3.6	X-Ray Powder Diffraction (XRPD).....	48
3.3.7	Water Absorption Index (WAI).....	48
3.3.8	Water Solubility Index (WSI) .....	49
3.3.9	Differential Scanning Calorimetry (DSC) .....	49
3.3.10	Dynamic Mechanical Thermal Analysis (DMTA) .....	51
3.3.11	Statistical Analysis .....	52
3.3.12	Sensory Analysis.....	52

**Chapter 4 Results: Material Characterisation of raw maize grits and intermediate product 1 (IP1).....54**

4.1	<i>Introduction</i> .....	54
4.2	<i>Materials and Methods</i> .....	55
4.3	<i>Results and Discussion</i> .....	56
4.3.1	Macrostructure .....	56
4.3.2	Microstructure .....	57
4.3.3	Absorption and Solubility.....	62
4.3.4	Crystallinity.....	64
4.4	<i>Conclusions</i> .....	68

**Chapter 5 Results: Twin-screw extrusion of IP1 with intermediate and final product characterisation..69**

5.1	<i>Introduction</i> .....	69
5.2	<i>Materials and Methods</i> .....	70
5.2.1	Materials .....	70
5.2.2	Processing Methods.....	70
5.2.3	Analytical Methods .....	72
5.3	<i>Results and Discussion</i> .....	73
5.3.1	Processing Observations .....	73
5.3.2	Expansion properties of twin-screw extruded intermediates .....	76
5.3.3	Microstructure of twin-screw extruded intermediates .....	78
5.3.4	Molecular properties of twin-screw extruded intermediates .....	82
5.3.5	Water loss mechanisms of intermediate products during heating .....	97
5.3.6	Product microstructure and textural attributes .....	101
5.4	<i>Conclusion</i> .....	104

<b>Chapter 6 Single-screw extrusion of IP1 with intermediate and final product characterisation .....</b>	<b>106</b>
6.1 Introduction.....	106
6.2 Materials and Methods.....	107
6.2.1 Materials .....	107
6.2.2 Processing Methods.....	109
6.2.3 Analytical Methods .....	112
6.3 Results and Discussion.....	113
6.3.1 Processing Observations .....	113
6.3.2 Characterisation of differences in single- and twin-screw extrusion intermediates .....	115
6.3.3 Characterisation of IP3 intermediates with additional semi-crystalline material .....	121
6.3.4 The microstructural properties of semi-crystalline materials before and after expansion ..	127
6.3.5 The impact of semi-crystalline material on the expansion and texture of final products ...	131
6.4 Conclusion .....	140
<b>Chapter 7 Final conclusions and future work.....</b>	<b>143</b>
<b>Chapter 8 Appendices .....</b>	<b>146</b>
<b>Chapter 9 References .....</b>	<b>152</b>

## Symbols and Abbreviations

AM:AP	Ratio of amylose to amylopectin
cP	Centipoise
CP	Continuous Phase
Da	Daltons
DMTA	Dynamic Mechanical Thermal Analysis
DP	Dispersed Phase
DSC	Differential Scanning Calorimetry
Dwb	Dry weight basis (%)
E'	Storage modulus (Solid-like)
E''	Loss modulus (Liquid-like)
ER	Expansion Ratio
IP1	Intermediate Product 1
IP2 40	Intermediate Product 2 at 40 % moisture
IP2 55	Intermediate Product 2 at 55 % moisture
IP3	Intermediate Product 3

IP4	Intermediate Product 4
LVR	Linear Viscoelastic Region
MCC	Microcrystalline Cellulose
$M_w$	Molecular Weight
Pa	Pascal
Pa.s	Pascal second
PEP	PepsiCo
PS	Potato Starch
RF	Rice Flour
RVA	Rapid Viscometer Analyser
SME	Specific mechanical energy (kJ/kg)
Tan $\delta$	Tangent Delta ( $E''/E'$ )
$T_g$	Glass transition temperature
TGA	Thermogravimetric Analysis
$T_m$	Melting temperature
WAI	Water Absorption Index
WSI	Water Solubility Index

Wwb	Wet weight basis (%)
XRPD	X-ray Powder Diffraction
XRT	X-Ray Tomography
$\Delta H$	Change in Enthalpy (J/g)
$\Delta P$	Change in Pressure (bar)
$\Delta T$	Change in Temperature ( $^{\circ}\text{C}$ )
$\eta$	Viscosity (eta)

## Table of Figures

Figure 1. (A) Anatomy of a maize kernel and (B) Scanning electron micrograph of compacted starch granules in the endosperm (Gwirtz and Garcia-Casal, 2014; Pineda-Gómez <i>et al.</i> , 2012).....	3
Figure 2. (A) Native maize starch granules and (B) native potato starch granules under cross polarised light microscopy.....	6
Figure 3. Schematic of the crystalline and amorphous lamellae within a starch granule that are associated with the clusters and branch chains of amylopectin (Jenkins and Donald, 1995).....	8
Figure 4. Diagrammatic representation of A-type and B-type polymorphs of crystal packing of amylopectin double helices (not to scale) (Wang <i>et al.</i> , 1998) .....	10
Figure 5. Wide angle x-ray diffraction patterns of the semi-crystalline polymorphs: A-type (Cereal), B-type (Tuber), C-type (Tuber and Seed) and V-type (Helical Amylose Lipid Complexes) (Zobel, 1988).....	11
Figure 6. Scanning Electron Micrographs of (A) swollen starch granules and (B) ruptured starch granules, during heating of semi-crystalline starch in an aqueous environment (Copeland <i>et al.</i> , 2009).....	13
Figure 7. (A) RVA profile of gelatinisation of native semi-crystalline starch granules through to a macromolecular solution. The key parameters are notated: pasting temperature, peak viscosity and final viscosity (adapted from Saunders <i>et al.</i> , 2011). .....	14
Figure 8. Change in physical state of aged amorphous glass to melt through glass transition and crystallisation (adapted from Bhandari <i>et al.</i> , 1997). .....	21
Figure 9. Diagram of co-rotating and counter-rotating twin screw profiles (Tangram Technology, 2014)..	23
Figure 10. Light microscopy of an intermediate-product (A) and final product (B) depicting the CP and DP microstructure that exists following processing (Scale bar = 50 µm).....	26

Figure 11. Diagrammatic representation of the change in viscosity ( $\eta$ ) of an intermediate starch matrix during frying with respect to time. Bullet points highlight key physical and molecular changes and arrows depict key drivers in reducing or increasing $\eta$ (adapted from Kristiawan <i>et al.</i> , 2016; van der Sman, 2016; van der Sman and Broeze, 2013; Chanvrier <i>et al.</i> , 2006; Kokini and Moraru, 2003; Tuorila <i>et al.</i> , 1998) ...	29
Figure 12. State diagram on the expansion process of potato based intermediates (adapted from van Der Sman, 2016) .....	31
Figure 13. Outline of the manufacturing steps to utilise bulk processed maize (IP1) into 2 separate manufacturing processes (IP2 and IP3) in addition to a comparison product manufactured from native maize (IP4) and the corresponding chapters presenting results from characterisation of intermediate and final products. ....	38
Figure 14. Screw profile of twin-screw extrusion process in the manufacture of IP1.....	40
Figure 15. (A) Average percentage (%) of particle diameter of IP1 from 0 to 2000 $\mu\text{m}$ $\pm$ standard deviation based on 3 replicates, (B) Light microscopy micrograph of IP1 particles following milling. ....	56
Figure 16. Light Micrographs of (A, C) hydrated IP1 following milling, (B, D) Cross polarised light micrographs of hydrated IP1 following milling.....	58
Figure 17. Average viscosity of IP1 in excess water. Error bars represent standard deviation based on 3 replicates.....	59
Figure 18. Average Water Absorption Index (%) and Water Solubility Index (%) of native maize grits and IP1. ....	63
Figure 19. Light microscopy of IP1 with (A) iodine staining (B) iodine stained with excess water.....	64
Figure 20. XRPD of native maize grits and IP1. Numbers correspond to the peaks in IP1. ....	65
Figure 21. DSC thermographs of hydrated raw maize grits (black) and IP1 (grey) (at least 1 solid: 1 water). (A) Hydrated raw maize grits and IP1 up to 100 $^{\circ}\text{C}$ in aluminium pans. (B) Replicates of IP1 to 150 $^{\circ}\text{C}$ in stainless steel pans. Lines displaced by $\pm 0.25$ mW/g for ease of observation. Heating rate 5 $^{\circ}\text{C}/\text{min}$ . ....	66

Figure 22. Photos demonstrating (A) expansion of IP1 dough on exit of the extruder at water contents <30 %, (B) Browning of dough at 40 % water content (IP2 40). .....	73
Figure 23. Photo depicting pale yellow dough of IP2 55. ....	74
Figure 24. State diagram of the pathway of transitions. Colours correspond to individual processes and numbers indicate the steps within that process from native maize grits through to IP3 (red), into the manufacture of IP2 40 (dark blue) and the expansion of IP2 40 into FP2 40 (light blue) relative to water content (%) and temperature (°C).. ....	75
Figure 25. Average expansion ratio (volume basis) $\pm$ standard deviation based on 5 replicates of FP4, FP2 55 and FP2 40. All final product expansions are statically significantly different ( $P < 0.05$ ). Pictures show cross-sectional expansion of corresponding samples. ....	76
Figure 26. (A) Confocal light micrograph of IP2 55 intermediate cross-section (scale bar = 100 $\mu$ m) (B) Scanning electron micrograph of FP2 55 cross section (scale bar = 1 mm).....	77
Figure 27. Light microscopy with iodine and fast green staining of FP4. (A) Native starch granules surrounded by protein matrix (green), (B) Alerone layer associated with endosperm.....	78
Figure 28. Light microscopy of microtomed intermediates following iodine staining. (A & B) IP2 40, (C & D) IP2 55 and (E & F) IP4. Fibre = light green, protein = yellow, fat = dark brown.....	80
Figure 29. Light microscopy with iodine and fast green staining of intermediates (A) IP2 40 and (B) IP2 55 .....	81
Figure 30. Average viscosity (cP) $\pm$ standard deviation with respect to time and temperature. ....	83
Figure 31. State diagram of starch. Black dotted line represents $T_g$ with respect to water content and temperature. Red dotted lines demonstrate the influence of intermediate dough water content on time to $T_g$ during air drying at 25 °C. Purple box highlights area in which retrogradation can occur (adapted from van der Sman, 2016). ....	84

Figure 32. Relative heat flow (mW/g) of intermediate-products during DSC measurements in excess water. For ease of interpretation IP4 has been offset by +0.03 mW/g and IP2 55 by -0.03 mW/g. Heating rate 5 °C/min.....	85
Figure 33. XRPD of Native maize grits, IP1, IP4 and IP2 55.....	87
Figure 34. (A & B) Storage modulus (E') and tan $\delta$ (E''/E') vs. temperature (°C) of whole intermediates at 1 Hz frequency. (C) Peak tan $\delta$ (T <sub>g</sub> ) of IP4 and IP2 40 at 0.3 Hz, 1 Hz and 10 Hz. (D) E' (T <sub>g</sub> + 30 °C)/E' (30 °C) of IP4 and IP2 40 at 0.3 Hz, 1 Hz and 10 Hz. Heating rate 5 °C/min. ....	90
Figure 35. Light microscopy of final product 4 (FP4) following microtoming. Purple/blue = starch matrix, green= fibre, yellow = protein. (A) Scale bar = 20 $\mu$ m, (B) scale bar = 10 $\mu$ m. ....	93
Figure 36. (A) Relative E' and (B) Tan $\delta$ (E''/E') of ground intermediates in aluminium pockets at 1 Hz frequency IP4 < 1 mm, IP4 >1 mm, IP2 40 <1 mm and IP2 40 >1 mm. ....	96
Figure 37. Fast rate (40 °C/min) thermo-gravimetric analysis of ground intermediates at ~1 mm in diameter from 25 °C to 250 °C. (A) Weight loss (B) 1 <sup>st</sup> derivative. IP4 (black lines), IP2 40 (grey lines).....	97
Figure 38. (A) Slow rate (5 °C/min) thermo-gravimetric analysis (TGA) of ground intermediates from 30 °C to 250 °C. (A1) Black = IP4 weight loss, green= IP2 40 weight loss. (A2) 1 <sup>st</sup> derivative of IP4 (black) and IP2 40 (green). (B) Fast rate (40 °C/min) TGA of intermediates (B1) weight loss (%) (B2) 1 <sup>st</sup> derivative. ....	99
Figure 39. Scanning electron micrographs of final products (A, C, E) FP2 40 cross section, (B, D, F) FP4 cross section. ....	102
Figure 40. (A) Particle size distribution of Superior Native Potato Starch and (B) Cross polarised light microscopy.....	107
Figure 41. (A) Particle size distribution of Rice Flour, (B) Hydrated Light microscopy and (C) hydrated cross polarised light microscopy.....	108
Figure 42. (A) Light microscopy and (B) cross polarised light microscopy of micro-crystalline cellulose...	109

Figure 43. Pictures demonstrating stretching device attached to extruder to thin the dough sheet achieving thinner intermediates following cutting and drying.....	110
Figure 44. Graph demonstrating the impact of dough water content from 30 % to 40 % (wwb) on average pressure, die temperature and torque within a single-screw extruder based on 3 recipes. Error bars are based on standard deviation of 3 replicates. ....	114
Figure 45. Average viscosity (cP) $\pm$ standard deviation with respect to time and temperature of intermediates.....	116
Figure 46. XRPD of IP1, IP2 55, IP2 40 and IP3. Numbers correspond to peak $2\theta$ ( $^{\circ}$ ) positions of extruded intermediate-products.....	117
Figure 47. Light microscopy of IP3 following microtoming and iodine staining (A) Micrograph with scale bar 200 $\mu\text{m}$ and (B) Scale bar 50 $\mu\text{m}$ .....	118
Figure 48. Final products following expansion of intermediates (A) FP2 55, (B) FP2 40 (C) FP3.....	118
Figure 49. Thermo-gravimetric analysis of ground intermediates to 1 mm in diameter at (A) slow rate (5 $^{\circ}\text{C}/\text{min}$ ) and (B) fast heating rates (40 $^{\circ}\text{C}/\text{min}$ ). (1) IP3 weight loss and (2) IP3 1st derivative.....	120
Figure 50. DSC thermographs of native material, intermediate (IP3) and final product (FP3) of (A) + 10 % Potato Starch (PS), (B) + 10 % Rice Flour (RF), (C) + 10 % Micro-crystalline cellulose (MCC) and (D) IP3 with no additional crystalline material. IP3 + MCC, IP3 + RF, FP3 + MCC and FP3 + RF have been offset by -0.05 mW/g for ease of interpretation. Heating rate 5 $^{\circ}\text{C}/\text{min}$ and >50 % water content.....	124
Figure 51. X-Ray Diffraction patterns of raw materials, intermediates and final product. ....	126
Figure 52. Confocal light micrograph of intermediate cross-sections. (A) IP3, (B) IP3 + 10% PS, (C) IP3 + 10% MCC and (D) IP3 + 10% RF. White lines in top right corner relate to 100 $\mu\text{m}$ scale bar.....	127
Figure 53. Light microscopy of intermediates and final products following microtoming and iodine staining. (A) IP3, (B) FP3, (C) IP3 + 10 % PS, (D) FP3 + PS, (E) IP3 + 10 % MCC (F) FP3 + 10 % MCC (G) IP3 + 10 % RF and (H) FP3 + 10 % RF.....	128

Figure 54. Average expansion ratio (volume basis) $\pm$ standard deviation of IP3, IP3 + PS, IP3 + RF and IP3 + MCC.....	131
Figure 55. Scanning electron micrographs of final products (A) FP3, (B) FP3 + PS, (C) FP3 + RF and (D) FP3 + MCC. Small micrographs show final product microstructures of trial repeats at x22 objective, Scale bar = 1 mm.....	134
Figure 56. Thermo-gravimetric analysis (TGA) of intermediates at 40 °C/min. 1) Weight loss (%) and 2) 1 <sup>st</sup> derivative. (A) IP3, (B) IP3 + PS, (C) IP3 + RF, (D) IP3 + MCC. 3 replicates per sample code. ....	136
Figure 57. Average degree of difference score $\pm$ standard deviation based on an un-trained sensory panel of 5 people. FP3 is 0 across all attributes as a reference, FP3 + RF, FP3 + MCC and FP3 + PS. ....	138

## Table of Tables

Table 1. Raw material costs within emerging markets supplied by PepsiCo Procurement.....	1
Table 2. Nutritional specification of maize grits (Whitworth Bros. Ltd.; Appendix 1). ....	5
Table 3. Typical characteristics of starch granules from different botanical sources (adapted from (Majzoubi, 2004; Alczar-Alay and Meireles, 2015; Jane, 2009). ....	7
Table 4. Common differences between directly and in-directly expanded manufacturing processes (van der Sman and Broeze, 2013). ....	25
Table 5. Nutritional results of maize grits measured by Covance Laboratories Inc. ....	39
Table 6. Steps 1 to 7 for sample preparation prior to microtoming of intermediate and final products (SP Bioscience; Goteberg).....	43

Table 7. Degree of differences score definitions .....	53
Table 8. Average $\pm$ standard deviation of peak viscosity temperature ( $^{\circ}$ C), peak viscosity (cP) and final viscosity (cP) for native maize grits and IP1 based on 3 replicates.....	60
Table 9. Twin-screw extrusion parameters for IP4, IP2 at 40 % and 55 % barrel water content. ....	71
Table 10. Frying temperatures and times of intermediate products to expand into final products.....	71
Table 11. Average % water loss $\pm$ standard deviation of IP2 40 and IP4 between different temperature ranges. * represent statistically significant differences in each data set ( $P < 0.05$ ). ....	100
Table 12. Processing conditions for single-screw extruder intermediate manufacture.....	110
Table 13. Frying conditions for intermediates.....	111
Table 14. Average % water loss $\pm$ standard deviation of IP2, IP3 and IP4 between the temperature ranges of 30-130 $^{\circ}$ C (a) and 130-250 $^{\circ}$ C (b). The average ratio of a/b $\pm$ standard deviation is also presented. All figures are based on three replicates. ....	121
Table 15. Average enthalpy (J/g) $\pm$ standard deviation of raw materials, intermediates and final products. Raw material refers to the crystalline material alone and not dry mixes. ....	125

## Chapter 1 Introduction

### 1.1 Project Background

Market growth of crisps within developed countries has become saturated (Walton, 2015). As a result, PepsiCo (PEP) is focusing on emerging markets to increase global market share. Here snack consumption forecasts are extremely attractive, contributing to the forecasted global savoury snack market value of \$129 billion by 2019 (CPS Industry News, 2015). To provide affordable snacks, it is essential they are manufactured using the cheapest raw materials. Consequently, throughout Asia, South America and South Africa snacks need to be manufactured from cereals rather than tubers (Table 1).

**Table 1. Raw material costs within emerging markets supplied by PepsiCo Procurement**

<b>Ingredient</b>	<b>India Cost (\$/kg)*</b>	<b>South Africa Cost (\$/kg)*</b>	<b>Brazil Cost (\$/kg)*</b>
Potato Starch	0.77	0.75	0.90
Potato Flakes	1.65	1.14	1.80
Maize Grits	0.34	0.37	0.33
Wheat Flour	0.34	0.42	0.62
Rice Flour	0.40	0.77	0.71

\*correct as of November 2016

The research presented is focused on understanding the material properties of cereal intermediate-products, and how these properties influence differences in associated final product characteristics such as: expansion ratio (ER), cell size distribution and sensory attributes. Coupled with this, there is a need to build an understanding of the key levers to manipulate these characteristics enabling PEP

to meet the desired consumer experience, whilst still providing an affordable snack. The cereal selected was maize as this is the cheapest of cereal materials and is widely available.

The project is based on extruded snacks due to pre-existing extrusion capabilities within emerging markets. Indirectly expanded snacks are a primary focus due to the advantage of creating a long shelf-life intermediate with high bulk density and low water content.

Based on the broader needs of the project, the initial work focused on investigating:

- 1) The fundamental properties of starch based ingredients before and after processing
- 2) The key processes required to manufacture intermediates and final products from cereal based ingredients
- 3) How changes during processing drive differences in the microstructure of intermediates and more specifically the function of the two phases developed
- 4) How the intermediate microstructure changes can drive differences in final product microstructures following expansion and how this influences sensory attributes

## Chapter 2 Literature Review

### 2.1 Maize grits

Maize originated approximately 7,000 years ago in Mexico and due to its adaptability to grow in different regions is now the most abundant commodity worldwide. In 2011, it was reported that more than 830 million metric tonnes are produced annually; 45 % of which is utilised as animal feedstock, 43 % for ethanol production and the remaining 12 % for human consumption (Gwirtz and Garcia-Casal, 2014).

The anatomy of a maize kernel can be split into four major structures: endosperm (83 %), germ (11 %), pericarp (5 %), and tip cap (1 %) (Figure 1).

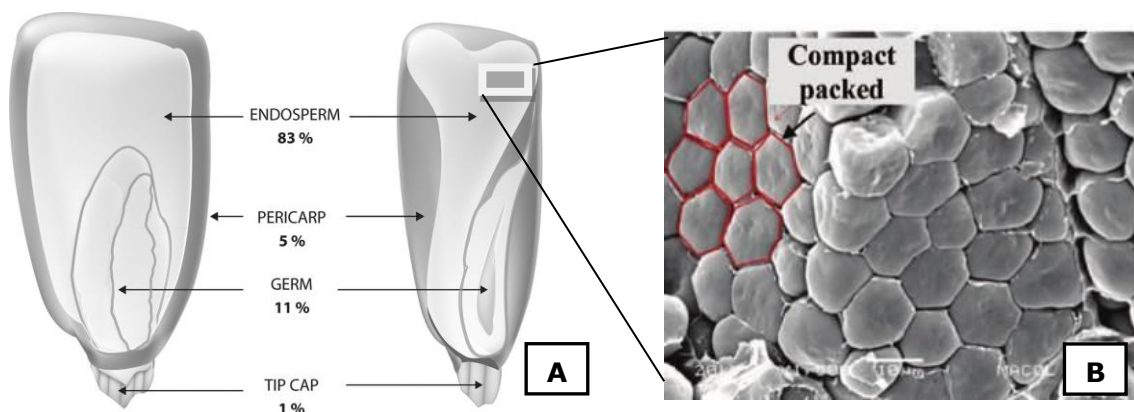


**Figure 1. (A) Anatomy of a maize kernel and (B) Scanning electron micrograph of compacted starch granules in the endosperm (Gwirtz and Garcia-Casal, 2014; Pineda-Gómez *et al.*, 2012).**

The endosperm is primarily for carbohydrate storage and therefore consists of starch within a surrounding protein matrix. The endosperm can be split further into floury (soft) and vitreous (hard);

which are separated during processing to deliver different functional ingredients (Louis Alexandre *et al.*, 1991).

The major protein associated with the endosperm is zein. Approximately 75 % of zein sits in the endosperm, uniformly distributed between starch granules as protein bodies. Rich in non-essential amino acids: glutamic acid, leucine and proline; zein has a high proportion of non-polar residues responsible for the alcohol soluble characteristic of the protein (Shukla and Cheryan, 2001).

The germ of the kernel is the primary storage for fat with an average content of 33 %. The majority of fat is in the form of polyunsaturated fatty acids and additional fat soluble vitamins B and E. The pericarp consists of the largest proportion of fibre within the kernel surrounding both the endosperm and germ regions with a semipermeable barrier. Finally, the tip cap is attached to the pericarp and is the point at which the kernel reaches the stalk, largely consisting of fibre (Chaudhary *et al.*, 2013).

Maize grits are manufactured from the vitreous endosperm. Following softening of the kernel with warm water, the germ is extracted and fed into a dry milling process where the majority of the remaining germ and pericarp are removed (Peplinski *et al.*, 1984). Dry milling tends to render poorer quality isolates with traces of fibre, protein and lipid. Dry milling also causes damage to the endosperm and leaching of the starch granules from the encapsulated protein matrix (Carvalho *et al.*, 2010). Following milling, fluted rollers and screens are used to meet the specified particle size. A typical nutritional specification of maize grits supplied in the UK is displayed in Table 2.

**Table 2. Nutritional specification of maize grits (Whitworth Bros. Ltd.; Appendix 1).**

<b>Nutrient</b>	<b>%</b>
Energy (KJ/kcal)	1265/300
Total Fat	1.6
of which Saturates	0.2
of which mono-unsaturates	0.4
of which poly-unsaturates	0.8
Total Carbohydrate:	56.7
of which Sugars	1.1
Fibre	16.9
Protein	6.4
Water	14

## 2.2 Semi-crystalline starch

Cereal starch is stored in the endosperm in granular form and is typically synthesised as two polymers; amylose and amylopectin. These granules are thought to compose of an amorphous bulk core area surrounded by concentric semi-crystalline growth rings with alternating amorphous regions (Wang and Copeland, 2015). Under cross polarised light microscopy, native starch granules can be detected with the interference pattern that reveals a unique Maltese cross pattern (Figure 2).

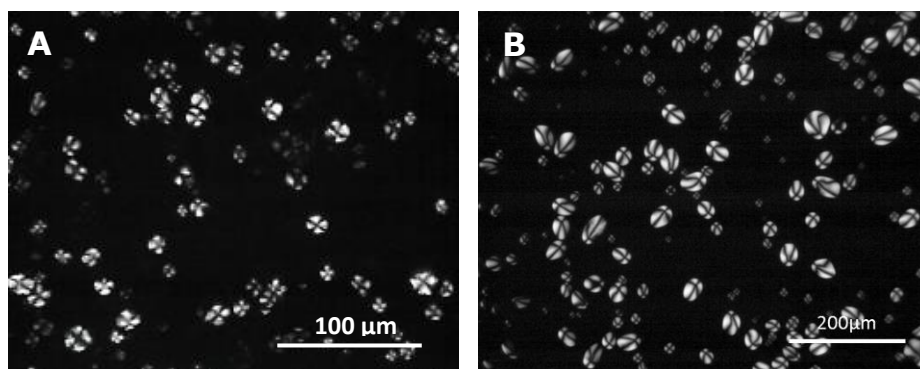


**Figure 2. (A) Native maize starch granules and (B) native potato starch granules under cross polarised light microscopy.**

Starch granule characteristics are dependent on starch origin, with clear differences between tuber and cereal granules (Table 3). Tubers, such as potatoes, have a far larger size and swelling capacity when subjected to heat in an aqueous system. It is hypothesised these differences are driven by molecular differences in starch polymerisation, specifically amylose (Table 3). Additionally, tuber starch has on average 0.5 % amylopectin bound phosphate compared with cereal starch which has less than 0.01 % (Xu *et al.*, 2017). A difference in phosphate content dramatically alters starch functionality including pasting properties, gel strength and viscosity (Xu *et al.*, 2017). The increase in

peak viscosity associated with tuber starches is attributed to the repelling charge between phosphate groups (Jane, 2009).

**Table 3. Typical characteristics of starch granules from different botanical sources (adapted from (Majzoubi, 2004; Alczar-Alay and Meireles, 2015; Jane, 2009)).**

Characteristic	Wheat	Maize	Potato
Average Diameter ( $\mu\text{m}$ )	1-45	5-30	5-100
Shape	Spherical Lenticular	Irregular Polyhedron	Oval Spherical
Degree of polymerisation of amylose	1300	930	2100-4900

### 2.2.1 Amylose and Amylopectin

Amylose is described in literature as a linear helical polymer with  $\alpha$ -D glucose units linked by  $\alpha$  (1, 4) glycosidic bonds and a limited number of  $\alpha$  (1, 6) branch points. Amylose is thought to be primarily in the form of single helices within native starch granules (Ring *et al.*, 1985). However, it can be found in the form of double helices or single helices that have complexed with non-starch molecules, such as lipids and iodine (Jane, 2009). There is some speculation over the amylose location in the granule; but is most commonly reported in the form of individual chains that sit radially-orientated between crystalline amylopectin (Wang *et al.*, 2015).

Amylopectin is a highly branched polymer of  $\alpha$  (1, 4) linked glucose units with branch chains at the  $\alpha$  (1, 6) positions. It has a proposed three-dimensional cluster structure composed of A, B and C chains,

with one reducing end C chain per cluster (Manners, 1989). The reducing end is suggested to sit within the disordered bulk core of the starch granule associated with amylose (Wang *et al.*, 2015).

The crystalline region of the granule corresponds with the aligned cluster of the short chain amylopectin, whilst the amorphous region is thought to be associated with the (1, 6) branch points (Jenkins and Donald, 1995). The compaction of these molecules forms a composition of alternating regions of crystalline and amorphous lamellae (Figure 3). For maize starch, the degree of crystallinity is reported in the range of 15 - 17 % (Frost *et al.*, 2009; Sahai and Jackson, 1996; Zobel *et al.*, 1988).

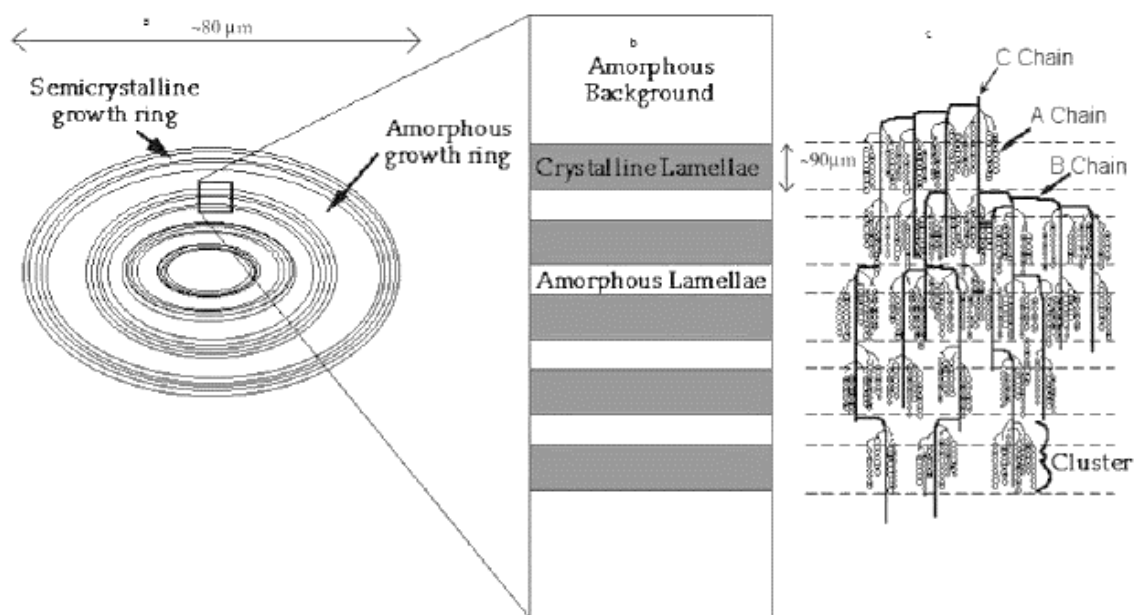


**Figure 3. Schematic of the crystalline and amorphous lamellae within a starch granule that are associated with the clusters and branch chains of amylopectin (Jenkins and Donald, 1995).**

The ratio of amylose to amylopectin (AM:AP) is dependent on botanical source with native cereals commonly having higher amylose content than tubers. Generally, the ratio falls within the region of 20 - 30 % amylose and 70 - 80 % amylopectin for wild-type starches (Alczar-Alay and Meireles, 2015). The amylose and lipid content of starch granules is directly correlated; with cereal starches having enriched radially aligned lipid at the granule surface (Jane, 2009; Morrison *et al.*, 1984).

### 2.2.1.1 Amylose Complexes

Upon heating of starch in an aqueous system with the presence of free lipids, amylose can form amylose-lipid complexes (Tang *et al.*, 2016). These complexes are defined as a helical amylose polymer in which the hydrophobic chain of a lipid is embedded (Gudipati *et al.*, 2013; Putseys, 2010). Similarly, the chemical element iodine associates with amylose helices and is commonly used in microscopy to stain amylose.

For cereals, amylose lipid complexes are thought to exist naturally within the amorphous region of the granule (Tang *et al.*, 2016; Jane, 2009). However, they cannot be detected until they are complexed in the lamellar crystalline form following processing (Biliaderis and Galloway, 1989). The crystalline structure of amylose-lipid complexes are defined as V-type polymorphs.

### 2.2.1.2 Semi-crystalline polymorphs

The amylopectin double helices that alternate between the amorphous regions have been characterised into the crystalline polymorphs: A-type and B-type. Tuber based starches are predominately B-type and cereals, A-type (Wang *et al.*, 1998) (Figure 4). For seeds and pulses, a combination of A- and B-type are prevalent, referred to as C-type. The differences between A-type

and B-type are primarily found in the packing density and consequently the proportion of bound water within each crystal differs (Wang *et al.*, 1998). A-type crystals have a greater density of packing and bind a smaller number of water molecules than B-type; 12 and 36 respectively (Tomasik, 2003). Perez and Bertoft (2010) provide a detailed critical review on the research conducted to build an understanding of amylopectin crystalline polymorphs.

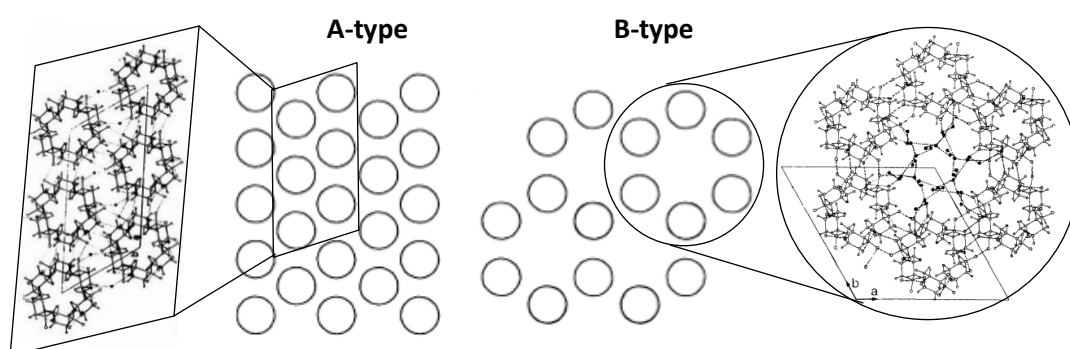


**Figure 4. Diagrammatic representation of A-type and B-type polymorphs of crystal packing of amylopectin double helices (not to scale) (Wang *et al.*, 1998). The channel of well-localised water molecules (filled black dots) between the crystal packing of double helices in A-type starch was proposed by Imberty *et al.* (1988) and B-type by Imberty and Perez (1988).**

Polymorphs A, B, C and V can be identified within materials using X-Ray Diffraction (XRD) where wide angle X-rays are used to detect long range order of molecules. The peaks correspond to X-ray intensities scattered by the electrons at different diffraction angles. Through Bragg's Law the diffraction angle ( $2\theta$ ), interplanar distance ( $d$ ) and x-ray wavelength ( $\lambda$ ) are interconnected (Equation 2.1) (Ida, 2012).

$$n\lambda = 2d \sin\theta \quad \text{(Equation 2.1)}$$

The differentiation between A-type and B-type crystal polymorphs is primarily determined through the position and intensity of the peaks, particularly between the 0 to 10° and 17 to 25° 2 $\theta$  positions (Jane *et al.*, 1999). For amylose-lipid complexes, crystalline forms correspond to peaks at the 7.3°, 12.7° and 19.8° 2 $\theta$  positions (Shogren *et al.*, 2006; Hanna and Bhatnagar, 1994) (Figure 5).

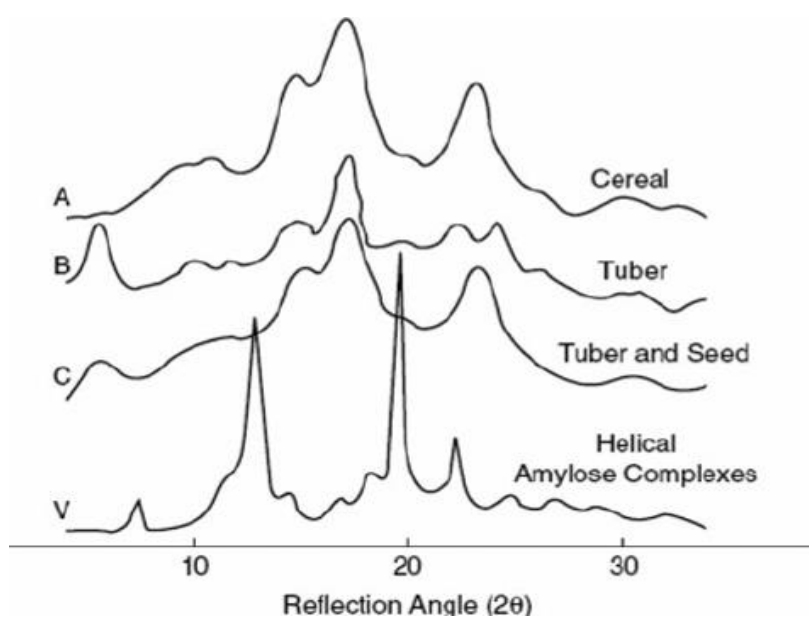


**Figure 5. Wide angle x-ray diffraction patterns of the semi-crystalline polymorphs: A-type (Cereal), B-type (Tuber), C-type (Tuber and Seed) and V-type (Helical Amylose Lipid Complexes) (Zobel, 1988).**

### 2.2.2 Starch gelatinisation (semi-crystalline to amorphous)

The term starch gelatinisation over the last decade has evolved to generalise key events that result in the loss of crystalline polymorphs in native starch. Thus, it has become an umbrella term; now referred to in aqueous (Fallahi *et al.*, 2016; Alcázar-Alay and Meireles, 2015) and non-aqueous environments (van der Sman and Broeze, 2013), with loss of crystallinity defined as both melting and breaking of intermolecular hydrogen bonds (Ubwa *et al.*, 2012; Lai and Kokini, 1991). A comprehensive review on the evolution of starch terminology has recently been published by Matignon and Tecante (2017).

For the purpose of this research, the term refers to any of the following five events:

1. Water uptake within the amorphous regions causing plasticisation and disruption of crystalline regions
2. Temperature and shear disruption of hydrogen bonding within amylopectin resulting in melting of crystalline regions
3. Granule swelling and leaching of amylose
4. Granular rupture (Figure 6) and continued leaching of amylose and amylopectin
5. Granular breakdown

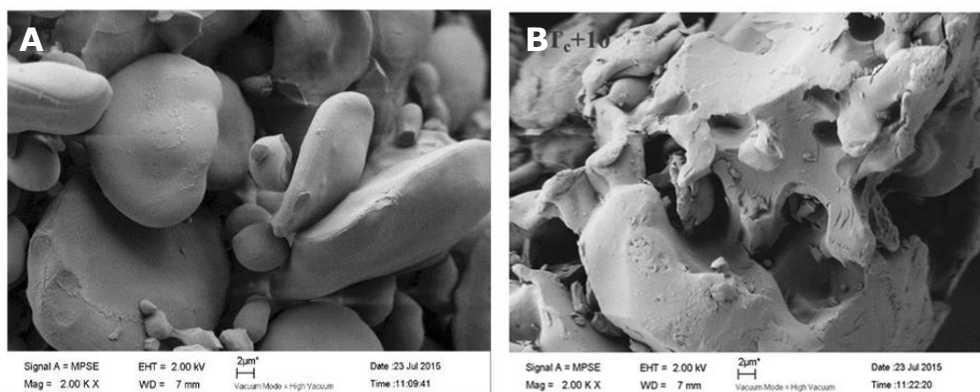


**Figure 6. Scanning Electron Micrographs of (A) swollen starch granules and (B) ruptured starch granules, during heating of semi-crystalline starch in an aqueous environment (Copeland *et al.*, 2009)**

### 2.2.2.1 Rapid Viscometer Analyser (RVA)

Gelatinisation of starch is often demonstrated in an RVA whereby the native starch is subjected to temperature and shear in an aqueous environment. The resistance of the starches to shear forces as the starch transforms from a semi-crystalline granule to a macromolecular suspension causes changes to the viscosity as demonstrated in Figure 7.

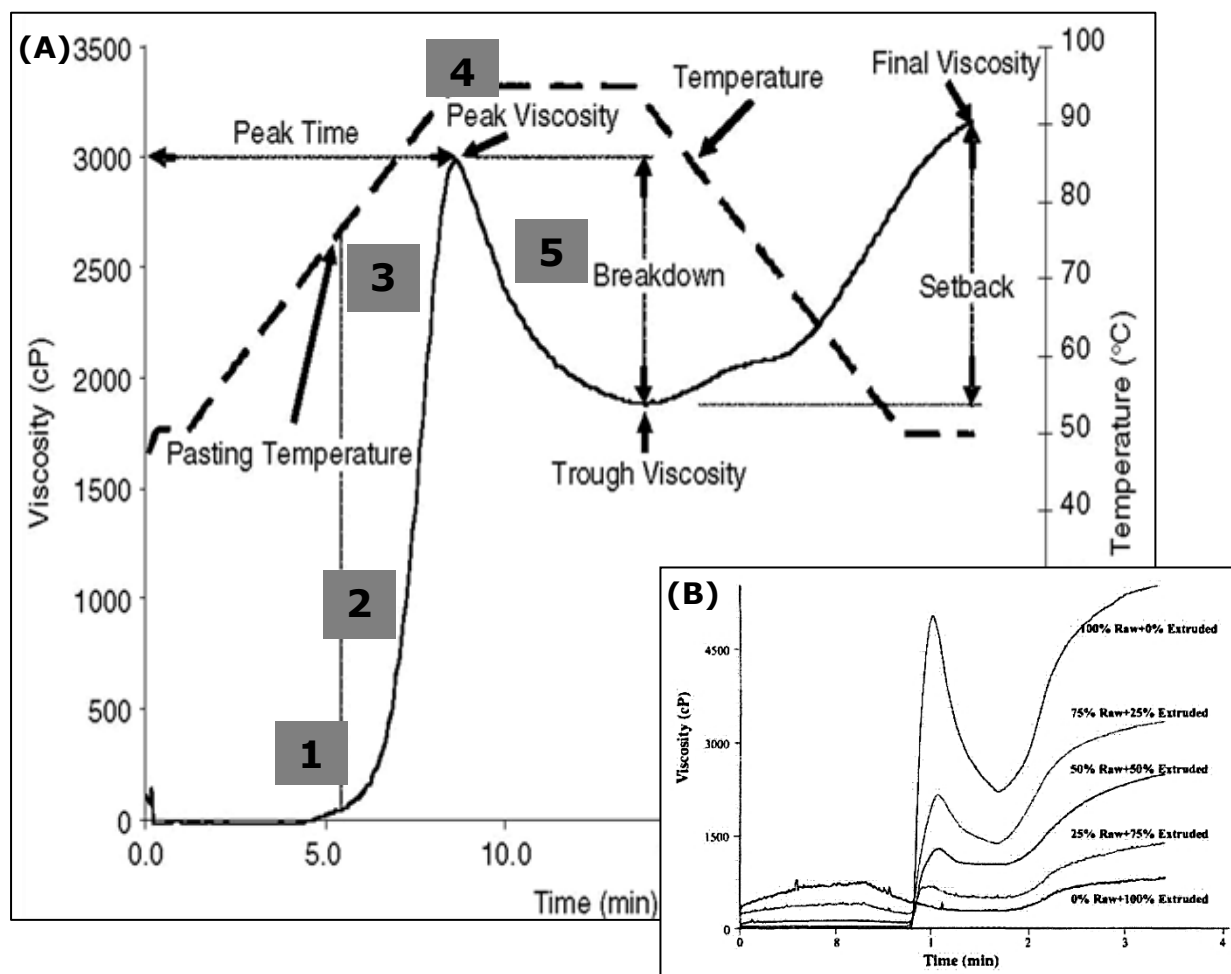


Figure 7. (A) RVA profile of gelatinisation of native semi-crystalline starch granules through to a macromolecular solution. The key parameters are notated: pasting temperature, peak viscosity and final viscosity (adapted from Saunders *et al.*, 2011). Numbers correspond to key events described on page 12. (B) RVA profiles of ingredients with an increased proportion of extruded starch to raw (native) starch, to show the influence of 'pre-gelatinised' starch on an RVA profile (adapted from Ozcan and Jackson, 2005).

When native starches are compared under the same conditions in an RVA, the pasting temperature is typically dependent upon botanical source. High amylose starches (cereals), are found to have higher pasting temperatures, thought to be a consequence the presence of non-starch components (lipids, fibres) that restrict access of water into the granule (Fallahi *et al.*, 2016; Mishra and Rai,

2006). Conversely, starches with pasting at room temperature, as displayed in Figure 7 B, are indicative of having amorphous starch granules that have been damaged prior to the measurement, often termed as 'pre-gelatinised'. Hence, the viscosity of the paste can increase prior to being exposed to a higher temperature. Of course, if the pre-gelatinisation process has rendered non-granular soluble starch, then it is likely the increase in viscosity during the RVA measurement will be a consequence of particle swelling and not starch granule swelling; as demonstrated in the 100 % extruded profile in Figure 7 B.

Pre-gelatinisation can also be characterised under cross polarised light microscopy by loss of birefringence. Additionally, Differential Scanning Calorimetry (DSC) in excess water can be used to identify the temperature at which crystalline order of amylopectin is lost from the change in enthalpy ( $\Delta H$ ) upon heating; corresponding to the endothermic transition of melting. If during the DSC measurement an endothermic transition is not witnessed, it is assumed the starch granules have lost their crystalline order prior to the measurement.

Peak viscosity is the point at which the granules (or particles) reach maximum swelling capacity prior to breaking down. Peak viscosity also differs significantly between botanical sources with native potato reaching  $\sim 14000$  centipoise (cP) compared with native maize at  $\sim 4000$  cP. It is hypothesised this difference is driven by the differences in granule diameter and the high proportion of phosphate monoesters within the amylopectin of potato granules that promote chain repulsion (Blennow *et al.*, 2000).

On cooling, the increase in viscosity is associated with the gelation of leached amylose and is an indirect measure of the concentration and size of solubilised macromolecules (Vesterinen *et al.*, 2001; Fredriksson *et al.*, 1998). Within extrusion, final viscosity has been related to the specific mechanical

energy (SME) to which the starch has been subjected during extrusion processing (Equation 2.2) (Moisio *et al.*, 2015; Majzoobi, 2004).

Loss of granular integrity facilitates water solubility and as a result Water Solubility Index (WSI) is also correlated with the mechanical energy through the Meuser Model, of which is specific to certain starches (Oikonomou and Krokida, 2012; Meuser *et al.*, 1984) (Equation 2.3).

$$\text{SME (Whr. kg}^{-1}\text{)} = \frac{\text{Motor Power (W)}}{\text{Throughput (kg.hr)}} \quad \text{(Equation 2.2)}$$

$$\text{WSI (\%)} = 0.289 \times \text{SME (W. hr. kg}^{-1}\text{)} - 4.0 \quad \text{(Equation 2.3)}$$

### 2.2.3 Melting

In limited water conditions (<20 %), when starch is subjected to heat; melting of crystalline regions can occur. Melting is a 1st order transition that results in the loss of crystallinity. Although this phenomena is considered part of the gelatinisation process; alone or in limited water the melting phenomena does not result in the swelling of starch granules and often if mechanical damage is limited, the granular integrity of the starch is retained.

Similarly to gelatinisation process, the melting temperature ( $T_m$ ) of starch is dependent on the water content (%) and type of crystal packing, with A-type amylopectin starch having a higher melting temperature than B-type (Zobel, 1988; Whittam *et al.*, 1990). V-type polymorphs are particularly resistant with melting temperatures in excess of 100 °C.

## 2.2.4 Starch conversion

The term 'gelatinisation' has become such a broad term that often in literature, when 'gelatinised' is used to characterise a material, the specific state of the starch is unknown. As already defined, gelatinised starch can describe the granular swollen state of starch to the non-granular macromolecular solution, which alone determines significantly different functionalities of the starch itself. When considering the relevancy of gelatinisation with extrusion processing, the term starch conversion seems more appropriate to cover the spectrum of starch states. Particularly, as within the relevant area of research, the processing conditions of extrusion are so severe that granular integrity of starch is unlikely to be sustained and depolymerisation is likely to have occurred.

### 2.2.4.1 Depolymerisation

Depolymerisation is defined as mechanical, thermal, chemical or enzymatic breakdown of starch into lower molecular weight ( $M_w$ ) polysaccharides and is covered under the term starch conversion. During processing, mechanical and thermal depolymerisation is more likely to occur in low water (<30 %) and high shear environments (Sarifudin and Assiry, 2014; Tester, 1997). Therefore, following gelatinisation of starch granules, further alteration to the physical structure of the starch can occur.

A significant amount of research has been carried out on defining the effect of processing on the depolymerisation of both amylose and amylopectin following gelatinisation. Characterised through a variety of methods, amylopectin is often found to be more susceptible during extrusion to mechanical depolymerisation than amylose (Majzoobi, 2004; Baud *et al.*, 2001). It is hypothesised that the high level of branching promotes the sensitivity of amylopectin, driving a greater effect of highly processed amylopectin on the starch material properties (Tang and Ding, 1994).

### 2.2.5 Retrogradation

Retrogradation is the re-association of amylose and amylopectin molecules through hydrogen bonding, forming helices and aggregates, crystallising the polymer. The process occurs in the temperature region between the glass transition and melting of the polymer and is an on-going process with rapid crystallisation of amylose molecules and slower re-crystallisation of amylopectin (Bhandari *et al.*, 1997).

For amylose, the double helical structure reforms and aggregates causing alignment of molecules and phase separation of the polymer-rich and polymer-deficit phases (Wang *et al.*, 2015). In excess water, retrograded amylose has been found to melt between 80 and 100 °C (Sievert and Pomeranz, 1989). Due to the restrictions driven by a high degree of branch chains within amylopectin; typical re-association causes the side chains to form shorter double helices. Consequently, re-crystallised amylopectin is in a less thermodynamically stable crystalline form and has a melting temperature between 60 and 65 °C (Majzoobi, 2004).

Retrograded starch is associated with A- and B-type crystal packing depending on the physical conditions; temperature and water content (Mihhalevski *et al.*, 2012; Shamaï *et al.*, 2004; Hellman *et al.*, 1954). High water and low temperature conditions promote formation of B-type polymorphs; which are found more prevalent amongst retrograded food following storage (Wang *et al.*, 2015; Hoover *et al.*, 2010; Bowen *et al.*, 2006).

## 2.3 Glass transition and aging of glasses

### 2.3.1 Glass transition

Depending on the temperature conditions and plasticiser level, amorphous polymers including amylose and amylopectin, can exist in a glassy state. In this form, large molecular motions are prevented by the locking of chains in a high viscosity network structure ( $>10^{12}$  Pascal second (Pa.s)) (Biliaderis, 2009). On heating to the glass transition temperature ( $T_g$ ), large scale segmental motions commence, shifting the polymer into a mobile viscous rubber. This second order transition is detectable within a DSC trace by the change in base line (due to the change in specific heat capacity) or by the significant changes in mechanical properties or volume occupancy.

Mechanical properties are most commonly measured using Dynamic Mechanical Thermal Analysis (DMTA). With DMTA, the response of a material to a deformation force is measured as a function of time, temperature or frequency (Menard, 2008). Through applying a sinusoidal deformation, changes in stiffness and damping are measured and used together with a geometry factor to obtain modulus information (Equation 2.4, 2.5 and 2.6) (Ehrenstein *et al.*, 2004).

$$\text{Complex Modulus (E}^*) = \frac{\sigma}{\varepsilon} \times \frac{l^3}{wt^3} \quad \text{(Equation 2.4)}$$

Where  $\sigma$  = force applied (Force/Area) and  $\varepsilon$  = deformation amplitude (Change in length/original length),  $l$  = length,  $w$  = width and  $t$  = thickness.

$$\text{Storage Modulus (E')} = E^* \times \text{Cos } \delta \quad \text{(Equation 2.5)}$$

$$\text{Loss Modulus (E'')} = E^* \times \text{Sin } \delta \quad \text{(Equation 2.6)}$$

Storage modulus ( $E'$ ) measures a material's ability to store elastic energy and loss modulus ( $E''$ ) is related to energy dissipation. Tangent delta ( $\tan \delta$ ) is the ratio of  $E''$  to  $E'$  and is therefore used to characterise the viscoelastic-solid ( $E'$ ) and -ideal liquid ( $E''$ ) behaviour of a material along with the  $T_g$  (peak  $\tan \delta$ ).

The  $T_g$  of a polymer is dependent on thermal history, composition of ingredients and plasticiser level. Such that, a more semi-crystalline polymer will have a higher  $T_g$  than amorphous. Within foods, due to the complexity of biopolymers,  $T_g$  is often reported as a broad range rather than an absolute value.

The  $T_g$  can be lowered by the addition of additional materials, known as the plasticisation effect; increasing mobility. This is often demonstrated with sugar (Kraus *et al.*, 2014; Bhandari and Howes, 1999), glycerol and water (Tuorila *et al.*, 1998), the effect of which on final products has recently been reviewed in detail by Bhattacharya (2017).

### 2.3.2 Aging of glasses

Although a transition into the glassy state constrains translational motions; side group motions still persist. Consequently, storage of polymers below the  $T_g$  can enable a process referred to as glassy state relaxation or physical aging, to enthalpy equilibrium (Chung and Lim, 2006). De-aging of an aged polymer reveals what appears to be an endothermic peak during calorimetric measurements below the  $T_g$  (Enrione *et al.*, 2012). The peak is driven by a change in specific heat capacity following thermodynamic relaxation, induced by structural rearrangements (Biliaderis, 2009). De-aging of a material in relation to the  $T_g$ , crystallisation (retrogradation) and melting is proposed in Figure 8.

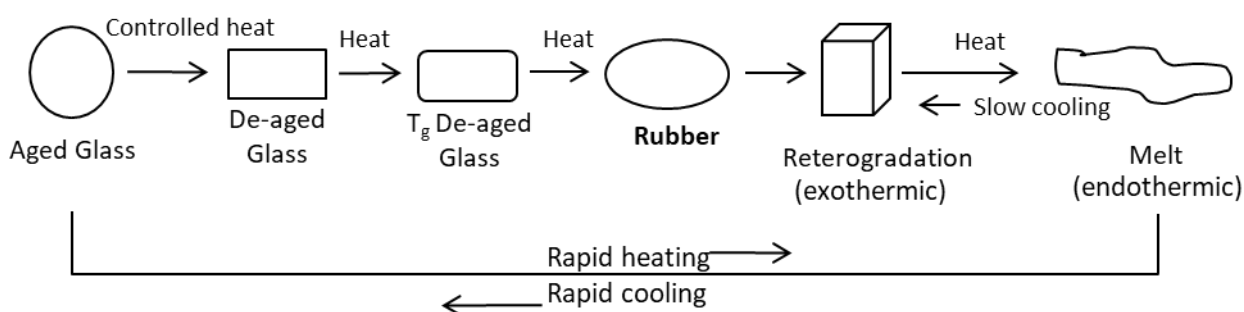


**Figure 8. Change in physical state of aged amorphous glass to melt through glass transition and crystallisation (adapted from Bhandari *et al.*, 1997).**

As a result, when dry calorimetric measurements are taken revealing de-aging, this can be misinterpreted as the melting of the polymer or even the glass transition as suggested for Liu *et al.* (2009). Details on recent findings for analytical methods and interpretation are summarized in the review by Chung and Lim (2006), where the significance of time, water and crystallinity on the likelihood of aging to occur is also detailed.

## 2.4 The manufacture of extruded snacks

The relationship between the fundamentals of starch structure, starch conversion, and glass transitions for snacks production will become apparent following the introduction of the transformations during processing of raw materials into both intermediates and final products. Extruded snacks are important as they provide a high quality snack that can be manufactured at low cost in very high volumes from a variety of different ingredients. By altering the extrusion process and driving differences in ingredient functionality, extrusion offers the potential to deliver a variety of different products from the same ingredient source.

### 2.4.1 Hydration and pre-conditioning

For the manufacture of starchy snacks, typically the process is initiated by blending dry ingredients such as native starches and grits in addition to functional ingredients such as salt, sugar and oil. Since these ingredients are of low water content and in the glassy or crystalline state, to plasticise the materials, the following stage involves hydration to the required dough water content in a mixer. At this point, the plasticised materials can pass through a pre-conditioning stage where they are subjected to hot steam; promoting starch conversion of the native starch. Pre-conditioning is more likely to be required in a milder extrusion process where starch conversion is minimal (van der Sman and Broeze, 2013). After the formation of hydrated dough, the material is then fed into a screw extruder to transition the materials into a cohesive melt, through mechanical and/or thermal energy. At this stage, water is critical in facilitating the processability of the melt and transformations of starch, through both the glass transition and melting.

## 2.4.2 Single and Twin-screw extrusion

Extrusion is the key transformational process during the manufacture of final products. It is defined as a high-volume manufacturing process where material is passed through a stationary heated barrel with forward feeding rotating screw(s) that convey and melt the material to achieve the desired physical and molecular properties. With twin-screw extrusion, co-rotating and counter-rotating screw models are available, which determine the flow of the material through the barrel (Figure 9). Typically, due to the associated loss of localised pressure points and self-cleaning capabilities, co-rotating screws are more commonly used in food manufacture (Harper, 1992).

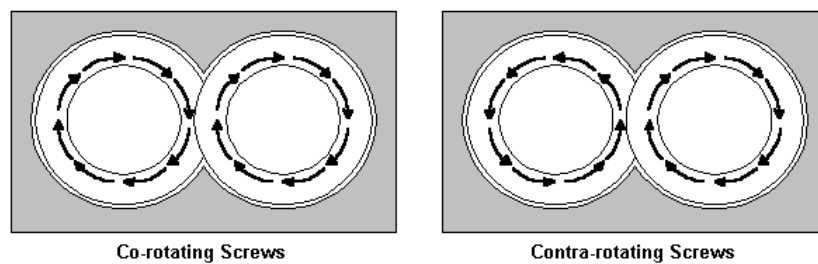


**Figure 9. Diagram of co-rotating and counter-rotating twin screw profiles (Tangram Technology, 2014)**

Twin-screw extrusion is associated with more severe process conditions (particularly mechanical damage) and therefore is often used to process cereal starches which are commonly more resistant to starch damage, through high thermal and mechanical energy. Conversely, since lower gelatinisation temperatures are associated with tubers; single-screw extrusion is more commonly used.

Extrusion offers the capability of controlling a variety of parameters including: screw profile, screw speed, water content and temperature; all of which can alter the material characteristics (Majzoobi, 2004). Typically, due to the associated changes in SME, shear stresses and temperature, these parameters determine the degree of molecular breakdown of the substrate through viscous dissipation (Kokini *et al.*, 1999). In the case of starch based food, this relates to the extent to loss of crystallinity and macromolecular depolymerisation, which dramatically alters material functionality (Kirby *et al.*, 1988). However, there are complex interactions between material and operational variables, with one variable change often directly influencing two or three additional variables; as demonstrated in the work by Fallahi *et al.* (2016).

On exiting the extruder, the material passes through a die of the desired cross-section. At this point the material is passed through a very small diameter which drives packing of the material at the end of the barrel. This packing section generates further shear, temperature and viscous dissipation; likely to drive further starch conversion.

### 2.4.3 Direct and in-direct expansion

On exiting the extruder, the viscous melt can either be directly or in-directed expanded. Direct expansion is the expansion of the melt immediately on exiting the extruder at the die face. It is induced by high temperature within the barrel and flash off of water at the die when the melt is subjected to atmospheric pressure, which drives matrix expansion. In-direct expansion however, is associated with milder conditions, preventing sudden flash off of water, creating a dense intermediate-product (often simplified to intermediate), which is dried and later expanded in hot oil

or air. The key differences in processing of direct and in-directly expanded snacks are detailed in Table 4.

**Table 4. Common differences between directly and in-directly expanded manufacturing processes (van der Sman and Broeze, 2013)**

Directly expanded	In-directly expanded
Low barrel water content (10 - 15 %)	High barrel water content (30 - 40 %)
High barrel temperature (>200 °C)	Milder barrel temperature (<130 °C)
High change in pressure ( $\Delta P$ ) on extruder exit	Low $\Delta P$ on extruder exit
Exit dough water content 10 %	Exit dough water content 20 - 25 %
Drying to 1 %	Drying to 10 - 12 %
No further processing (straight to seasoning following drying)	'intermediate-products' are required to be in-directly expanded after in oil or air
Short shelf life <4 months	Long shelf life >1 year (intermediates)

## 2.5 Structure creation of in-directly expanded snacks

### 2.5.1 Intermediate-product microstructure

For in-direct expansion, the final microstructure of the intermediate-product plays an important role in determining the degree of expansion and more specifically, the sensory attributes of the final product (Kristiawan *et al.*, 2016; van der Sman, 2016; Chanvrier *et al.*, 2015; van der Sman and Broeze, 2013; Robin *et al.*, 2012).

Within colloidal science, the concept describing the material states; typically the continuous phase (CP) and the dispersed phase (DP), has been adapted to describe the microstructure that may occur following extrusion of starch-based materials (Day and Golding, 2016). It has been suggested for intermediate-products, that the CP is made from the leached amorphous starch (gel former), and is the phase that is critical for the expansion of the intermediate during heating. In addition, it is hypothesised to function as the glue between the particulates holding the structure together (Figure 10).

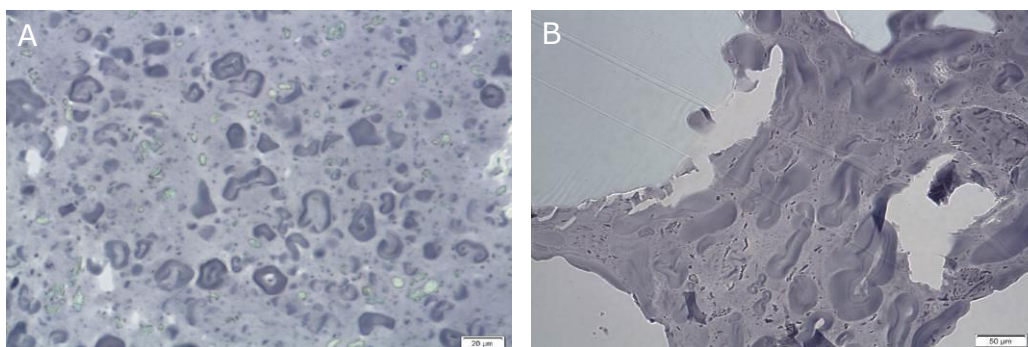


**Figure 10. Light microscopy of an intermediate-product (A) and final product (B) depicting the CP and DP microstructure that exists following processing (Scale bar = 50 μm).**

Literature defines the DP as 'filler particles' which may reinforce cell wall structure of the aerated structure leading to thicker cell walls and a greater density following expansion (van der Sman, 2016; van der Sman and Broeze, 2013). The DP could be made from: fibre (plant cell wall material), protein aggregates, amylose-lipid complexes and native or swollen starch granules, and these materials could increase the viscosity of the wall, thereby not allowing it to expand. Additionally, as the cell wall thins it is suggested these more solid particles rupture the bubble walls acting in a similar way to a hole in a balloon, limiting expansion.

The proportion of amorphous to crystalline starch, that remains following processing, can directly influence the ratio of CP:DP and has a linear relationship with expansion rate (Case *et al.*, 1992). A microstructure that is weighted more on the CP is likely to have a higher degree of expansion (Kokini and Moraru, 2003). It is hypothesised this is partly driven by a reduction in bulk viscosity with an increase in amorphous material. Alternatively, a microstructure consisting of a greater amount of DP is thought to have limited expansion due to the associated influence on cell wall viscosity, bubble cell wall rupture and facilitation of water escape; which directly impacts  $T_g$ .

Semi-crystalline starch granules have unique DP properties due to the potential for melting during the expansion stage. The effects of this on expansion are not fully understood but it is thought that melting enables the interaction of amorphous amylopectin with water which could:

1. Increase the viscosity of the matrix
2. Reduce available water for nucleation and growth (van der Sman and Broeze, 2013)

The combined effect of these on the properties is likely to limit expansion as seen in recent literature (Davies, 2016; van der Sman, 2016). On the contrary, the opposite effect could be argued as a result of increased water bound within the B-type polymorphs, that has the potential to be accessible for plasticisation upon melting, which could decrease the  $T_g$  and viscosity of the matrix.

## 2.5.2 Intermediate-product to final-product expansion

For an in-direct expansion process, change in pressure ( $\Delta P$ ) on exit of the extruder to drive matrix expansion is eliminated. Thus, water content (%), rheology of the starch matrix and frying temperature ( $^{\circ}C$ ) are thought to be the key determinants of how the final product expands (Mohammadi Moghaddam *et al.*, 2015). The relationships of these constituents on the events during frying of intermediates are proposed in Figure 11. The key events being:

- 1A. Transition of the intermediate from a glassy state into a rubber state\*
- 1B. Bubble nucleation\*
2. Bubble growth and matrix expansion
3. Transition of expanded intermediate from a rubber to a glass as a result of water loss
4. Setting of expanded starch matrix on cooling (stabilisation)

\*not yet determined which phenomena occurs first in the expansion process

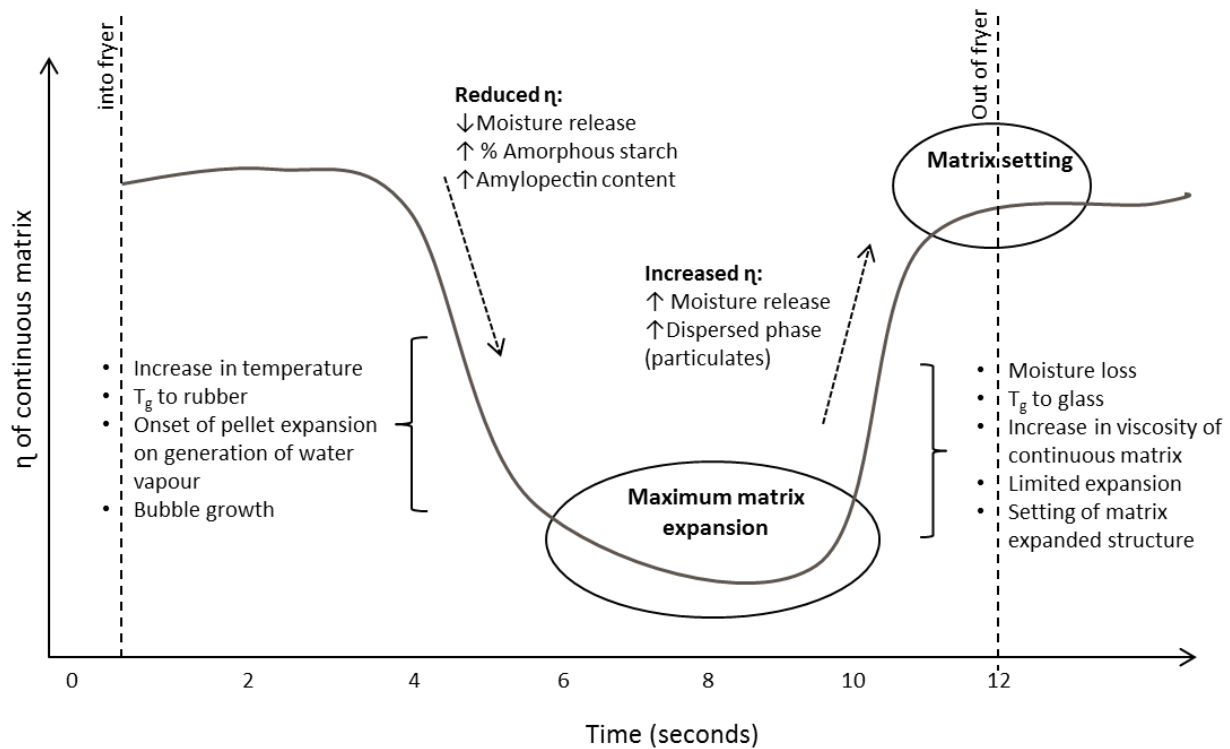


**Figure 11. Diagrammatic representation of the change in viscosity ( $\eta$ ) of an intermediate starch matrix during frying with respect to time. Bullet points highlight key physical and molecular changes and arrows depict key drivers in reducing or increasing  $\eta$  (adapted from Kristiawan *et al.*, 2016; van der Sman, 2016; van der Sman and Broeze, 2013; Chanvrier *et al.*, 2006; Kokini and Moraru, 2003; Tuorila *et al.*, 1998)**

### 2.5.2.1 Bubble nucleation and growth

Bubble nucleation, growth and stabilisation are vital processes for expansion; primarily governing the number and size of cells in a final product. Nucleation is hypothesised to take place at the point of contact between two phases and within the hilum of native starch granules (van der Sman, 2016; Kokini and Moraru, 2003). Bubble growth is dependent upon differences in pressure exerted within the bubble and the external bubble pressure, in addition to the radius of the gas nucleus and surface tension.

The three fates for an expanding bubble are collapse, rupture and stabilisation (van der Sman and Broeze, 2013). Collapse occurs when the vapour pressure cannot overcome elastic stresses; rupture when the cell wall thins to the point that the rupture stress is exceeded; and stabilisation when  $T_g$  is passed during bubble expansion or equilibrium. Bubble rupture, commonly known as cell coalescence, is suggested to promote bubble stabilisation by facilitating water vapour to escape from the internal matrix (Kokini and Moraru, 2003).

### 2.5.2.2 Water vaporisation and $T_g$

More recently, the original hypothesis relating to specific intermediate-product transitions during expansion, has been optimised (van der Sman, 2016; Kokini and Moraru, 2003). Numerical simulations have identified water vaporisation (the blowing agent) to be more accurate at a pressure of 4 bar. Therefore, the boiling point of water is more likely to occur at temperatures in excess of 140 °C; which corresponds more similarly to expansion temperatures measured in real time (Patel *et al.*, 2017; Norton *et al.*, 2011; Kloker *et al.*, 2003). In addition, optimum expansion has been identified at the boiling line and glass transition intersect, which has been demonstrated as a function of water and temperature in Figure 12 (van der Sman, 2016; van der Sman and Broeze, 2013).

The  $T_g$  gradient in Figure 12 demonstrates the influence of water content on the temperature at which the amorphous starch transitions from a glass to a rubber, which is likely to impact expansion. An intermediate with high initial water content will reduce the viscosity of the intermediate and consequently minimised pressure differences across the bubble wall will prevent bubble growth.

Norton *et al.* (2011) supported this model but partly attributed limited expansion to case hardening of high water content intermediates as a result of surface dehydration.

Alternatively, a very low initial water content will increase  $T_g$ , preventing reaching  $T_g$  due to the continued loss of water upon heating. This will result in the external bubble pressure continuously exceeding the internal bubble pressure, preventing bubble nucleation and growth. Water also facilitates heat transfer throughout the matrix, enabling  $T_g$  and water vaporisation to occur more rapidly; doubling the effect of low water on preventing expansion. In fact, optimum water content of intermediate-products for expansion has been identified in the region of 9 - 13 % (dwb) (Davies, 2016; van der Sman and Broeze, 2013; Kokini and Moraru, 2003)

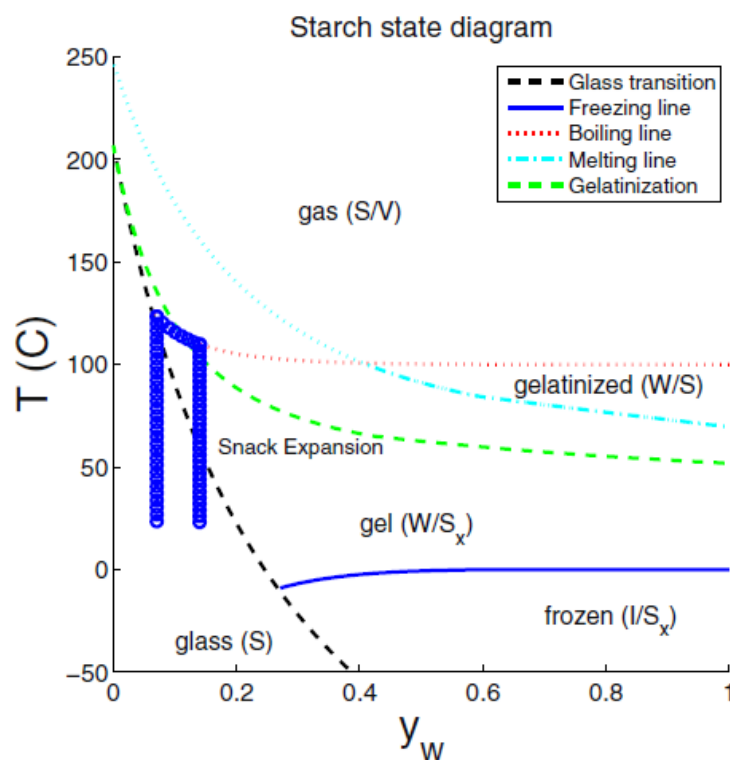


**Figure 12.** The most recently published starch state diagram on the expansion process of potato based intermediates (adapted from van Der Sman, 2016). The thick blue circles represent the pathway of transitions from right to left. Original work presented by Kokini and Moraru (2003).

As previously mentioned, at high frying temperatures, the crystalline regions of starch in the intermediate can become amorphous (Figure 12). More specifically, native and partially swollen starch granules in the presence of water can gelatinise and/or melt, losing crystallinity. This introduces the complication when moving from model systems to complex recipes with multiple botanical sources of starch. Such that, A-type starches in low water environments have higher melting temperatures and have consequently been found to remain crystalline during frying, unlike B-type starches (Patel *et al.*, 2016). Finally,  $T_g$ , gelatinisation and melting lines relative to water content and temperature in Figure 12 are specific to potato starch and therefore likely to shift with alternative bulk botanical starches as demonstrated by Riaz (2002).

### 2.5.2.3 Bulk viscoelastic properties

Following nucleation and glass transition, the bulk viscoelastic properties primarily determine the rate of expansion; governing the matrix resistance to the pressure differences across a bubble. The lower the matrix resistance to bubble growth, the greater the promotion of cell coalescence (Babin *et al.*, 2007). The point at which bubble growth ceases is when the melt either reaches  $T_g$  or a critical viscosity where the internal bubble pressure drops to below that of the atmosphere, hypothesised to be in the temperature region of  $T_g + 30\text{ }^\circ\text{C}$  (Fan, 1994).

In literature, the AM:AP has been found to partly govern the viscoelastic properties of the starch matrix (Kristiawan *et al.*, 2016). Such that, at low amylose contents expansion is often enhanced (van der Sman and Broeze, 2013; Adesso *et al.*, 1995). However, one important factor to consider here is the nature of the starch. High amylose granules are often characterised as more resistant to starch conversion than low amylose granules and therefore this may be a consequence of differences in the

amorphous to semi-crystalline ratio; which will directly influence the CP:DP (Brent *et al.*, 1997). In the case of amorphous starches, it is hypothesised a high amylose CP drives fast molecular entanglement of the polymer (retrogradation) that is more difficult to pull apart during expansion (Kristiawan *et al.*, 2016; van der Sman and Broeze, 2013; Babin *et al.*, 2007).

DMTA is the most common method to characterise the bulk viscoelastic properties, where samples are mounted in a clamp as whole intermediates or ground particles within pockets. The sample is then subjected to sinusoidal deformation (stress) relative to temperature and time and the response measured (strain) is used to calculate  $E'$  and  $E''$  (Equation 2.4, 2.5 and 2.6). DMTA measurements are carried out in the linear viscoelastic region (LVR) where modulus is considered independent of strain. Thus, the relationship between DMTA measurements to bulk viscoelastic properties during frying has been questioned, where the materials could be subjected to conditions outside of the LVR. Della Valle *et al.* (1997) suggested that, since expansion is extremely rapid (< 12 seconds); it is likely the elongational strain rate is very high. Therefore, elongational viscosity of the melt during expansion could exceed the linear viscoelastic limit. To overcome this Chanvrier *et al.* (2015) have correlated the ratio of DMTA measurements  $E'(T_g + 30\text{ }^\circ\text{C}) / E'(30\text{ }^\circ\text{C})$  to elongational viscosity; measured by a capillary rheometer.

### 2.5.3 Final product microstructure

Final product microstructure can be characterised to understand the impact of ingredients and process on the expansion properties of final products. Typically, methods aim to characterise cell size distribution, cell wall thickness, number of cells, expansion ratio (ER) and density; where the word “cell” refers to open space filled with air, surrounded by a solid phase. Cell size distribution characterises the inhomogeneity of the final product and coupled with number of cells gives an indication into the degree of cell coalescence during expansion. Typically, ER is a measure of the degree of expansion which negatively correlates with final product density.

Methods used to characterise microstructures include Scanning Electron Microscopy (SEM), Micro-CT X-Ray Tomography (XRT) and C-Cell Analysis; where image processing can be used on SEM micrographs to extract quantitative data. XRT is considered the gold-standard method due to the reconstruction of the final product microstructure into 3D images; where whole products can be analysed rather than basing data on one image following sample cutting. To characterise open or closed cells within snacks, pycnometry is often used with expanded starch-based products.

In literature, maize grits are typically associated with direct-expanded extrusion due A-type starches requiring more severe processing to convert the starch. As a result of low water content; high SME and temperatures are generated when processing the starch which often results in loss of both crystallinity and granular integrity. Consequently, maize grits final products are often reported to be highly expanded and of low density when compared with alternative products (Nor *et al.*, 2013).

Much of the recent work within expanded maize snacks is focused upon the addition of functional ingredients, often with the aim to increase the positive nutrition of snacks. The added ingredients

often restrict expansion; increasing density, cell wall thickness and decreasing cell size (Reddy *et al.*, 2014; Nor *et al.*, 2013; Robin *et al.*, 2012; Ahmed, 1999). As a result, the impact of altering final product microstructure on sensory attributes has been investigated.

Particular interest is focused on the link between 'crispness' of snacks and microstructure; defined as 'the combination of noise produced during the initial bite with the front teeth and the breakdown of the product when bitten with the back molars'. Duizer (2003) found crispiness to have a binomial distribution when correlated against mean closed porosity and an inverse relationship with hardness. Similarly, decreasing cell sizes of directly expanded corn extrudates have been found to have an inverse relationship with the mechanical strength of final products, thus impacting the fracture behaviour of the structure (Dogan *et al.*, 2008). The understanding of how density and mechanical strength influence food fracture and failure, spans across a variety of food categories, as detailed in the review by Lillford (2001). A significant amount of work has also been researched internally within the PEP sensory science centre. Following the beginning of work linking microstructure to texture both internally and externally, developing snacks with a designed microstructure that deliver a defined final product attributes has become a key platform of research.

## 2.6 Business Focus for the future of snacks

The global demand for salty snacks is expected to grow at a rate of 6% over the next 4 years. This growth is largely driven by emerging markets, as developed regions such as Europe and America, are restricted by market maturity (Bakery and Snacks, 2016).

Particular focus for PEP growth is in the Philippines and Bangladesh, where market growth has an exponential forecast. Currently, the salty snack market sizes of these countries are 180,000 tonnes (\$1 billion) and 92,000 tonnes (\$0.35 billion) respectively. Both countries have an annual GDP growth in excess of 6%, in addition to large, youth dominated populations greater than 100 million (Central Intelligence Agency, 2001).

Specifically for the Philippines, 57 % of market snacks are extruded, of which 24 % are maize-based. The main competitors are Universal Robina Corporation and LWW with a combined market share of 83 %, compared with PEP's 3 %.

The facts presented highlight two important factors:

- 1) Current extrusion capabilities within these emerging markets consist of high shear extrusion processes (typically used to manufacture maize) such as twin screw extrusion.
- 2) PEP currently has limited manufacturing capabilities within these regions (only producing 3 % of total market).

To utilise the current manufacturing capabilities within emerging markets and provide further control over product functionality, the current research project has been approached by processing

maize grits first, using high-shear extrusion, to create a homogenous bulk ingredient. Due to the nature of the manufacturing facilities in which the maize has been processed, the output will be homogenous and consistent throughout; providing control over the functional properties of the material into intermediate manufacture. This research will then aim to build an understanding of how the functionality of the bulk material during expansion of intermediates can be altered using additional ingredients.

## 2.7 Objectives

Following the initial investigative work, the specific objectives of the project were to:

- 1) Characterise the material properties and molecular structure of directly expanded twin-extruded maize grits (IP1)
- 2) Manufacture intermediates from IP1 using single-screw and twin-screw extrusion and characterise their properties using appropriate analytical methods
- 3) Link the key intermediate-product characteristics to the final product microstructure; identifying a strategy to optimise final microstructure
- 4) Deliver proof of principle of altering final product microstructure and attributes by incorporating additional ingredients; taking a design-led microstructure approach.

The manufacturing processes throughout this thesis and the associated samples are highlighted in Figure 13 whereby the twin-screw extruded directly expanded maize grits, utilised as a bulk ingredient, has been simplified to intermediate product 1 (IP1) and the following manufactured intermediate-products 2 and 3 (IP2 and IP3). As a comparison of intermediates manufactured from IP1, native maize grits were also processed under identical twin-screw extrusion conditions to IP2, notated as intermediate product 4 (IP4). IP2, IP3 and IP4 following expansion in hot oil are notated as final-product 2 (FP2), final-product 3 (FP3) and final-product 4 (FP4) respectively.

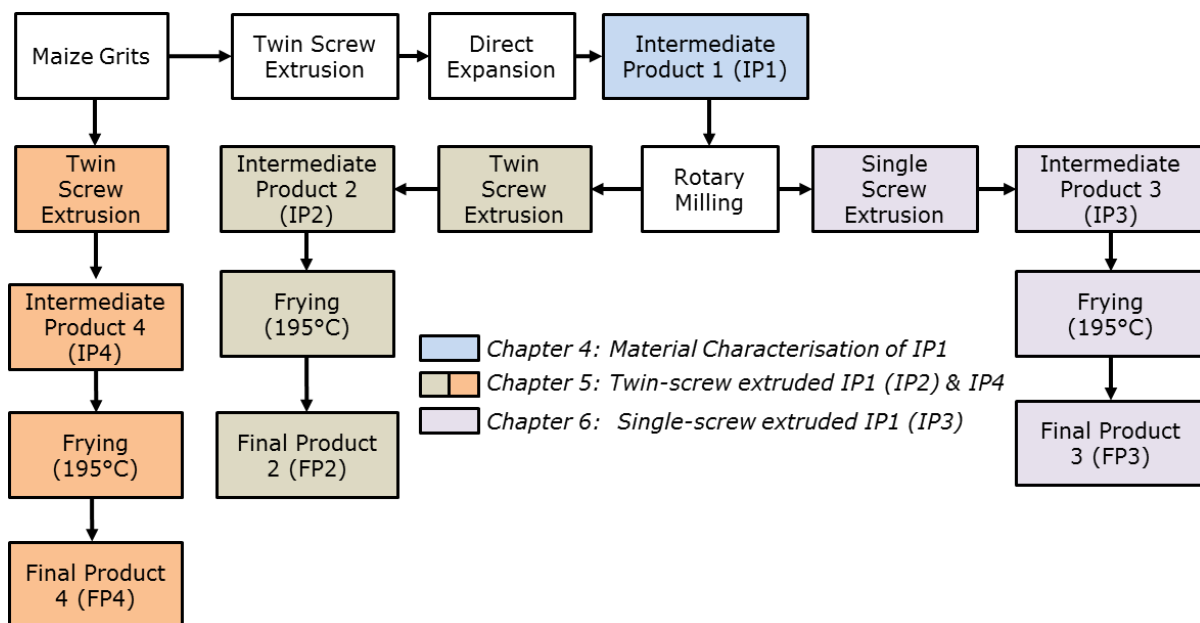


**Figure 13. Outline of the manufacturing steps to utilise bulk processed maize (IP1) into 2 separate manufacturing processes (IP2 and IP3) in addition to a comparison product manufactured from native maize (IP4) and the corresponding chapters presenting results from characterisation of intermediate and final products.**

## Chapter 3 Materials and Methods

Materials and methods considered generic in this research and therefore prevalent in more than one results chapter have been presented in this main materials and methods section. Any materials or methods specific to a results chapter have been detailed in the materials and methods of that chapter.

### 3.1 Ingredients

Yellow YG560 Maize Grits (Whitworth Bros. Ltd., Worksop UK) were used for the initial manufacture of the bulk ingredient with  $11.60 \pm 0.28$  % water content (dwb). The nutritional profile of the maize utilised in this research is displayed in Table 5, highlighting the impurities in the system with the presence of protein, cellular wall material (fibre) and fat.

**Table 5. Nutritional results of maize grits measured by Covance Laboratories Inc.**

<b>Nutrient</b>	<b>%</b>
Fat (by acid hydrolysis)	1.7
Dietary Fibre	4.54
Total Starch (by difference)	73.03
Total Sugar	1.6
Protein (Dumas Method N x 6.25)	6.93
Ash	0.7

## 3.2 Processing Methods

### 3.2.1 Direct Expansion (IP1)

Maize grits were processed at 14 % water content using a full scale BC 72 twin-screw extruder (Cletral: France) with a GPS2 high shear screw configuration (Figure 14). Screw speed was set at 340 rpm with a throughput of 750 kg/hr. Torque was set to 75 % of maximum with a 226 Kw motor and SME of 192.1 Whr.kg<sup>-1</sup>.



Figure 14. Screw profile of twin-screw extrusion process in the manufacture of IP1.

The extruder temperature zones were split into 5, of which zone 1 naturally increased in temperature to 40 °C due to conduction of temperature from zone 2. The temperatures of zones 2 to 5 are confidential and are therefore not disclosed in this research.

On exit of the extruder the melt expanded and was cut by a rotary die facing cutter at a speed of 760 rpm. Following cutting, samples were transported to a depositing port and collected in sealed plastic bags at water content of ~10 %.

### 3.2.2 Milling and Particle Separation

Milling of IP1 was carried out prior to incorporation into further manufacturing processes and before all analytical analysis on IP1. A pilot scale rotary mill (Urschel Laboratories; Leicester) was used with a 30 B-type head attached with 0.75 mm gaps and 28 columns.

## 3.3 Analytical Methods

### 3.3.1 Expansion Ratio (ER)

ER of the intermediate-product to final product was calculated on a volume basis by Equation 3.1.

$$ER = \frac{(W \times L \times T)_{final\ product}}{(W \times L \times T)_{intermediate\ product}} \quad \text{(Equation 3.1)}$$

Where W= Width (mm), T= Thickness (mm) and L = Length (mm)

### 3.3.2 Microscopy

Various methods of microscopy were used to characterise raw materials, intermediate products and final products. Hence, methods have been described separately, dependent on the sample format.

#### *3.3.2.1 Raw materials*

Micrographs of dry and hydrated samples in Chapter 5 were taken using an BX61 Microscope (Olympus; Germany) with a BX-UCB motorised stage. Prior to analysis samples were dispersed on a glass slide, and if hydrated, water was dispersed onto the sample with a pipette and covered with a glass slide. Magnifications of 5X and 10X were used for micrographs presented in Chapter 5.

#### *3.3.2.2 Intermediate and final products*

Micrographs presented in Chapter 5 and 6 of intermediate and final products were carried out externally by RISE Agrifood and Bioscience (Goteborg, Sweden) due to the limited availability of resources internally. Sample preparation steps carried out prior to microtoming are detailed below in Table 6 indicating the key events: fixation, dehydration, plastic embedding and sectioning of samples prior to microscopy. The steps detailed were carried out to preserve the structure of the samples and allow very thin slices ( $\sim 1 \mu\text{m}$ ) to be taken; enabling detailed interpretation.

**Table 6. Steps 1 to 7 for sample preparation prior to microtoming of intermediate and final products (SP Bioscience; Goteberg).**

Step	Step Name	Details	Time
1	Sample prep	Cutting of samples using laboratory blade to 0.5 x 1 x 2 mm size	10 minutes
2	Pre-fixation	Samples suspended above vapour mix of 50:50 25 % glutaraldehyde and 37 % formaldehyde in sealed pan	Minimum of 48 hours
3	Post Fixation	Sample suspended above 2 % osmium tetroxide (OsO <sub>4</sub> ) in sealed pan	3 hours
4	Dehydration	Sample dropped into 8 ethanol solution (10ml) washes using Leica EM TP in the following order of concentration: 50 %, 50 % 70 %, 70 %, 95 %, 95 %, 99 %, 99 %.	10 minutes per solution wash. 99 % concentration for 30 minutes each
5	Plastic Embedding	Sample dispersed in ethanol 99 % solution and Technovit 7100 at 1:1 ratio	1 hour
6	Plastic solidifying	Sample dispersed in 100 % Technovit 7100 solution (~15 ml)	6 hours
7	Polymerisation	Leave for plastic to harden throughout sample at 20 °C	2 hours

Following plastic embedding, samples were sectioned using a RMC Power Tome XL Ultramicrotome with a glass knife and sections were mounted onto glass slides.

### 3.3.2.3 Scanning Electron Microscopy

Cross-sections of final products were cut to 5 mm x 3mm and directly mounted onto circular aluminium stubs with carbon disks (Agar Scientific; Essex). A Leica SCD005 Sputter coated samples with Au alloy under vacuum for 300 seconds at 25mA current. Micrographs were taken using a Jeol 6060LV Scanning Electron Microscope (Jeol UK Ltd; Herefordshire) under vacuum. Magnifications of 5X, 12X, 20X, 43X and 65X were used on cross sections.

### 3.3.2.4 Staining

Staining of microtomed samples was used for light microscopy. The iodine solution to stain amylose blue, amylopectin brownish-mauve and protein yellow was mixed with the following components:

- Potassium iodide (KI) 2.0 g
- Iodine (I<sub>2</sub>) 1.0 g
- Distilled water 300 ml

Microtomed samples with protein were stained green with the following solution and left on the slides for 2-3 minutes before being rinsed with distilled water prior to microscopy:

- Light green powder 0.17 g
- 33 % Acetic Acid 100 ml

### *3.3.2.5 Confocal Light Microscopy*

All Confocal light micrographs displayed in this thesis were conducted externally by RISE Agrifood and Bioscience (Goteborg, Sweden) due to the limited availability of resources internally.

Intermediate samples were firstly cut and then placed directly under the SP5 confocal light microscope (Leica; Cambridge) displaying either the cross section or the intermediate surface following staining (of the starch phase) using Acriflavine in combination with Texas red and Bodipy.

### 3.3.3 Dry Particle Size Distribution (PSD)

Dry PSD was determined using a LS 13320 Series Particle Size Analyser (Beckman Coulter; High Wycombe) with an attached Tornado Dry Power System and optical model glass. Prior to analysis a calibration was carried out using a LS control G35D set (Beckman Coulter; High Wycombe) and optical model Silica Carbide.

Samples were placed into the loading cell no more than 1 cm in depth prior to analysis and measured using a 5mW diode laser. A minimum of three replicates were taken for results reported. Obscuration was set at 7 % with background and alignment measurements every 30 seconds and 30 minutes, respectively.

### 3.3.4 Thermogravimetric Analysis (TGA)

TGA was carried out to calculate water content (%) and characterise water loss mechanisms of intermediate products during expansion using slow and fast heating rates.

#### *3.3.4.1 Fast Rate TGA*

A Thermo-gravimetric Analyser, Model: TGA/DSC-1 (Mettler Toledo; Leicester), was used to measure weight loss of samples using fast heating rates. Prior to analysis samples were broken using a pestle and mortar. Broken samples were then sieved into 1 mm particle sizes and weighed separately until all samples were between 6.5 and 7.5 mg. All samples were heated at a rate of 40 °C/min from 25 °C up to 250 °C. Blank subtraction was based on loss of empty pans, measured prior to analysis. Graphs presented in Chapters 5 and 6 are based on relative % weight loss and 1<sup>st</sup> derivatives plotted using the STAR Software.

#### *3.3.4.2 Slow Rate TGA*

Slow rate TGA was carried out using a Thermo-gravimetric Analyser, Model: TGA/DSC-1 (Mettler Toledo; Leicester). Sample preparation was carried out in the same way as Section 3.3.4.1 with a heating profile from 25 °C to 250 °C at 5 °C/min.

### 3.3.5 Rapid Visco Analyser (RVA)

A 4500 RVA (Perten Instruments; Hägersten) was used to analyse the molecular properties of raw materials, intermediate and final products. Prior to analysis samples were tested for water content using TGA (*see Section 3.3.4.2*). Samples from the same set were then ground using a Retch Mill (Model ZM 200) at 1400 rpm with a 1 mm sieve catcher attached. Ground samples were then sieved to achieve an average particle size of <250  $\mu\text{m}$  with an Octagon Digital 2000 (CamLab; Cambridge). A small amount of each sample ( $3.5\pm 0.01$  g) was then added to  $25.0\pm 0.05$  g of distilled water, allowing for the original water content.

Samples were then placed in the aluminium sample pans with an attached polycarbonate stirring paddle. For the measurement, the stirring speed was set to 960 rpm for the first 10 seconds and 160 rpm for the rest of the experiment. The temperature profile consisted of samples being initially held at 22 °C for 2 min to study the cold-water viscosity; then, they were heated to 95 °C at a constant rate of 14 °C/min, and were held at that temperature for 3 min, then, cooled down to 22 °C at the same rate and were held at that temperature for 5 min. Analysis of results was carried out using the ThermoCline software (Version TCW3).

For Chapter 4, micrographs of the paste immediately before and after the measurement was taken. Refer to *Section 3.3.2.1* for details on the microscope used.

### 3.3.6 X-Ray Powder Diffraction (XRPD)

X-ray diffraction patterns were recorded on a D5005 X-Ray diffractometer (Siemens; Birmingham) in the angular range of 3-38° (2θ), with a step size of 0.05° (2θ) and an acquisition time of 2.5 seconds per step. The Cu K alpha-1 radiation (λ= 0.1542 nm) from the anode was generated at 40 kV and 40mA. For sample preparation, raw materials and intermediate products were ground using a pestle and mortar until <1 mm in diameter and evenly distributed in a mounting plate. The rotational speed for the plate was set to 60 rpm.

### 3.3.7 Water Absorption Index (WAI)

2g of sample following milling (Section 3.2.2) was placed in a centrifuge tube with 30 ml of distilled water. The sample was then subjected to vortex mixing for 2 minutes, repeated intermittently every 10 minutes for 30 minutes at 25 °C. The tube was then placed into a centrifuge and spun at 3000 rpm for 15 minutes. The supernatant was decanted and the precipitate was weighed. WAI was calculated using Equation 3.2.

$$WAI (\%) = \frac{\text{Weight (tube+precipitate)} - \text{Weight (tube)}}{\text{Weight (original sample)}} \times 100 \quad \text{(Equation 3.2)}$$

### 3.3.8 Water Solubility Index (WSI)

Following decanting of the supernatant into a pre-weighed dish, reported in Section 3.3.7, the supernatant was dried for 24 h at 105 °C. The dish following drying was then weighed and WSI was calculated from Equation 3.3.

$$WSI (\%) = \frac{\text{Weight (dish+dried sample)} - \text{Weight (dish)}}{\text{Weight (original sample)}} \times 100 \quad \text{(Equation 3.3)}$$

### 3.3.9 Differential Scanning Calorimetry (DSC)

DSC was carried out to characterise the loss of order of the starches following processing in addition to highlighting the glass transition temperatures ( $T_g$ ) of materials processed differently. As a result, both hydrated and dry DSC was carried out.

#### 3.3.9.1 Hydrated DSC

For hydrated DSC, a sample from the same set was taken and measured for water content using the slow rate TGA method (see Section 3.3.4.2). Samples were then analysed using a Q20 DSC (TA Instruments; Newcastle) with an attached refrigerated cooling system. For sample preparation, materials were ground using the ZM 200 Retch Mill (Hann; Germany) at 1400 rpm with a 1.0 mm sieve attachment to obtain a 5 to 15 mg sample size.

8 - 13 mg of sample was then placed into an aluminium pan and deionised water was added on a basis of 1:1 ratio (g/g) ensuring samples were greater than 50 % water content to prevent water content influencing transition temperatures (Coral *et al.*, 2009; Zobel *et al.*, 1988; Donovan, 1979). Pans were hermetically sealed and samples were left to hydrate for 60 minutes prior to analysing. An empty pan and lid was used as a reference. Samples were then heated from 10 °C to 120 °C at a rate of 5 °C/min. Following the measurement the heat flow was normalised to sample weight (g) and plotted against sample temperature (°C) using the STAR Software.

### 3.3.9.2 Dry DSC

Dry DSC was carried out using a DSC 3+ (Mettler Toledo; Leicester) whereby the water content of the same sample set was measured by slow rate TGA prior to analysis (see *Section 3.3.4.2*). Samples were prepared using a pestle and mortar to achieve a particle size between 750 µm and 1.5 mm and weight between 6.5 and 7.5 mg. 1 piece at a time was placed into a stainless steel pan and hermetically sealed prior to analysis. An empty pan and lid was used as the reference sample. Samples were heated from 25 to 250 °C at 40 °C/min. The pan was then cooled from 250 °C to 25 at 40 °C/min and the ramp was repeated up to 250 °C to account for de-aging of the material following storage. Following the measurement the heat flow was normalised to sample weight (g) and plotted against sample temperature (°C) using the STAR Software.

### 3.3.10 Dynamic Mechanical Thermal Analysis (DMTA)

#### 3.3.10.1 *Whole products*

Intermediate products were analysed using an 8000 SYS Dynamic Mechanical Analyser (PerkinElmer; Beaconsfield) with whole intermediate samples mounted and heated from -20 °C to 200 °C at a heating rate of 5 °C/min. Three frequencies of 0.3, 1 and 10 (Hz) were used to characterise the frequency dependency of the materials. A 0.005 mm displacement was used following a strain sweep that identified 0.005 mm in the linear viscoelastic region (*see Appendix 2*). Lower temperatures were reached by feeding in liquid nitrogen through an attached canister. The force during measurements was calibrated daily by applying a force of 0.04 Newton. Prior to mounting samples, to reduce geometry variability, samples were cut with a knife to the dimensions of ~11 mm x 12 mm. An average of the final dimensions; width, length and thickness were taken based on four measurements.

DOW Corning<sup>®</sup> High Vacuum Grease was used to seal the intermediates during specific whole product DMTA measurements to promote water retention. Where grease has been used it is stated in the figure description.

#### 3.3.10.2 *Pockets*

To prevent water loss during measurements, samples were milled to <1 mm in particle size and deposited into aluminium pockets. Pockets were then sealed with UniBond Silicone sealant and left for a minimum of 18 hours for the sealant to set prior to analysis. Samples were heated from -20 °C

to 200 °C at a heating rate of 5 °C/min with three frequencies 0.3, 1 and 10 (Hz) and a 0.005 mm displacement.

### 3.3.11 Statistical Analysis

In order to analyse the data collected, where data sets were greater than two, Design-Expert 6.0.11 (Stat-Ease; Minneapolis) was used applying a two-factor ANOVA with a Tukey Post Hoc Multiple Comparison test and a 0.05 level of significance. For comparison of two results, a two-tailed T-Test in Excel was used with a 0.05 level of significance. The test used for each Figure or Table is detailed in the materials and methods section of that specific chapter.

### 3.3.12 Sensory Analysis

In Chapter 6, final products were analysed by an untrained panel of 5 people using a degree of difference test to characterise differences between final products from a sensory perspective, specifically on the following defined attributes:

*Hardness:* First bite force required to bite through the product with front teeth

*Rate of breakdown:* How quick the product breaks down when chewing to a state where it can be swallowed

*Melting:* The ease with which the product disappear to a liquid / pulp without chewing

*Tooth packing:* The degree to which the product packs into the teeth following swallow and full clearance

A degree of difference scale was used where reference (IP3) was 0 and additional samples were compared for the following attributes on a +3 to -3 scale (Table 7). A non-related example of slightly and obviously different was provided prior to the analysis to aid in calibrating the panels understanding of the scaling. For further details on the degree of difference methodology please refer to Aust *et al.* (1985). Prior to analysis, intermediates were fried at 195 °C for 10 seconds and seasoned with 1.2 % fine salt 50 (Glacia; Cheshire).

**Table 7. Degree of differences score definitions**

<b>Score</b>	<b>Description</b>
-3	Sample is obviously less than reference on most samples
-2	Sample is slightly less than reference on all samples
-1	Sample is slightly less than reference on most samples
0	Sample is the same as reference
1	Sample is slightly more than reference on most samples
2	Sample is slightly more than reference on all samples
3	Sample is obviously more than reference on most samples

## **Chapter 4 Results: Material Characterisation of raw maize grits and intermediate product 1 (IP1)**

### **4.1 Introduction**

The milled intermediate product 1 (IP1) was characterised by physico-chemical methods to understand the molecular integrity and physical properties of the material, prior to utilisation as a bulk ingredient within intermediate manufacture (refer to Figure 13).

Prior to milling, the high expansion of IP1 on exit of the die was driven by the low water content, high shear processing, which was likely to promote loss of both crystalline order and granular integrity within the maize grits starch granules (*see Section 2.4.2*). Therefore, it was hypothesised much of the native crystalline structure would be amorphous.

As a result of the process conditions during and post extrusion, it was thought that IP1 should transition almost immediately into an amorphous glassy material following processing. Consequently, large chain movements for re-association could be restricted, preventing retrogradation of starch.

## 4.2 Materials and Methods

The methods used to characterise IP1 are listed below. Prior to analysis, IP1 was required to be milled to enable suitable geometry for testing. Specific details of the milling method and general analytical methods are detailed in Chapter 3.

Material characterisation methods:

- Light and Cross Polarised Light Microscopy (Olympus BX61, 5X objective)
- Particle Size Distribution (PSD)
- Rapid Visco Analyser (RVA)
- Water Solubility Index (WSI)
- Water Absorption Index (WAI)
- X-Ray Powder Diffraction (XRPD)
- Differential Scanning Calorimetry (Hydrated) (DSC)
- Statistical Analysis (Excel T-Test)

## 4.3 Results and Discussion

### 4.3.1 Macrostructure

Following milling, particle size of IP1 fell within the region of 40  $\mu\text{m}$  to 1800  $\mu\text{m}$ , with the greatest proportion of particle diameters between 500 and 650  $\mu\text{m}$  (Figure 15 A). Dry particle shape was identified as being angular by light microscopy, which is typically associated with rotary hammer milling (Figure 15 B). The angularity is assumed to be due to the high energy input causing singular breakage events, promoted by the fine material structure (Kaya *et al.*, 2002; Gaudin, 1926).

Light microscopy also supported quantitative data with the majority of particulates having a diameter great than 100  $\mu\text{m}$ . Additionally, it can be observed that more rounded particles are present at smaller particle sizes, which is hypothesised to have driven the reduction in errors below 500  $\mu\text{m}$  in Figure 15 A, concordant with published data (Kaya *et al.*, 2002).

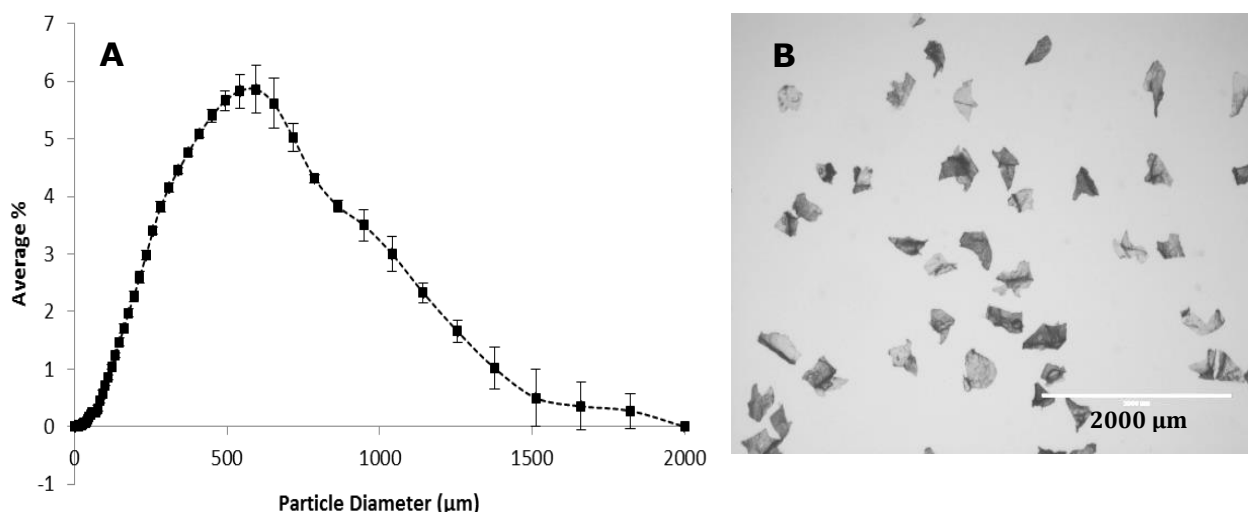


**Figure 15. (A) Average percentage (%) of particle diameter of IP1 from 0 to 2000  $\mu\text{m}$   $\pm$  standard deviation based on 3 replicates, (B) Light microscopy micrograph of IP1 particles following milling. Scale bar = 2000  $\mu\text{m}$**

### 4.3.2 Microstructure

Hydration of milled IP1 in excess water resulted in significant particle swelling (from ~500  $\mu\text{m}$  to ~900  $\mu\text{m}$ ), which was associated with the material being gelatinised (Majzoobi *et al.*, 2011; Carvalho *et al.*, 2010) (Figure 16 A). The micrographs suggest a presence of limited intact starch granules, with the large majority of starch having ruptured and broken down; indicating significant starch conversion.

It is important not to neglect the presence of other non-starch components associated with maize grits which have been previously addressed (*see Section 3.1*). In Figure 16, IP1 in excess water is displayed prior to shearing under the glass slide with light microscopy (A) and cross polarised light microscopy (B) and following shearing with light microscopy (C) and cross polarised light microscopy (D). It is hypothesised the majority of constituents within Figure 16 A are associated with the amorphous starch matrix. Following shearing, in an aqueous environment, the matrix breaks apart to form a CP with dispersed particulates, highlighted with arrows (Figure 16 C). These particulates are assumed to be the cellular material (fibre) and protein, present in low quantities (Table 5). Surprisingly, cellular material was identified as particularly resistant to extrusion with large intact cellular material persisting into the final product. Under cross polarised light, this cellular material appears crystalline; corresponding to the lipid bilayer structure within the cell wall (refer to X and Y notated on Figure 16 D) (Bagnell, 2012). This structure is typical of the alerone layer that surrounds the endosperm. Due to its mechanical resistance during the dry milling process; it remains associated with the endosperm into the processed material.

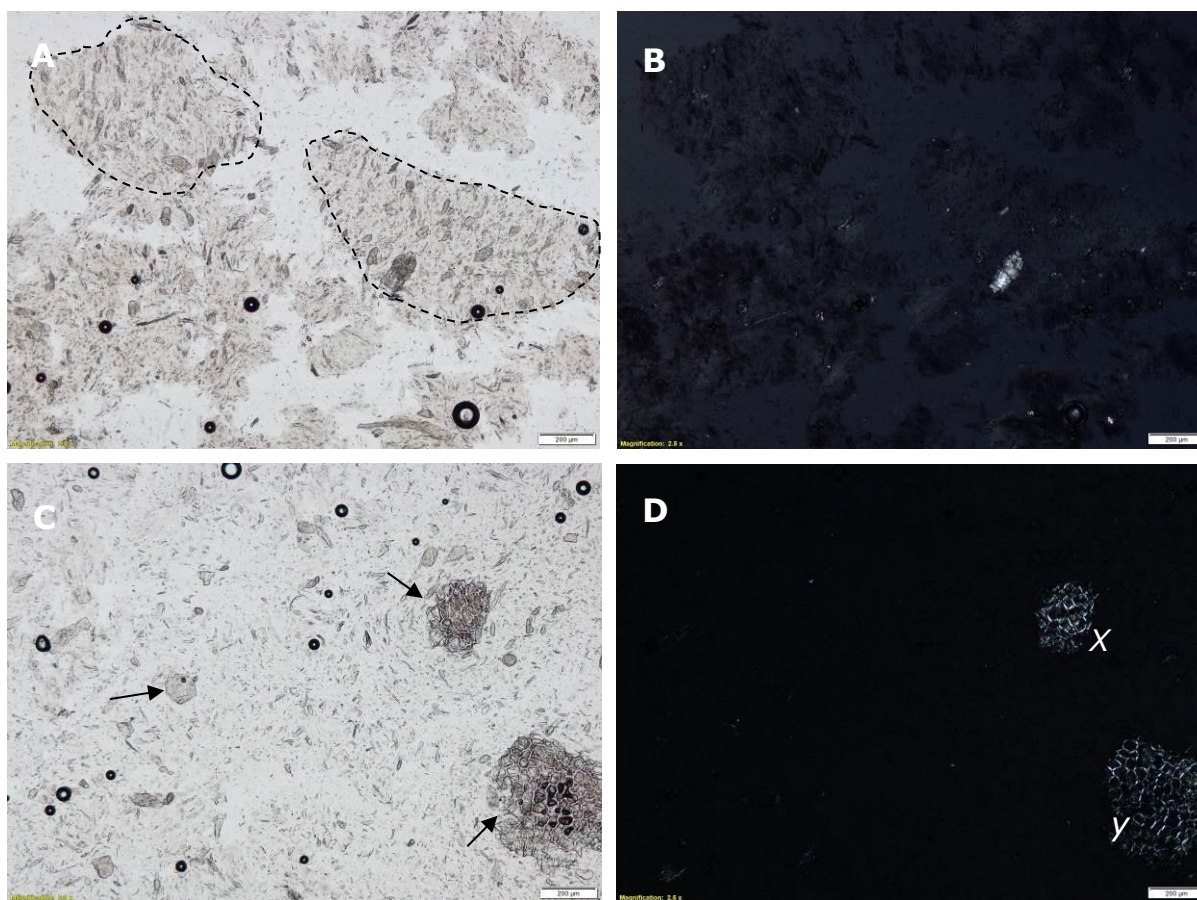


**Figure 16. Light Micrographs of (A, C) hydrated IP1 following milling, (B, D) Cross polarised light micrographs of hydrated IP1 following milling. Scale bar = 200  $\mu\text{m}$ . X and Y notations highlight intact cellular wall material.**

The low viscosity profile of the material, when subjected to shear and temperature in a high water environment is indicative of a gelatinised material with loss of granular structure (Figure 17); in agreement with Majzoobi *et al.* (2011) and Carvalho *et al.* (2010). The peak viscosity of  $618 \pm 7.09$  cP at room temperature indicates the immediate uptake of water promoting particle swelling. When comparing the peak viscosity temperature of IP1 to raw maize grits, clear differences can be seen; whereby the native starch requires a higher temperature ( $94.8$  °C) to enable granule disruption and promote water uptake (Table 8).

The differences in temperature peak viscosity could also be a result of the presence of non-starch components. In particular lipids, which are hypothesised to sit at the surface of intact granules preventing water uptake; limiting swelling until significant granule disruption.

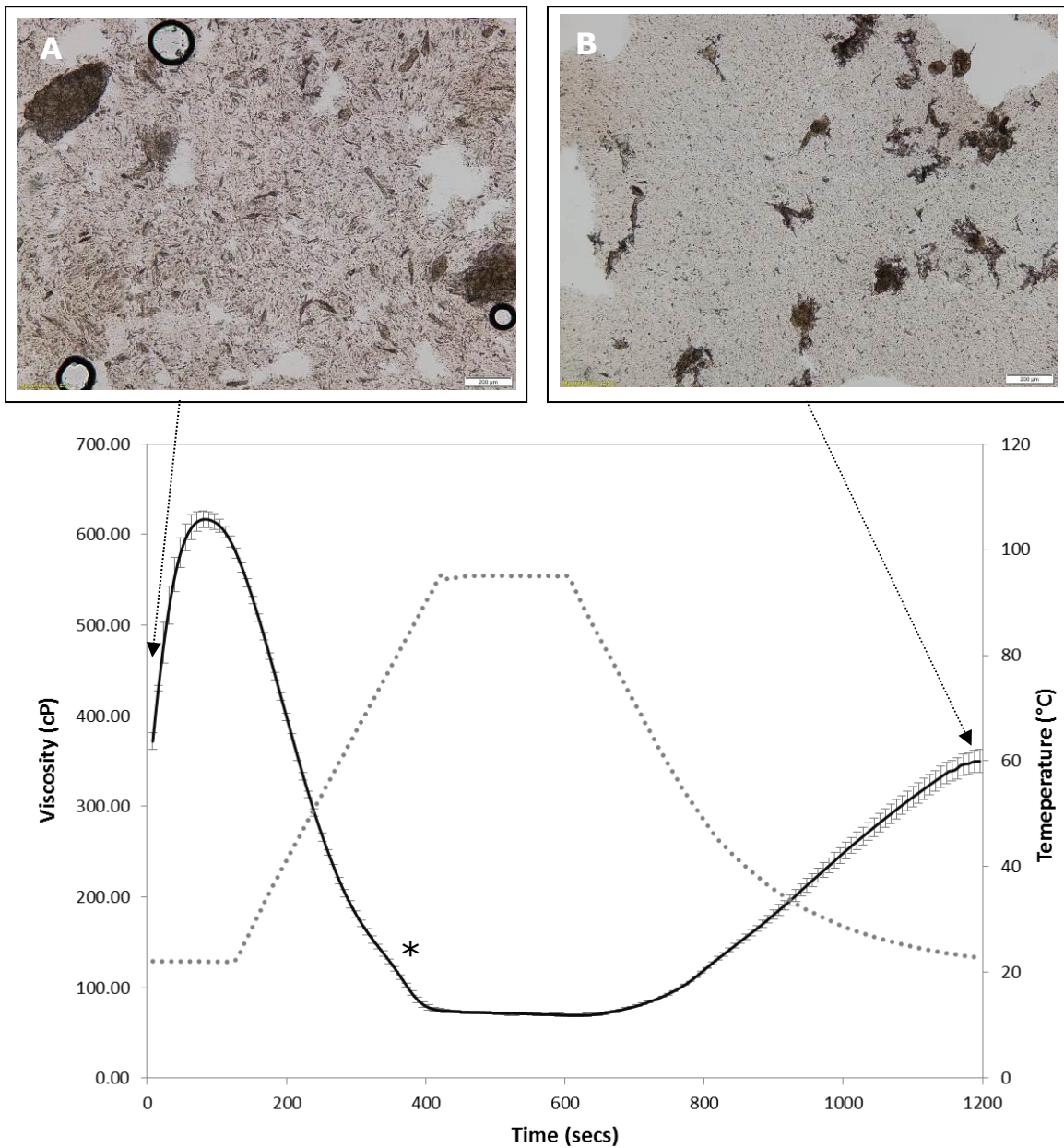


**Figure 17. Average viscosity of IP1 in excess water. Error bars represent standard deviation based on 3 replicates. .... Temperature (°C), — Average viscosity (cP). Micrograph (A) IP1 paste microstructure prior to measurement, (B) IP1 paste microstructure following measurement. Scale bar = 200 µm. Asterisk indicates slight shoulder peak at 350 seconds.**

**Table 8. Average  $\pm$  standard deviation of peak viscosity temperature ( $^{\circ}$ C), peak viscosity (cP) and final viscosity (cP) for native maize grits and IP1 based on 3 replicates.**

Parameter	Native maize grits	IP1
Peak Viscosity Temperature ( $^{\circ}$ C)	94.8 $\pm$ 0.03	22.1 $\pm$ 0.06
Peak Viscosity (cP)	2937.3 $\pm$ 19.4	618.3 $\pm$ 7.09
Final Viscosity (cP)	8357.3 $\pm$ 65.5	349.7 $\pm$ 12.5

Due to the loss of starch granule integrity of IP1, peak viscosity in Figure 17 is likely to be a representation of maximum particle swelling rather than inter-molecular changes (Kang *et al.*, 2016). The differences between IP1 and raw maize grits demonstrate the impact of a reduction in granular integrity on peak viscosity (Table 8) where starch granules swell to a greater volume than gelatinised particles (Fallahi *et al.*, 2016; Balasubramanian *et al.*, 2012; Carvalho *et al.*, 2010). For IP1 specifically, the impact of particle volume on viscosity is demonstrated in the micrographs presented before and after shearing (Figure 17 A and B). Whereby, the decrease in viscosity is hypothesised to be a result of particle breakdown during the measurement. Carvalho *et al.* (2010) performed a similar experiment on maize extrudates and demonstrated the state of starch at significantly higher magnifications. It showed at peak viscosity the pre-gelatinised starch had formed a discontinuous gel matrix. However, one thing that wasn't demonstrated was aggregation of particulates following heating that was observed in this study, as evident in Figure 17 B.

Denaturation and aggregation is a typical property of proteins upon heating and shearing. Therefore, the aggregation observed in the micrograph could be a result of the protein (zein) associated with the endosperm (Simmons *et al.*, 2007). However, the initial processing method of IP1, which involved a significant heating step, should also be considered as it is likely the protein was denatured

during the extrusion process and the shear during the measurement promoted aggregation. Simmons *et al.* (2007) suggested aggregation of proteins to occur at temperatures in excess of 70 °C and therefore it is likely this phenomenon occurred between 300 - 700 seconds (Figure 17). In the RVA trace, the slight shoulder peak that appears between 300 and 400 seconds (highlighted with an asterisk) could be an effect of the aggregation influencing the viscosity of the paste. In literature, unless there is polydispersity in the aggregated solution, protein aggregation is reported to increase viscosity, explaining the slight reduction in the rate of viscosity drop at this point (Lattuada *et al.*, 2015; Amin *et al.*, 2014; Lilyestrom *et al.*, 2013).

The increase in final viscosity from 100 cP to 350 cP upon cooling from 95 °C to room temperature, demonstrates the temperature dependence of dynamic viscosity (Messaâdi *et al.*, 2015). This phenomena is also related to the gelation properties of amylose starches upon cooling (Wang *et al.*, 2015; van der Sman and Broeze, 2013). The final viscosity of IP1 is significantly lower than raw maize grits, which suggests a lower hydrodynamic volume, that could be driven by differences in packing density (Kang *et al.*, 2016) (Table 8). The figures reported for final viscosity of both raw and directly expanded maize are supported by published data (Balasubramanian *et al.*, 2012; Carvalho *et al.*, 2010; Fallahi *et al.*, 2016). Literature is also in agreement that amylopectin is more susceptible than amylose to macromolecular depolymerisation during extrusion processes as a result of the  $\alpha$  (1, 6) branch points occupying a greater volume (Gomez and Aguilera, 1984; Majzoobi, 2004). Therefore, the differences in final viscosity of raw maize and IP1 could also be from the breakdown of amylopectin during the twin-screw extrusion process, which would directly impact the hydrodynamic volume of the soluble polymer.

### 4.3.3 Absorption and Solubility

Both the water absorption index (WAI) and water solubility index (WSI) of IP1 were statically significantly higher than native maize grits (Figure 18) ( $P < 0.001$ ). Although the absorption is greater for IP1 than native maize grits, it is likely if the starch granules were damaged but didn't lose granular integrity that the absorption capacity would be greater. As presented in literature, typically there is a bell curve associated with starch damage and WAI, such that following granular breakdown, absorption is reduced (Balasubramanian *et al.*, 2012). The temperature which appears to be critical is 150 °C, where WAI reaches a maximum (Fallahi *et al.*, 2016; Badrie and Mellowes, 1991). For IP1, barrel temperatures exceeded 150 °C which was likely to reduce WAI to 420 % as a result of granular breakdown. Conversely, the greater the extent of granular damage the greater the WSI, whereby increases are assumed to be promoted by further starch conversion, including depolymerisation, modelled by Gomez and Aguilera (1984). Therefore, suggesting significant starch damage has occurred for the WSI of IP1 to exceed 45 %. When taking into account the Meuser Model relationship between SME and WSI, SME at 192.1 W.hrk<sup>-1</sup> predicts a WSI for IP1 of 51.5 %; which is 2 % from the average measured (Figure 18) (Kirby *et al.*, 1988; Meuser *et al.*, 1984). However, due to the model being based on specific starches, it is unlikely to predict WSI for alternative botanical sources.

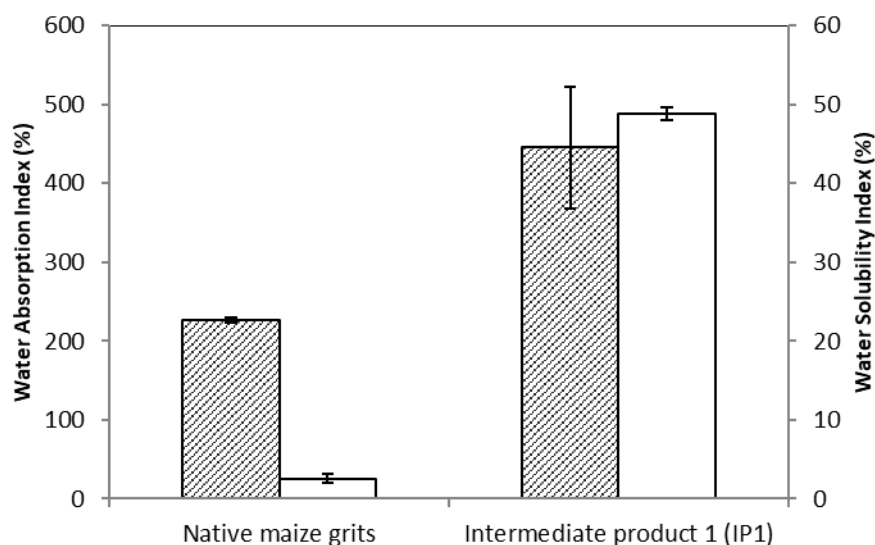


**Figure 18. Average  Water Absorption Index (%) and  Water Solubility Index (%) of native maize grits and IP1. Error bars represent standard deviation based on 5 replicates.**

The solubility capacity of IP1 is thought to be a result of leached amylose and amorphous amylopectin as a result of loss of granular integrity. Similarly, it is assumed as amylopectin is more susceptible to depolymerisation in extrusion processes, it is the key driver in changes in solubility between native maize and IP1 (Kibar *et al.*, 2010; Majzoobi, 2004) .

To test this further, staining of IP1 before and after hydration with iodine staining was carried out (Figure 19). It is clear upon staining in excess water (A vs. B) that the surrounding water matrix turns a strong blue colour suggesting the presence of only amylose. An explanation to this is that mechanical damage to the molecular structure of amylopectin during extrusion renders soluble amylose-like polymers (Harris and Little, 1993). This hypothesis is echoed in similar studies where following extrusion, a decrease in amylopectin content and increase in amylose content was found (Pushpadassa *et al.*, 2009; Baud *et al.*, 2001; Chinnaswamy and Hanna, 1990).

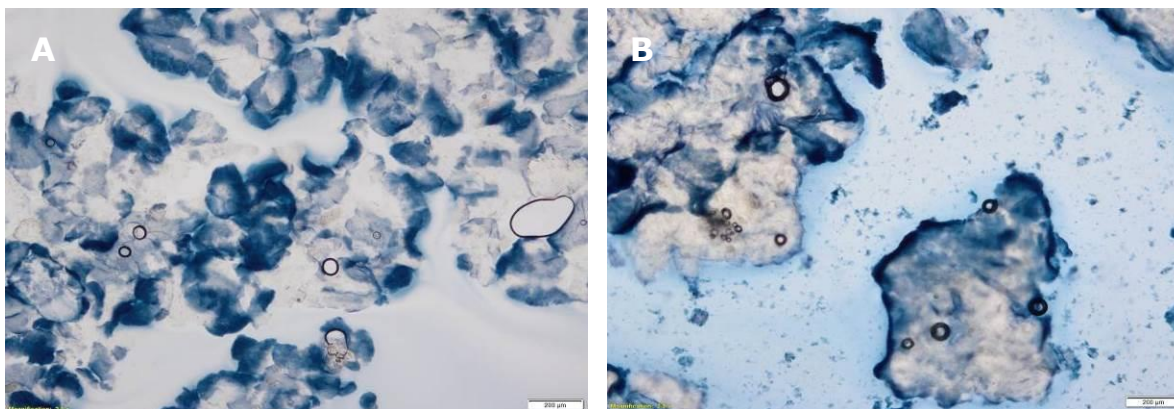


**Figure 19. Light microscopy of IP1 with (A) iodine staining (B) iodine stained with excess water. Scale bar = 200 µm.**

#### 4.3.4 Crystallinity

To characterise the crystalline polymorphs in both native maize grits and IP1; XRPD was used. Figure 20 shows XRPD for raw maize grits and IP1, where peaks correspond to single amylopectin crystal polymorphs.

Raw maize grits has sharp peaks at the  $17.46^\circ$ ,  $19.96^\circ$ ,  $20.62^\circ$  and  $26.92^\circ$   $2\theta$  positions; corresponding to A-type polymorphs of crystalline amylopectin (Jane *et al.*, 1999; Zobel *et al.*, 1988) (Figure 20). Following processing, the majority of amylopectin crystalline structure is lost with an amorphous halo demonstrated in Figure 20; the only peak that could correspond to remaining A-type crystalline amylopectin is the  $20.98^\circ$   $2\theta$  peak.

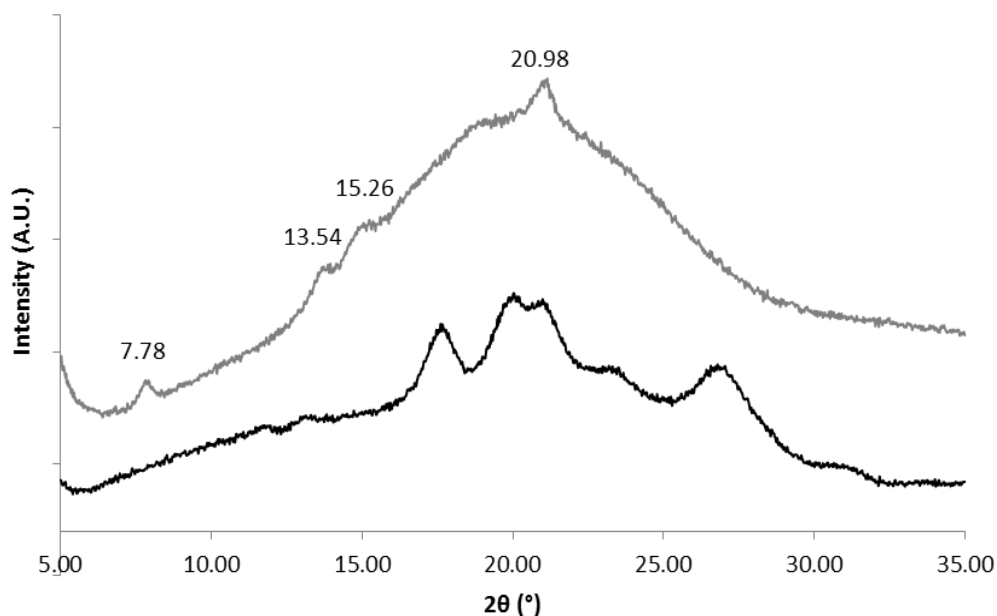


**Figure 20.** XRPD of — native maize grits and — IP1. Numbers correspond to the peaks in IP1.

Peaks corresponding to the 7.78°, 13.54° and 15.26° 2θ positions introduce the component commonly associated with cereal starches; amylose-lipid complexes. As previously mentioned in Section 2.2.1, amylose content is positively correlated with granule lipid content, where lipids are hypothesised to sit at the surface complexed with amylose. Following gelatinisation, the carbon chain of the fatty acid can complex again within the central cavity of the amylose helices forming amylose-lipid complexes that aggregate into a crystalline form (Finkenstadt *et al.*, 2016). Iodine cannot complex with amylose that is already associated with lipid, as this prevents iodine from being able to sit within the helices. Thus, XRPD and DSC are the main characterisation methods used to confirm amylose-lipid complexation following processing (Biliaderis and Galloway, 1989). However, literature on specific peaks within a XRPD trace that correspond to amylose-lipid complexes and other polymorphs is unclear. Shogren *et al.* (2006) reviewed these discrepancies and contest that differences in peaks are attributed to the number of glucose units associated with each turn around

the lipid core; 6 or 7, which alter the crystal inter-planar distance.  $V_6$  complexes are reported to have peaks at the  $7.50^\circ$ ,  $13.00^\circ$ ,  $\sim 20^\circ$   $2\theta$  positions and  $V_7$  at the  $\sim 15.30^\circ$  position (Mihhalevski *et al.*, 2012; Shogren *et al.*, 2006; Kawada and Marchessault, 2004). Therefore for IP1, it appears that there may be a combination of both  $V_6$  and  $V_7$  complex formation (Figure 20). The peak at the  $20.98^\circ$   $2\theta$  position, previously attributed to remaining crystalline amylopectin, could be argued as  $V_6$  crystal formation which has been reported at the  $19.8^\circ$   $2\theta$  position (Shogren *et al.*, 2006).

To further explore if ordered starch remains, DSC of IP1 was carried out in excess water up to  $150^\circ\text{C}$  (Figure 21 A and B), whereby an endothermic peak corresponding to the loss of crystalline order would be expected at a similar temperature to native maize grits ( $70 - 80^\circ\text{C}$ ). Amylose-lipid complexes would be expected to melt at temperatures in excess of  $100^\circ\text{C}$  (Pushpadassa *et al.*, 2009).

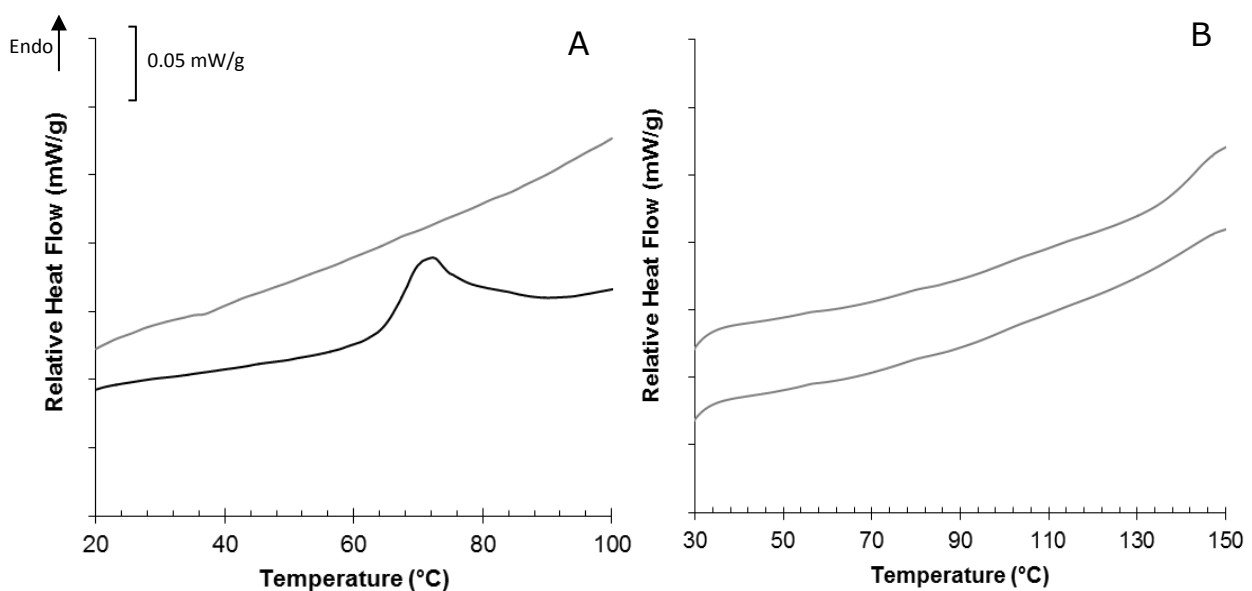


**Figure 21.** DSC thermographs of hydrated raw maize grits (black) and IP1 (grey) (at least 1 solid: 1 water). (A) Hydrated raw maize grits and IP1 up to  $100^\circ\text{C}$  in aluminium pans. (B) Replicates of IP1 to  $150^\circ\text{C}$  in stainless steel pans. Lines displaced by  $\pm 0.25$  mW/g for ease of observation. Heating rate  $5^\circ\text{C}/\text{min}$ .

The endothermic peak associated with the raw maize grits in excess water is attributed to the loss of helical order within the native starch. The average temperature and enthalpy of this endothermic peak was  $71.9 \pm 0.81$  °C and  $12.07 \pm 0.02$  J/g respectively, supported by published literature, who report mean endothermic temperatures of 72.3 °C and 76.74 °C and enthalpies of 12.8 J/g and 15.14 J/g (Ozcan and Jackson, 2005; Ratnayake *et al.*, 2009). It can be assured this is neither a glass transition nor aging of the material as the material is in excess water and therefore has passed the  $T_g$  line during hydration, prior to the measurement (Chung and Lim, 2006; Zeleznak and Hosene, 1987).

The thermograph of IP1 in excess water shows no endothermic peak between the temperatures of 40 to 100 °C; supporting the hypothesis that the crystalline regions associated with amylopectin in the native starch are amorphous. Similarly, retrogradation was restricted due to the sudden loss of water and glass transition on exit of the extruder, preventing large molecular movements. The small exothermic peak at lower temperatures (36 °C) could be a result of the amorphous starch solubilising. Measurements were repeated up to 150 °C to support XRPD data with the melting of amylose-lipid crystal structures (Figure 21 B). However, no definitive endothermic peaks were detected in excess of 100 °C. Since the proportion of amylose-lipid complexes in the bulk material will be relatively small, and there is no defined temperature for all complexes to melt, it is unsurprising that the endothermic peak is undetectable.

Thus, conclusions are unable to be made for the peak in Figure 20 at  $20.98^\circ 2\theta$ . The initial DSC data presented showing no amylopectin melting transitions supports the hypothesis that it is more likely to be attributed to amylose-lipid crystals than amylopectin. However, with no clear endothermic melting transition for the amylose-lipid complexes in excess of 100 °C, as often seen in literature,

final conclusions on the lipid complexes cannot be made within the scope of the project (Finkenstadt *et al.*, 2016; Cieřla and Eliasson, 2007).

#### 4.4 Conclusions

The molecular structure of maize grits is significantly damaged during processing, particularly in a high-shear, directly expanded process. Hence, the material following milling has complete loss of granular integrity and high absorption and solubility capacity in the presence of water. Upon shearing in excess water, measured peak viscosity and final viscosity were significantly lower for IP1 than native maize grits; suggested to be driven by the loss of granular integrity and macromolecular depolymerisation during extrusion.

Cereal starches are associated with lipids thus, following extrusion; there is thought to be formation of amylose-lipid complexes detected by peaks in XRPD analysis. However, melting of these amylose-lipid complexes were not detected in complementary DSC measurements.

Taking the material characterisation of IP1 into consideration and comparing this with the typical material properties of the CP and DP of intermediates, it is hypothesised that the starch within IP1 will function as the glue between the dispersed protein and cellular material, following intermediate product manufacture (van der Sman and Broeze, 2013). As a result, and as intended, IP1 is likely to provide a controlled bulk CP which can be manipulated to achieve a design-led approach to the final product microstructure.

## **Chapter 5 Results: Twin-screw extrusion of IP1 with intermediate and final product characterisation**

### **5.1 Introduction**

Following material characterisation of IP1, the milled material was manufactured into intermediates. Initially, a bench-top scale pasta maker was used to create dough using a low shear and temperature process with the aim of preventing further starch conversion of IP1. However, due to the limited temperature control and pressure within the system, uniform intermediate product manufacture was unsuccessful; with much of the IP1 dough blocking the die head. Hence, manufacture was moved to a pilot scale twin screw extruder. An increase in barrel temperature often drives a reduction in dough viscosity; therefore it was expected for extrusion to facilitate formation of processable dough. Additionally, twin-screw extruders can reach significantly higher pressures, enabling the dough to be pushed out of the die preventing blockages.

To compare the intermediates manufactured from pre-processed maize grits (IP1), native maize grits were fed through the extruder at the same processing conditions to manufacture preserved starch intermediates notated as intermediate product 4 (IP4) (refer to Figure 13). IP1 was processed using 2 separate dough water contents to render intermediates at lower (40 %) and higher (55 %) water, notated as IP2 40 and IP2 55 respectively. IP4 corresponds to intermediates manufactured from native maize grits but with same processing conditions as IP2 40.

The following results characterise and compare the expansion properties and microstructure of final products after frying (FP2 40, FP2 55 and FP4). Similarly, the results also characterise and compare

the molecular properties of corresponding intermediates IP2 40, IP2 55 and IP4 (amorphous vs. semi-crystalline) in an attempt to begin to link the expansion of intermediates to their molecular properties prior to frying.

## 5.2 Materials and Methods

### 5.2.1 Materials

Yellow YG560 maize grits (Whitworth Bros. Ltd., Worksop) (11.60% water dwb) were used to manufacture IP4.

Milled pre-gelatinised IP1 manufactured initially from Yellow YG560 maize grits (Whitworth Bros. Ltd., Worksop) was also utilised in intermediate product manufacture of IP2 40 and IP2 55 (for process refer to Chapter 3).

### 5.2.2 Processing Methods

#### 5.2.2.1 *Twin-Screw extrusion*

Manufacture of IP2 40, IP2 55 and IP4 was carried out using a 24 MC barrel co-rotating twin-screw, intermeshing extruder (ThermoFisher; Germany) with standard conveying low-shear screw profiles at a pitch ratio of 1:1. A rectangular die head was used with the dimensions of 1.5 mm x 3 mm. Screw speed was set to 250 rpm and initially the feeding rate was 9 kg/hr. Due to the low density of IP1, the solids feed rate was in fact lower than the set feeding rate and as a result a catch test was

used to validate the solids feed rate and adjust the water feed rate accordingly. The actual solids feed rate and additional extruder variables are detailed in Table 9.

**Table 9. Twin-screw extrusion parameters for IP4, IP2 at 40 % and 55 % barrel water content.**

Sample Name	Raw material moisture (dwb)(%)	Density (g/ml)	Die Temp (°C)	Torque (Nm)	Zone 2 Temp (°C)	Zone 3 Temp (°C)	Zone 4 Temp (°C)	Zone 5 Temp (°C)	Zone 6 Temp (°C)	Zone 7 Temp (°C)	Zone 8 Temp (°C)	Zone 9 Temp (°C)	Zone 10 Temp (°C)	Pressure (bar)	Solids Feed rate (kg/hr)	Water feed rate (ml/min)	Calculated Moisture (dwb) (%)
IP4	11.6	0.68	89	17	81	73	90	119	139	110	97	87	87	1	9	36	40
IP2 40	10.8	0.14	92	18	84	98	101	119	140	120	100	80	89	1	8	33	40
IP2 55	8.6	0.14	66	35	27	31	38	47	53	59	65	70	72	0	6	42	55

### 5.2.2.2 Drying

To prevent cracking or over-drying of intermediates, samples were left to air dry for 18 hours at 25 °C. Following drying, samples were stored in plastic sealed bags at room temperature and water contents were tested using a TGA to confirm intermediates were in the range of 10 to 13 % water.

### 5.2.2.3 Frying

Samples were fried at 195 °C until intermediates were at maximum expansion; ranging from 10 to 80 seconds in a 3 litre Magimix 350 fryer with sunflower oil (Table 10). An explanation for the different frying times is provided in Section 5.3.1.

**Table 10. Frying temperatures and times of intermediate products to expand into final products**

Sample Name	Temperature (°C)	Time (seconds)
IP4	195	31
IP2 40	195	45
IP2 55	195	80

### 5.2.3 Analytical Methods

The specific details of the analytical methods used in Chapter 5 can be found in Chapter 3. The following methods were used to characterise intermediate and final product molecular and microstructure properties:

- Expansion Ratio (ER)
- Confocal Light microscopy
- Scanning Electron Microscopy (SEM)
- Dynamic Mechanical Thermal Analysis (DMTA)
- Differential Scanning Calorimetry (Hydrated and Dry) (DSC)
- Thermogravimetric Analysis (TGA)
- X-Ray Powder Diffraction (XRPD)
- Rapid Visco Analysis (RVA)
- Light Microscopy
- Statistical Analysis (two-factor ANOVA with a Tukey Post Hoc Multiple Comparison test Figure 25 and 34, Excel T-Test Table 11)

## 5.3 Results and Discussion

### 5.3.1 Processing Observations

The pre-processing of IP1 prior to manufacture into intermediates enabled expansion of the melt on exit of the die (Figure 22 A). The expansion was most likely driven by the low shear viscosity of the material that favoured direct expansion, compared with native maize grits (Padmanabhan and Bhattacharya, 1991; Chanvrier *et al.*, 2015). As direct expansion was not desired, the water feed rate was increased to reduce die pressure and prevent this from occurring (Kokini and Moraru, 2003; Kokini *et al.*, 1992). 40 % barrel water content was identified as the most stable; where barrel pressure reduced to 1 bar preventing expansion (Table 9). However, at 40 % barrel water content, browning of the material on exit was still observed suggesting further macromolecular depolymerisation of the starch as a result of severe processing (Kirby *et al.*, 1988) (Figure 22 B).

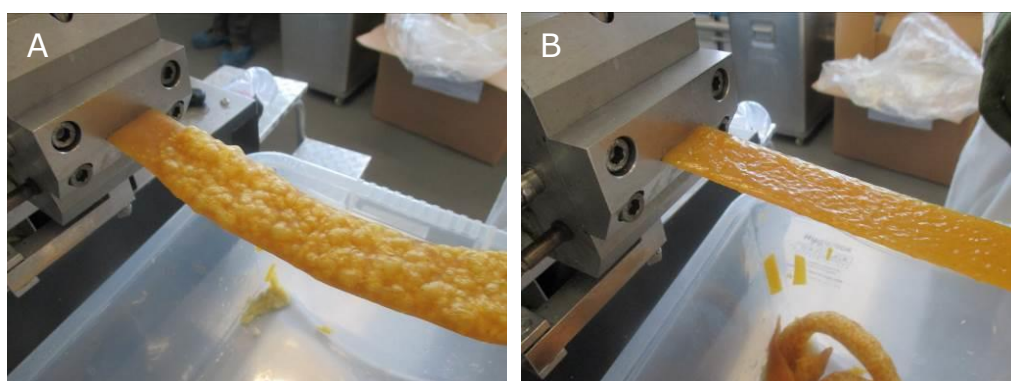


**Figure 22. Photos demonstrating (A) expansion of IP1 melt on exit of the extruder at water contents <30 %, (B) Browning of melt at 40 % water content (IP2 40).**

To reduce the observed mechanical and thermal damage during processing; barrel water content was increased to 55 %, with the assumption being that an increase in water content would reduce

the viscosity of the melt. This was expected to reduce the shear between the barrel screws, directly reducing generation of temperature and mechanical energy. Due to the high dough water content, a vacuum was used at the die head to remove water and prevent die swell on exit. Therefore, pressure was recorded as 0 bar (Table 9). Finally, the melt on exit of the die was a very pale yellow compared to dark brown; suggesting a reduction in depolymerisation of starch (Figure 23).



**Figure 23. Photo depicting pale yellow melt of IP2 55.**

The die dimension measured 1 mm thickness; however the dough on exit of the extruder had an average thickness of  $2.6 \pm 0.34$  mm with intermediates extruded at 55 % reaching as high as 3.7 mm. It is thought this was a result of “die swell” on exit of the extruder, even with the vacuum, attributed to the elasticity of the pre-gelatinised material driving partial recovery on exit (Fan, 1994; Ofoli *et al.*, 1993). Thus, intermediates had to be fried for significantly longer than industrial intermediates (10 - 15 seconds) to enable heat transfer into the centre of the product and reach  $T_g$  to enable expansion (Table 10).

To aid the reader in understanding the transformations of which the material has passed during the two extrusion processes, a state diagram relating to the work presented in Section 2.5.2 by van der Sman (2016), has been developed specifically for FP2 40. Figure 24 adapts the  $T_g$  and  $T_m$  of maize grits presented by Riaz (2002) to characterise how the native maize grits have transitioned through the primary extrusion process into IP1 (red), through to utilisation into the secondary extrusion process rendering intermediates IP2 40 (dark blue), to the in-direct expansion of IP2 40 into FP2 40 (light blue). The extremes of both extrusion processes, which were likely to exceed both the  $T_g$  and  $T_m$  of the native starch granules (not taking into consideration the significant mechanical damage), continue to explain the material properties of IP1 and begin to explain the characteristics witnessed in Chapter 5 of intermediates and final products that have been subjected to the secondary extrusion process.

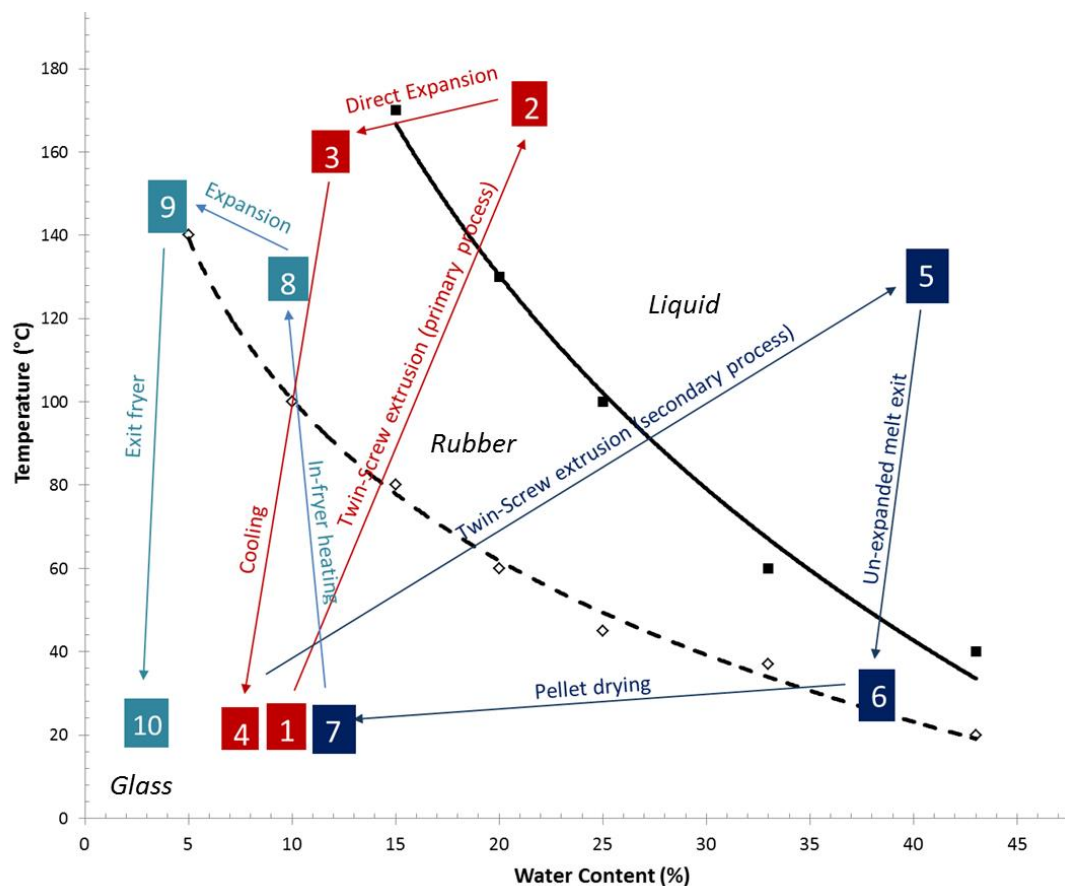
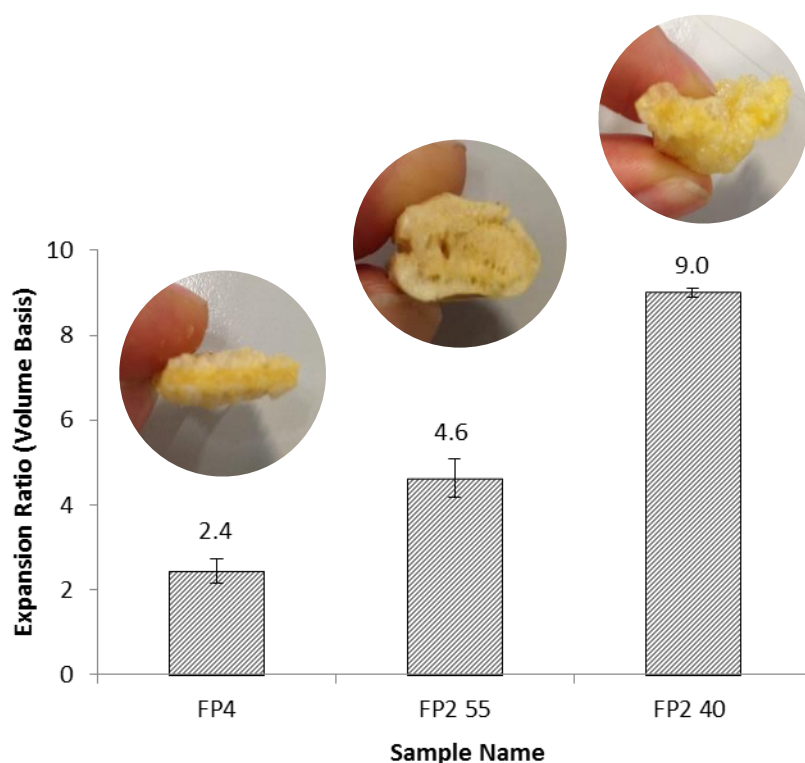


Figure 24. State diagram of the pathway of transitions. Colours correspond to individual processes and numbers indicate the steps within that process from native maize grits through to IP3 (red), into the manufacture of IP2 40 (dark blue) and the expansion of IP2 40 into FP2 40 (light blue) relative to water content (%) and temperature (°C). The ---- $T_g$  and ——— $T_m$  have been adapted from Riaz (2002).

### 5.3.2 Expansion properties of twin-screw extruded intermediates

Following frying of intermediates (Table 10), there were statistically significant differences in ER's between the 3 different final products ( $P < 0.05$ ) (Figure 25). For the final product of IP2 55 (FP2 55) anisotropic expansion occurred; hypothesised to be a result of case hardening upon air drying of the high water intermediate, which caused a water gradient within the intermediate product. Case hardening is thought to change bubble nucleation and growth on the intermediate surface as a result of less water; as demonstrated in Figure 26 B (Emerson *et al.*, 2011; Norton *et al.*, 2011). Similarly, intermediate thickness, as observed during processing, is likely to influence heat transfer mechanisms during frying, resulting in an extended frying time as well as a greater final product size attributed to a larger total mass.



**Figure 25.** Average expansion ratio (volume basis)  $\pm$  standard deviation based on 5 replicates of FP4, FP2 55 and FP2 40. All final product expansions are statically significantly different ( $P < 0.05$ ). Pictures show cross-sectional expansion of corresponding samples.

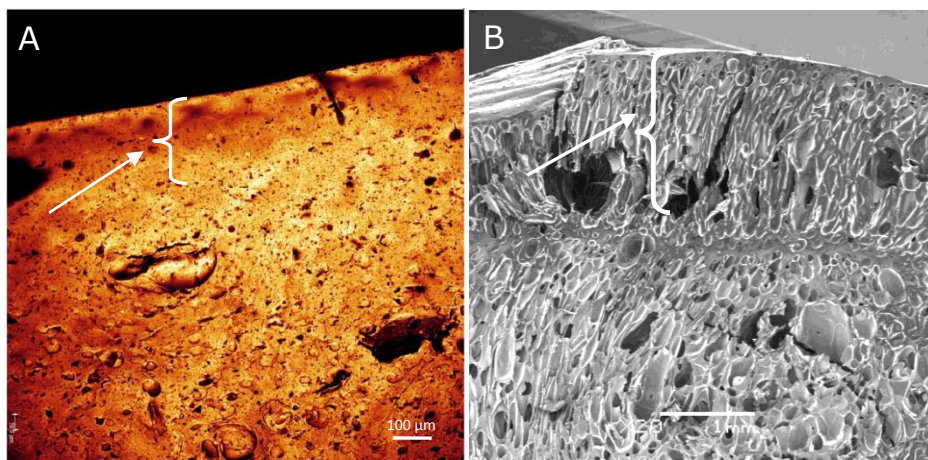


**Figure 26. (A) Confocal light micrograph of IP2 55 intermediate cross-section (scale bar = 100  $\mu\text{m}$ ) (B) Scanning electron micrograph of FP2 55 cross section (scale bar = 1 mm). Arrows indicate case hardening effect of air drying at high water content.**

The greatest difference in ER was found between the final product of IP2 40 (FP2 40) and final product of IP4 (FP4) (Figure 25). These final products were extruded at the same in-barrel water content and therefore differences were likely to be a result of differences in starting materials with FP2 40 being manufactured from amorphous non-granular starch and FP4 from semi-crystalline native starch. As previously described, loss of granular integrity during processing influences the ratio of CP:DP and has a linear relationship with expansion rate (van der Sman and Broeze, 2013). Therefore, it is hypothesised as a result of differences in the state of the starch prior to manufacture that the CP:DP in intermediates is significantly different. From initial micrographs of FP4, the retention of granular starch following frying is demonstrated (Figure 27). Additionally, large intact sections of the alerone layer, which are associated with the intact endosperm of maize, were only found in micrographs of FP4 and not FP2 40 or 55; confirming the CP:DP to be greater for that of IP2 intermediates than IP4.

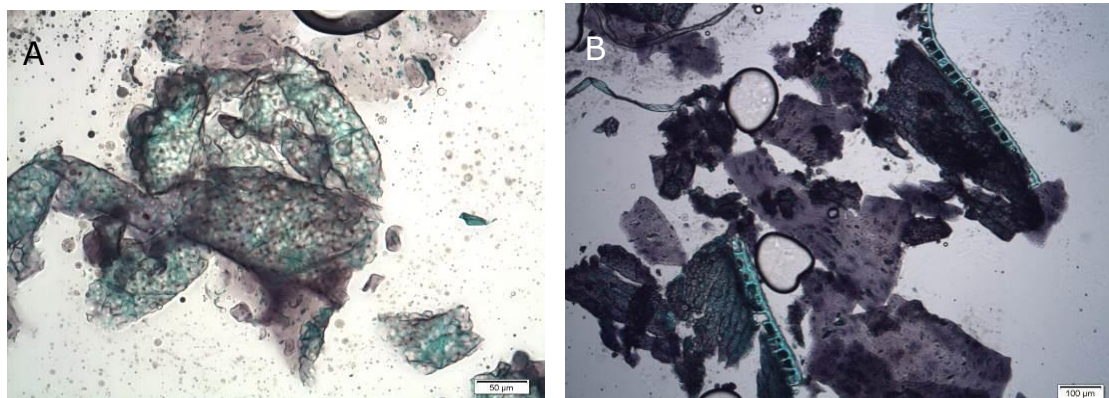


**Figure 27. Light microscopy with iodine and fast green staining of FP4. (A) Native starch granules surrounded by protein matrix (green), (B) Alerone layer associated with endosperm.**

### 5.3.3 Microstructure of twin-screw extruded intermediates

To identify the fundamental drivers in differences in expansion between intermediates; IP4, IP2 40 and IP2 55 were microtomed and examined under light microscopy to assess qualitatively the differences in CP:DP.

Figure 28 displays the micrographs of intermediates, where on a microstructure level no clear differences were observed between IP2 40 and IP2 55 (Figure 28 A and C). The figures demonstrate how for both the majority of starch is within the CP, with fine particulates of protein, fibre and fat sitting distributed throughout the amorphous starch matrix. In Figure 29 A, the interfacial association of fibre and protein particulates with the starch matrix is demonstrated in more detail. Here, the fibre seems to be entangled in large chains surrounding aggregated protein; where the fibre appears to have a greater affinity for the continuous starch matrix, than the protein. Similar results have been seen with protein aggregation amongst a starch matrix illustrated in confocal

microscopy by Chanvrier *et al.* (2015). Figure 29 B suggests much of the same for the IP2 55 with the protein and fibre sitting within the starch matrix as an entangled filler particle.

For IP4, micrographs demonstrate similar findings to FP4 with a large proportion granular starch sitting within the amorphous starch matrix, which suggests to function as part of the DP (Figure 28 E). Compared to IP2 40 and 55, the protein appears to be less evenly distributed with aggregation and larger intact protein matrices surrounding the starch granules (Figure 28 F).

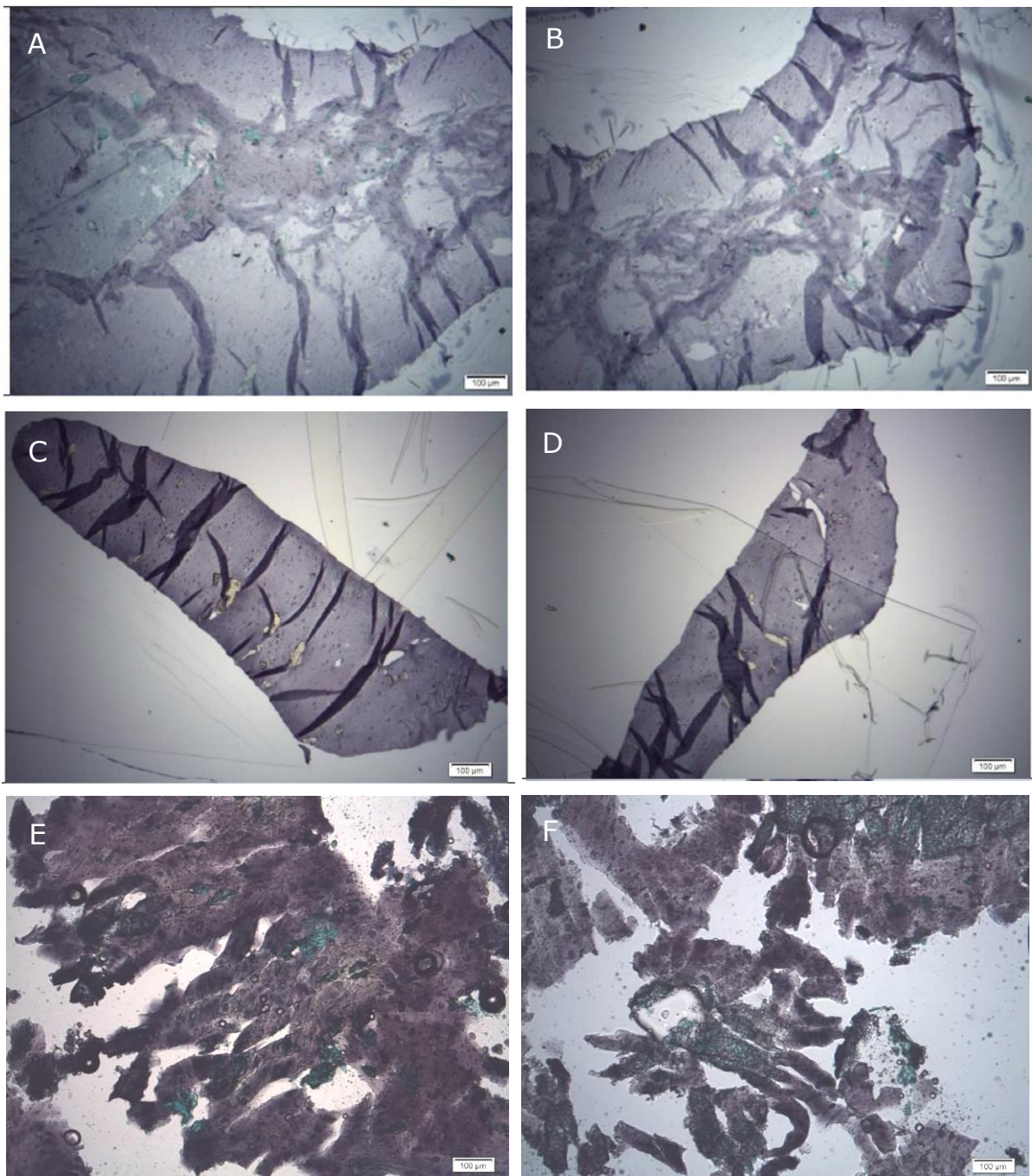


**Figure 28. Light microscopy of microtomed intermediates following iodine staining. (A & B) IP2 40, (C & D) IP2 55 and (E & F) IP4. Fibre = light green, protein = yellow, fat = dark brown. Scale bar= 100 µm.**

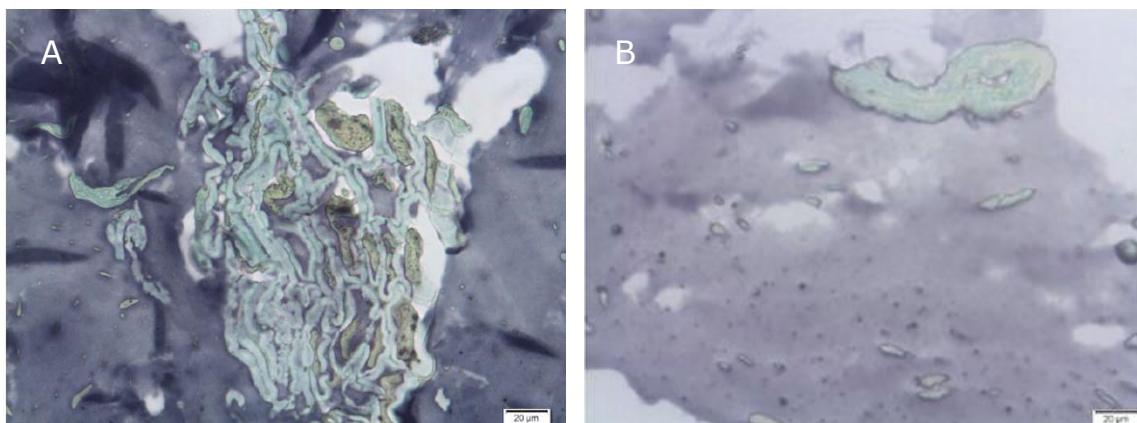


**Figure 29. Light microscopy with iodine and fast green staining of intermediates (A) IP2 40 and (B) IP2 55. Scale bar = 20 µm.**

From the results presented, it is clear that two extrusion processes impact not only the proportion of CP:DP but also the size and distribution of non-starch components throughout the starch matrix; with protein in IP4 reaching particulate diameters in excess of 400 µm, compared with IP2 ranging from 1 µm up to 100 µm. However, micrographs were not able to detect clear differences between IP2 40 and IP2 55, which suggested a CP heavy intermediate dominated by a smooth amorphous matrix for both. This is interesting as intermediates had significantly different processing conditions and as demonstrated in Figure 25; final products with very different expansion. As a result, the CP:DP is not the only driver in expansion and therefore further characterisation to a molecular level is required to continue to identify the additional drivers for differences in expansion of all intermediates; aiding the identification of the most useful analytical tools.

### 5.3.4 Molecular properties of twin-screw extruded intermediates

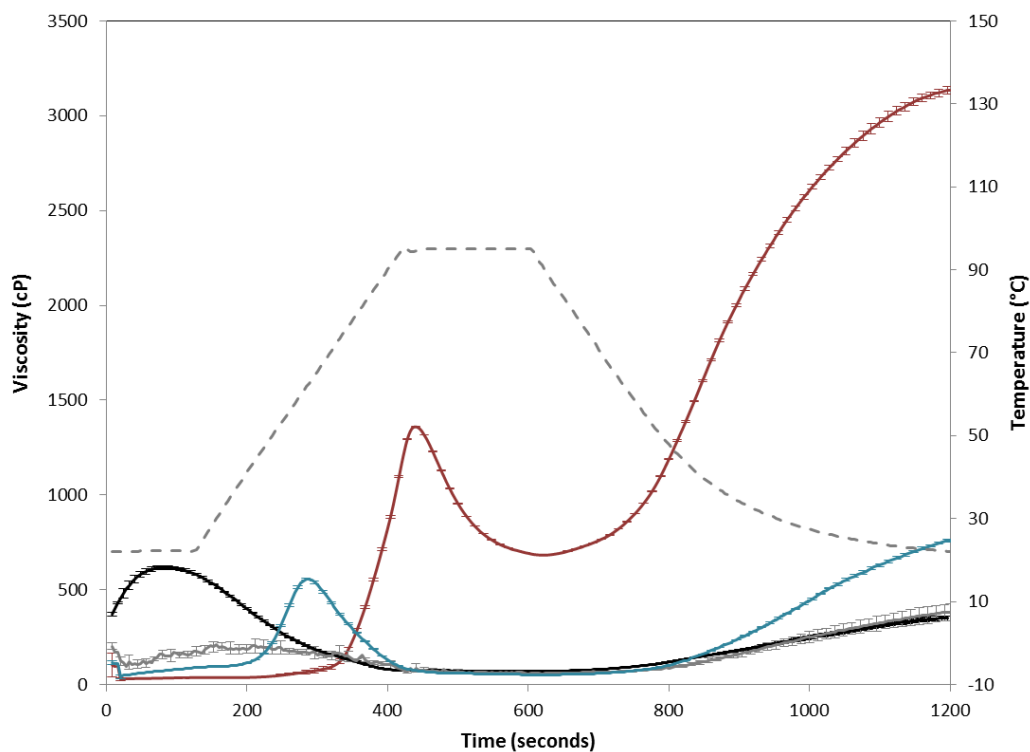
Intermediates were characterised on a molecular level to build an understanding of the impact of changes in processing on the state of the starch; linking intermediate molecular characterisation to expansion. Further description of methods and information to interpret results are presented in Section 2.2.2.

Figure 30 shows the RVA traces for IP2 40, IP2 55 and IP4 following milling, where clear differences can be found in pasting temperature, peak viscosity and final viscosity. The initial material utilised in intermediates (IP1) is also presented to facilitate interpretation and discussion. Both IP1 and IP2 40 have a cold swelling peak but with a significant reduction in peak viscosity of IP2 40; thought to be a result of further starch conversion during the second extrusion process following granular breakdown (Alcázar-Alay and Meireles, 2015). IP2 40 also resulted in a relatively noisy trace which was attributed to aggregation and clumping of the dispersion during the measurement.

Peak viscosity of IP2 55 was ca. 20 °C higher than temperatures of IP1 and IP2 40, indicative of starch re-crystallisation; confirmed later by DSC and XRPD. It was thought the high water content dough, when left to dry at room temperature, induced re-crystallisation of starch; termed as retrogradation.

Retrogradation occurs between the  $T_g$  and  $T_m$  of a polymer (Figure 8) therefore, in van der Sman's (2016) state diagram of starch at 25 °C, the time before the  $T_g$  of intermediates will be mostly dependent on the initial water content (although water holding capacity and water mobility may play some role). The impact of dough water content alone on retrogradation prior to  $T_g$  is demonstrated in Figure 31. As a result of retrogradation, a temperature of 80 °C is required to disrupt the hydrogen bonding within the crystalline regions and trigger onset of pasting. Preferential

retrogradation in IP2 55 is further supported by the greater increase in final viscosity; which could be attributed to retrograded amylose which would have been unlikely to melt out during the RVA measurement (Fredriksson *et al.*, 1998).



**Figure 30. Average viscosity (cP) ± standard deviation with respect to time and temperature. — IP1, — IP2 40, — IP2 55, — IP4 and - - - Temperature. Error bars are based on 5 replicates.**

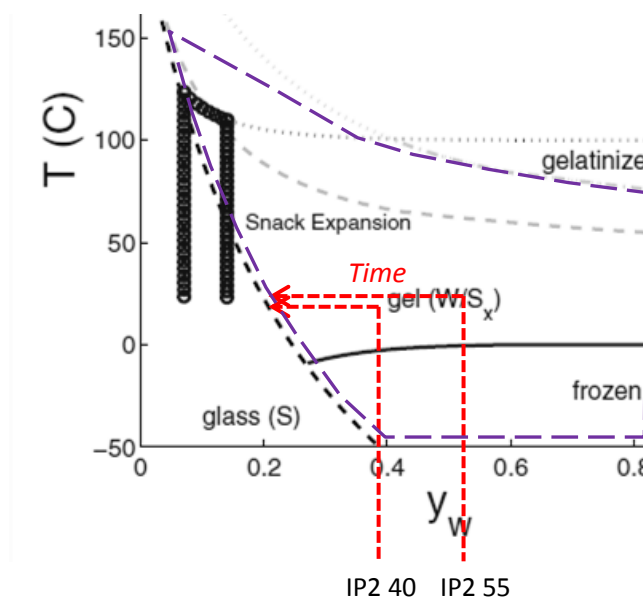


**Figure 31.** State diagram of starch. Black dotted line represents  $T_g$  with respect to water content and temperature. Red dotted lines demonstrate the influence of intermediate dough water content on time to  $T_g$  during air drying at 25 °C. Purple box highlights area in which retrogradation can occur (adapted from van der Sman, 2016).

IP4, similar to that of IP2 55, shows a peak viscosity at 95 °C and a significant increase in final viscosity (Figure 30). The shift in peak is thought to be a result of the higher gelatinisation temperature of A-type native starch. The peak viscosity and final viscosity of IP4 also suggest remaining granular starch in the intermediates. However, when compared with native maize grits, a reduction in peak viscosity by 2000 cP and final viscosity by 5000 cP is observed; likely to be a result of some starch conversion during extrusion (Table 8).

Hydrated DSC thermographs of intermediates are displayed in Figure 32, where small endothermic peaks (when compared to Figure 21) are observed, likely to be a result of the majority of the intermediate being amorphous. IP2 40 was confirmed to be amorphous with no endothermic peak in thermographs. Conversely, IP2 55 was found to have an endothermic peak of  $1.24 \pm 0.13$  J/g between

45 and 62 °C which corresponds to the melting temperature of retrograded B-type amylopectin; melting at a lower temperature than native cereal starch (Wang *et al.*, 2015; Fu *et al.*, 2013). IP4, which retained granular integrity had an endothermic peak at 80 °C of  $3.77 \pm 2.25$  J/g; associated with the loss of A-type amylopectin order in maize starch. However, when compared with raw maize, an 8.3 J/g reduction in enthalpy was observed; supporting the assumption that a decrease in viscosity was attributed to starch conversion of the native starch granules (Pushpadassa *et al.*, 2009) (Figure 21).

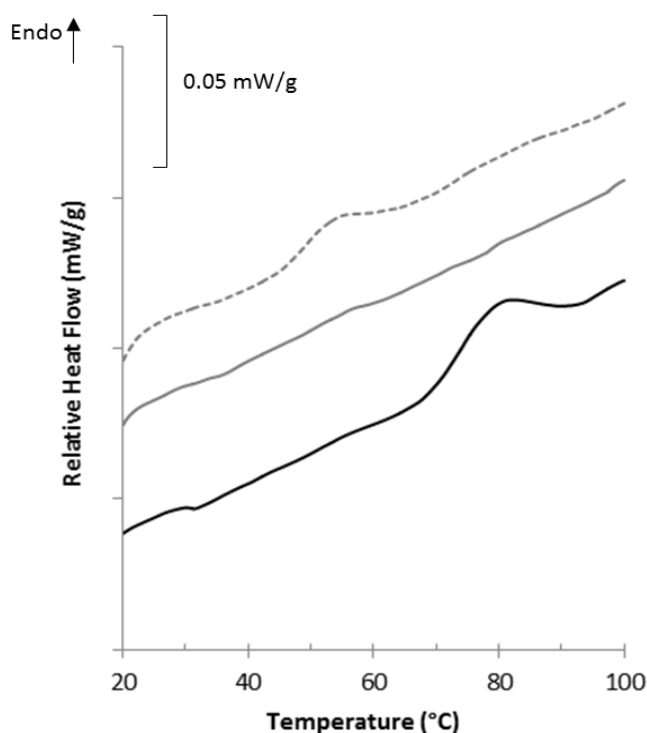


Figure 32. Relative heat flow (mW/g) of intermediate-products during DSC measurements in excess water. — IP4, — IP2 40 and ..... IP2 55. For ease of interpretation IP4 has been offset by +0.03 mW/g and IP2 55 by -0.03 mW/g. Heating rate 5 °C/min.

Relating Figure 24 to the DSC of IP4, which went through the second extrusion process (stages 3, 4, 5 and 6); it would be expected for all native crystalline amylopectin to have melted as the processing conditions exceeded the melting temperature at 40 % water content. The retention of crystalline amylopectin can be explained by local water content (%), which could differ throughout the melt if inhomogeneous during extrusion. Therefore, lower local water content (%) would increase the melting temperature in excess of the extruder barrel temperature (<20 %), retaining crystalline amylopectin into the intermediate.

Results from XRPD analysis found all intermediates to have a peak at  $19.75^\circ$  and  $12.95^\circ 2\theta$ ; relating to B-type amylopectin polymorphs and amylose-lipid complexes, respectively (Figure 33). This finding echoes literature of low water content (15 – 30 % wwb) starch based systems measured by XRPD following storage (Enrione *et al.*, 2012; Mihhalevski *et al.*, 2012). Comparably, IP1, IP2 40 and IP2 55 show loss of A-type crystalline polymorphs as a result of severe processing. Similarly to DSC, all intermediate traces have a dominant amorphous ‘halo’ which is associated with the majority of the intermediates being amorphous.

For IP4, as demonstrated in RVA and DSC, there is retention of A-type polymorphs corresponding to the peaks at  $18.20^\circ$  and  $23.12^\circ 2\theta$ ; associated with remaining native maize starch. As a result, IP4 appears to have a combination of both A-type and B-type starch, referred to in literature as C-type (Wang *et al.*, 2015).

Detection of B-type polymorphs supports previous DSC conclusions of retrograded IP2 55 as a result of high water intermediates. However, it also suggests retrogradation of IP2 40 and IP4, as B-type polymorphs are not present in native cereal starch; which was not apparent in DSC thermographs. It

is thought this could be a result of differences in the degree to which the starch is retrograded, with XRPD being significantly more sensitive to detecting crystal polymorphs.

One thing to note is that previously published data suggests water content and temperature conditions primarily determine the preferred crystal polymorph, with water contents in excess of >43 % promoting B-type crystals and <29 % promoting A-type crystals (Mihhalevski *et al.*, 2012). Consequently, it would be expected for IP2 40 and 55, which sit either side of the critical water content of 43 %, to have differences in XRPD traces. On closer inspection, it could be suggested for IP2 40 that the peak at  $18.20^\circ 2\theta$  appears more prominent, aligning with the peak in native maize starch. However, with the noisy trace making it difficult for interpretation and DSC thermographs showing no endothermic peak at higher temperatures; final conclusions could not be made on the influence of water on the preferential crystal polymorph formed during retrogradation.

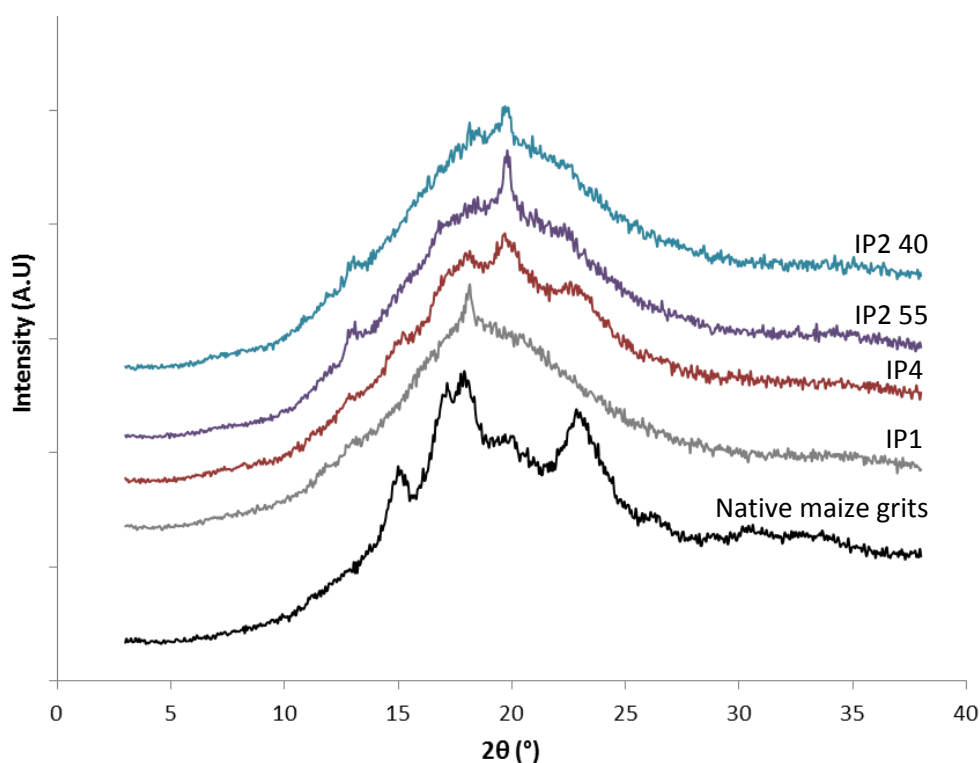


Figure 33. XRPD of — Native maize grits, — IP1, — IP4, — IP2 55, — IP2 40. Numbers correspond to peak  $2\theta$  (°) positions of extruded intermediate products.

### 5.3.4.1 Bulk viscoelastic properties of intermediate products

Bulk viscoelasticity of intermediates was analysed using DMTA to understand if the differences in molecular structure of starch altered viscoelastic properties; partly explaining the differences in expansion. Due to IP2 55 resulting in case-hardening and consequently differences in expansion mechanisms between the centre and surface of intermediates, it was concluded this could impact the measured viscoelastic properties. Therefore, IP2 55 was not analysed and the results presented correspond to IP2 40 and IP4 only.

Figure 34 displays the viscoelastic properties of intermediates between -20 °C to 200 °C at a heating rate of 5 °C/min and at 3 frequencies: 0.3, 1 and 10 Hz. Figure 34 A and B simplify the data by displaying storage modulus ( $E'$ ) and  $\tan \delta$  ( $E''/E'$ ) of IP2 40 and IP4 as a function of temperature at 1 Hz only (See Appendix 3 for Loss Modulus ( $E''$ )). In Figure 34 C, mid- $T_g$  calculated mechanically from the temperature at which peak  $\tan \delta$  occurred, is compared at three frequencies 0.3, 1 and 10 Hz for both IP2 40 and IP4. To compare  $E'$  of these intermediates within the same physical state from Figure 34 A, the  $E'$  at  $T_g + 30$  °C, following normalisation of data ( $E'/E'$  at 30 °C) is presented (Figure 34 D). In literature,  $E'(T_g + 30 \text{ °C}) / (E' \text{ at } 30 \text{ °C})$  of starch melts has been correlated with elongational viscosity (Chanvrier *et al.*, 2015) (refer to Section 2.5.2.3 for more detail). Figure 34 D also presents  $E'$  as a function of frequency to show the frequency dependency of the material. Here, increases in oscillation from 0.3 to 10 Hz drove the product to appear more elastic. This finding is in agreement with literature, such that at higher frequencies the relative motion between molecular chains is restricted, allowing a greater deformation energy to be stored; increasing  $E'$  (Ditudompo *et al.*, 2013; Babin *et al.*, 2007).

In Figure 34 A, the drop in  $E'$  at ca. 60 °C is associated with the onset of  $T_g$ . The continued drop in  $E'$  following  $T_g$  is a result of an increase in temperature which drives the intermediate into a more viscous-like state reducing stored energy. The peak  $\tan \delta$  (mid- $T_g$ ) of all maize samples were reported between 88 and 112 °C which aligns with the state diagram of maize grits published by Riaz (2002) (Figure 24 and 34 C).

The increase in  $E'$  at 130 °C is thought to be a result of water loss during the measurement which directly influences the rheological properties of the sample, preventing the rubbery plateau to be achieved (Chanvrier *et al.*, 2006). In literature, the loss of water is reported to be greater following  $T_g$  onset and therefore greatest water loss is likely to occur after 52 °C (Brent *et al.*, 1997). To validate this, a grease layer was spread on IP4 to retain water within the sample during the measurement (Figure 34 A and B). The grease layer retained water at  $T > T_g$  onset; reducing the storage modulus and increasing  $\tan \delta$  as a result of plasticisation. Similarly, IP2 40 and IP4 (after the addition of a grease layer), expanded within the clamp during measurements; thought to be the driver of the large error bars following 130 °C of  $\tan \delta$  (Figure 34 B).

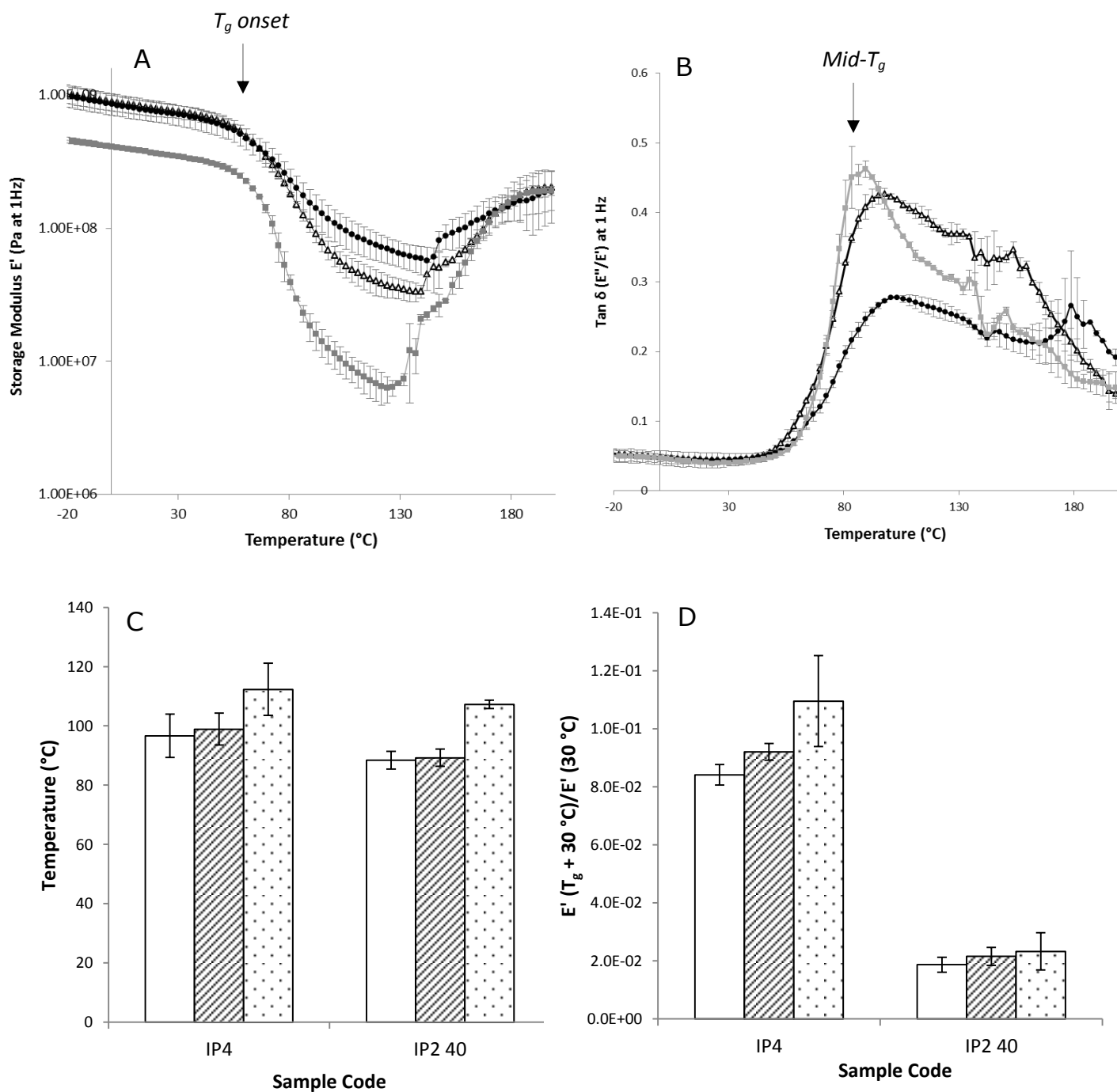


Figure 34. (A & B) Storage modulus ( $E'$ ) and  $\tan \delta (E''/E')$  vs. temperature ( $^{\circ}\text{C}$ ) of whole intermediates at 1 Hz frequency. ●●● IP4, ▲▲▲ IP4 + grease ■■■ IP2 40. (C) Peak  $\tan \delta (T_g)$  of IP4 and IP2 40 at □ 0.3 Hz, ▨ 1 Hz and ▩ 10 Hz. (D)  $E' (T_g + 30 \text{ }^{\circ}\text{C})/E' (30 \text{ }^{\circ}\text{C})$  of IP4 and IP2 40 at □ 0.3 Hz, ▨ 1 Hz and ▩ 10 Hz. Heating rate 5  $^{\circ}\text{C}/\text{min}$ .

When comparing  $E'$  during heating of intermediates at the same starting water content; significant differences were apparent in both glassy and rubber states of IP2 40 and IP4 (Figure 34 A). These differences were statically significantly different when comparing data points at the same physical state following normalisation ( $P < 0.001$ ) (Figure 34 D).

The differences presented in Figure 34 D could begin to partly explain differences in ERs of intermediates upon frying where a lower  $E'$  at  $T > T_g$  would be expected to promote bubble growth. However, other factors such as local bubble wall viscoelasticity will influence not only bubble expansion but bubble collapse and coalescence. Therefore, although DMTA gives an insight into the bulk viscoelastic properties of intermediates, it cannot be assumed that this is indicative of the properties during frying due to the differences in heating rate. Similarly, it is not a measurement of the viscoelasticity at the bubble wall.

Interestingly, when comparing  $T_g$  onset and mid- $T_g$  at the same frequency there were no statistically significant differences between intermediates ( $P > 0.05$ ) (Figure 34 A and C). Irrespective of  $T_g$ , the differences in  $E'$  of IP2 40 and IP4 could be a result of a number of inter-related factors which are further detailed below.

- 1) Molecular weight differences between samples
- 2) Amorphicity differences between the samples
- 3) The influence of DP to CP matrix interfacial adhesion
- 4) The AM:AP ratio of the matrix
- 5) Water retention differences between samples at  $T > T_g$  onset

Regarding point 1) the differences in molecular weight of the starch within the intermediate prior to analysis could be interpreted from Figure 30. Here, significant differences in the final viscosity of intermediate pastes following heating and cooling in a high moisture system are apparent. This is unsurprising since IP2 40 has gone through a significantly more severe process than IP4 and therefore it is likely the native starch is considerably damaged. Differences in molecular weight is also likely to explain why there are differences in the initial  $E'$  of the sample, prior to heating (Figure 34 A).

For point 2) the amorphicity differences between IP2 40 and IP4 were characterised in Section 5.3.4 where RVA, DSC and XRPD confirmed IP2 40 to have a greater proportion of amorphous material. The influence of amorphicity on viscoelasticity properties of materials is often demonstrated with amorphous and semi-crystalline plastics (Dos Santos *et al.*, 2013), where literature supports the theory that a greater proportion of amorphicity drives a reduction in storage modulus following  $T_g$ . It is thought this is a result of crystalline structures preventing molecular movement through interlinking of chains; rendering solid-like behaviour (Askadskii *et al.*, 2014; Doyle, 2000). For starch, this phenomena has also been demonstrated by Chanvrier *et al.* (2006) whereby an increase in processing temperatures of maize flour drove a decrease in  $E'$ . Similarly to the results reported in Figure 34, irrespective of  $E'$ , the  $T_g$  for all of these samples were reported at  $\sim 94$  °C (Chanvrier *et al.*, 2006).

Relating to point 3) in the case of starch intermediates, the state of the starch granules (intact or ruptured) directly influences the CP:DP (Chanvrier *et al.*, 2013). This is demonstrated in Figure 28 and 33, where the CP:DP is significantly altered with the retention of granular integrity in IP4 compared with IP2 40. Similarly, the size and distribution of the non-starch DP is altered by further processing, with larger cell wall and zein particulates present throughout the starch matrix of IP4.

The influence of zein interfacial adhesion to starch matrices has been addressed by Chanvrier *et al.* (2006), whereby an increase in zein mass within a starch CP increased  $E'$  at a heating rate of 3 °C/min and 0.2 Hz frequency, with the opposite observed for a protein CP and addition of starch. Similarly, an increase in particle content (including fibre, protein and intact starch granules) reduced the  $\tan \delta$  peak amplitude, echoed in Figure 34 B. This was thought to be a consequence of starch-zein or starch-granule interactions whereby, due to weak adhesion in the glassy state, particles weakened the matrix whereas in the rubbery state particles reinforced the material (Habeych *et al.*, 2008). The reinforcement of the intermediate in the rubber phase is supported by micrographs of final products where zein has elongated with the matrix (Figure 35). However, in this case, if particles were to weaken the matrix in the glassy state,  $E'$  would be expected to be lower for IP4 than that of IP2 40 at temperatures below 52 °C (Figure 34 A).

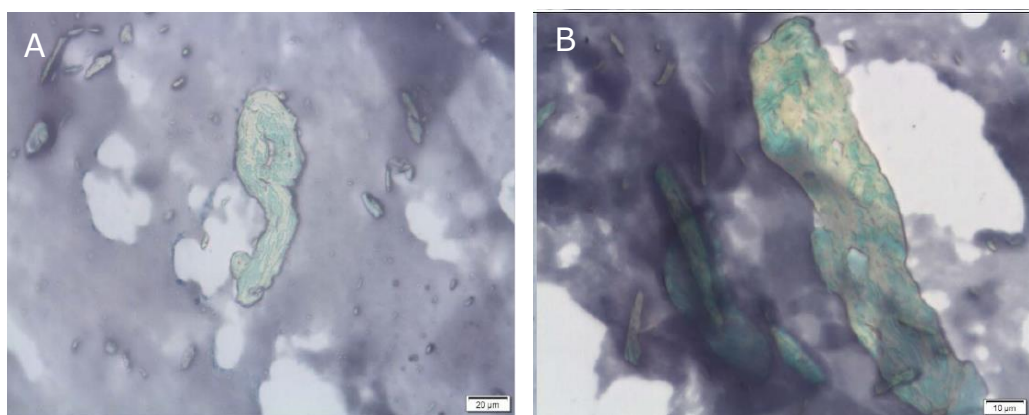


**Figure 35. Light microscopy of final product 4 (FP4) following microtoming. Purple/blue = starch matrix, green= fibre, yellow = protein. (A) Scale bar = 20 µm, (B) scale bar = 10 µm.**

Point 4) relates to the AM:AP which has recently been correlated in literature to viscoelastic properties of native moulded starch (Babin *et al.*, 2007). Here  $E'$  at  $T > T_g$  (137 °C) was found to rank in order of amylose content, such that the greatest amylose content (70 %) was associated with the highest  $E'$  value.

This supports data presented in the review by Kokini and Moraru (2003) where an increase in amylose content was found more commonly to reduce expansion of extrudates. However, the CP amylose content appears to have a binomial distribution, with maximum expansion in the region of 1:1 AM:AP (González *et al.*, 2013; Chinnaswamy and Hanna, 1987). Relating the work by Babin *et al.* (2007) to Figure 34, it would suggest a greater proportion of amylose within the CP of IP4, which is expected since milder processing will prevent loss of crystalline amylopectin.

One thing often not detailed in literature is the state of the starch following processing which even when amorphous, can still alter functionality (Matignon and Tecante, 2017). This is important as high amylose starches have been characterised as more resistant to processing as a result of the presence of lipid at the granule surface. Therefore, intermediates with different native amylose-content starches that have gone through the same process, could be suggested to have differences in the degree of order, granular integrity and retrogradation that directly influences measured  $E'$ ; as reported by González *et al.* (2013) following characterisation by microscopy. One must also consider the impact of where the amylose and amylopectin sit within the CP:DP microstructure. With much of IP4's native semi-crystallinity being retained into the intermediate, one would assume the majority of the CP is associated with leached amylose. For IP2 40, no granular structure remains, suggesting amorphous amylopectin to be sitting within the CP with the amylose.

Finally, point 5) as previously discussed, relates to the inevitable loss of water during DMTA measurements which directly increases  $E'$ . Figure 34 A demonstrates the differences in  $E'$  if water is retained following  $T_g$  through using a barrier. To relate this to frying, van der Sman and Broeze (2013) suggested that an increase in DP could facilitate water escape from the internal matrix during expansion by inducing weak points within the CP; transitioning the expanded product into the glassy

state sooner. Therefore, it could be suggested that the differences in  $E'$  of IP2 40 and IP4 at  $T > T_g$  could be further promoted by differences in water loss during the measurement. The data presented supports this with retention of water using a grease layer influencing  $E'$  of IP4 to be more similar to that of IP2 40 (Figure 34 A). However, it must be considered that the grease layer did not completely prevent water loss with a continued increase in  $E'$  following 130 °C (Kristiawan *et al.*, 2016) (Figure 34 A). In an attempt to eliminate water loss from directly influencing  $E'$ , samples were ground and mounted in aluminium pockets with a sealant. Figure 36 shows the relative  $E'$  (A) and  $\tan \delta$  (B) of pockets containing the powdered IP4 and IP2 40 at particle sizes greater than and less than 1 mm.

On observation, particle size appears to influence the reduction in  $E'$  relative to temperature, with the larger particle size (>1 mm) promoting a more significant drop in  $E'$  following  $T_g$  onset at 40 °C (Figure 36 A). The larger spacing between >1 mm particles could have enabled further movement within the aluminium pocket making the sample appear more mobile, reducing  $E'$ . Therefore suggesting with highly compacted pockets, movement is restricted between particles and consequently  $E'$  appears greater (*repeats presented in Appendix 4*).

When comparing IP2 40 and IP4 for both particle sizes, the differences in  $E'$  are no longer as apparent (Figure 34 vs. 36), with only a slight increase in  $E'$  drop of IP2 40 compared to IP4. Thus, the hypothesis that differences in  $E'$  of intermediates are driven partly by differences in water loss, is supported.

Interestingly, retention of water within starch based systems is often associated with a reduction in  $T_g$ , with as little as an increase in 3 % water content decreasing  $T_g$  onset by up to 20 °C (Ditudompo *et al.*, 2013; Robin *et al.*, 2012). When comparing Figure 36 B with Figure 34 B,  $T_g$  (peak  $\tan \delta$ )

appears to be at higher temperatures. This could be explained by the differences in heat transfer from the enclosed aluminium sealed pockets rather than directly onto the sample.

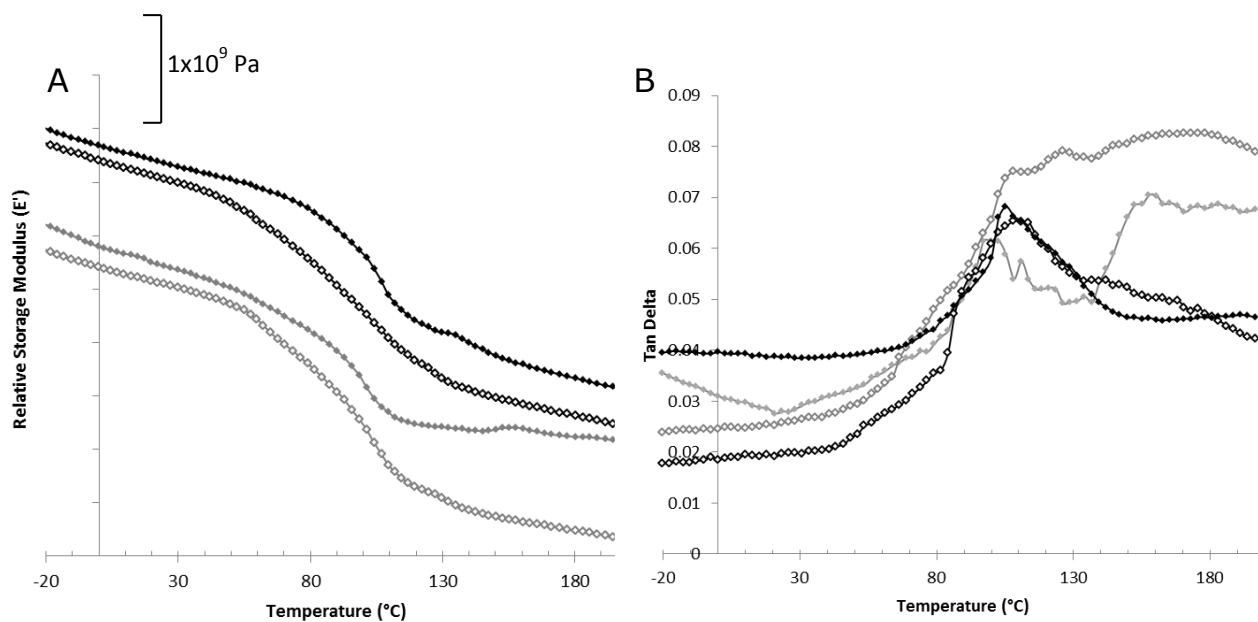


**Figure 36. (A) Relative  $E'$  and (B) Tan  $\delta$  ( $E''/E'$ ) of ground intermediates in aluminium pockets at 1 Hz frequency —◆◆◆ IP4 < 1 mm, —◇◇◇ IP4 > 1 mm, —◆◆◆ IP2 40 < 1 mm and —◇◇◇ IP2 40 > 1 mm. Repeats displayed in Appendix 4.**

In an attempt to correlate  $T_g$  measured mechanically by DMTA with alternative methods, dry DSC of intermediates was carried out at a heating rate of  $10\text{ }^{\circ}\text{C}/\text{min}$ . However, due to the broadness of the  $T_g$  detected by changes in heat flow base line, as often seen in literature, interpretation was subject to bias and therefore has not been presented as part of the formal results (Liu *et al.*, 2009) (see Appendix 5 for thermographs).

### 5.3.5 Water loss mechanisms of intermediate products during heating

To build on discussion point 4) in Section 5.3.4.1, TGA was carried out at both fast and slow heating rates to collect quantitative data on characterising weight loss differences between IP2 40 and IP4 below 250 °C. It is assumed for all following TGA data that weight loss of intermediates is a direct measure of water loss (Neher *et al.*, 1973).

Initial method development identified particles of the same size (1 mm in diameter) but at different weights to have a greater impact on water loss than sample composition. Figure 37 displays weight loss and 1<sup>st</sup> derivate of IP2 40 and IP4 with respect to temperature at a heating rate of 40 °C/min, whereby the greater the sample mass (density), the greater the sudden loss of water at higher temperatures. As a result, all following measurements were taken with samples at 1 mm in diameter and between 6.5 to 7.5 mg in an attempt to minimise the influence of density on water loss.

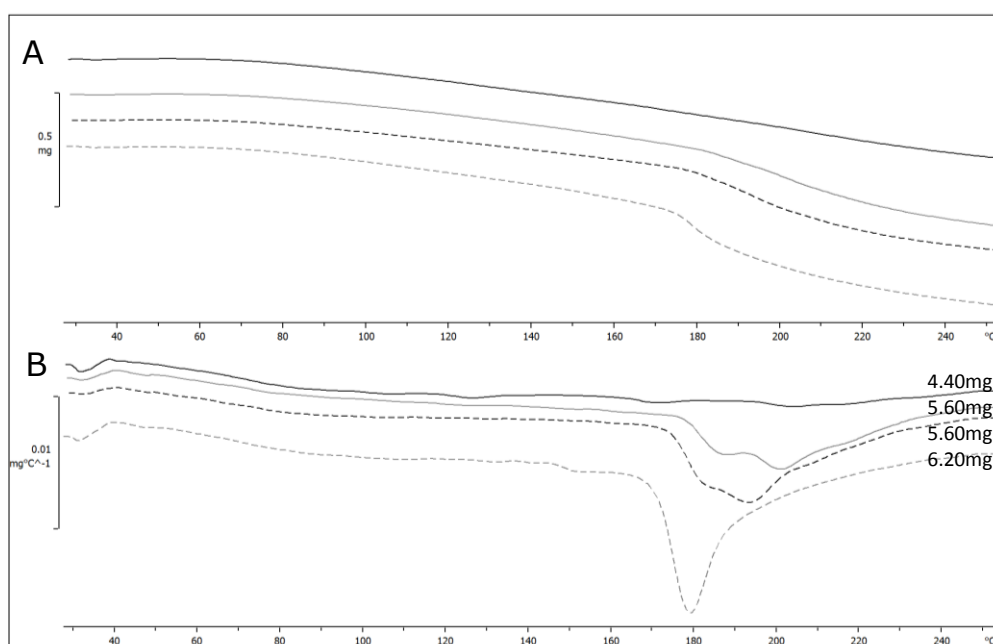


**Figure 37.** Fast rate (40 °C/min) thermo-gravimetric analysis of ground intermediates at ~1 mm in diameter from 25 °C to 250 °C. (A) Weight loss (B) 1<sup>st</sup> derivative. IP4 (black lines), IP2 40 (grey lines).

Figure 38 A shows the water loss and 1<sup>st</sup> derivative with respect to temperature from 25 to 200 °C of IP4 and IP2 40 at 5 °C/min heating rate. The differences in water loss mechanisms are demonstrated with the greatest rate of loss for IP4 between 60 and 80 °C. IP2 40 intermediates however had the greatest loss of water at temperatures in excess of 190 °C, whereby a sudden loss of water was apparent; likely as a result of pressure build up. Exact water loss % between specific temperatures is presented in Table 11. There are two hypotheses as to why the intermediate with a higher proportion of amorphous starch releases water at a higher temperature. Firstly, the crystalline particles within IP4 may aid in creating weak points within the internal structure which would facilitate a path for water to escape at a lower temperature. Similarly, as water will preferentially be absorbed into the amorphous region, a greater proportion of crystalline starch will increase the concentration of water within the amorphous region; directly influencing the samples ability to lose water.

Prior to the measurement, samples were ground to a diameter of 1 mm. Hence, measurements are not representative of whole intermediate samples; where geometry could influence the water release measurements in TGA measurements. Therefore, during DMTA measurements where the whole intermediate products are analysed, differences could be more significant. Similarly, the mechanism of heating is different, which could result in events occurring at slightly different temperatures.

To relate water release mechanisms to the differences seen in expansion following frying, faster heating rates were required. Figure 38 B presents the results of samples heated at a rate of 40 °C/min, expected to give a greater indication into water release mechanisms during frying.

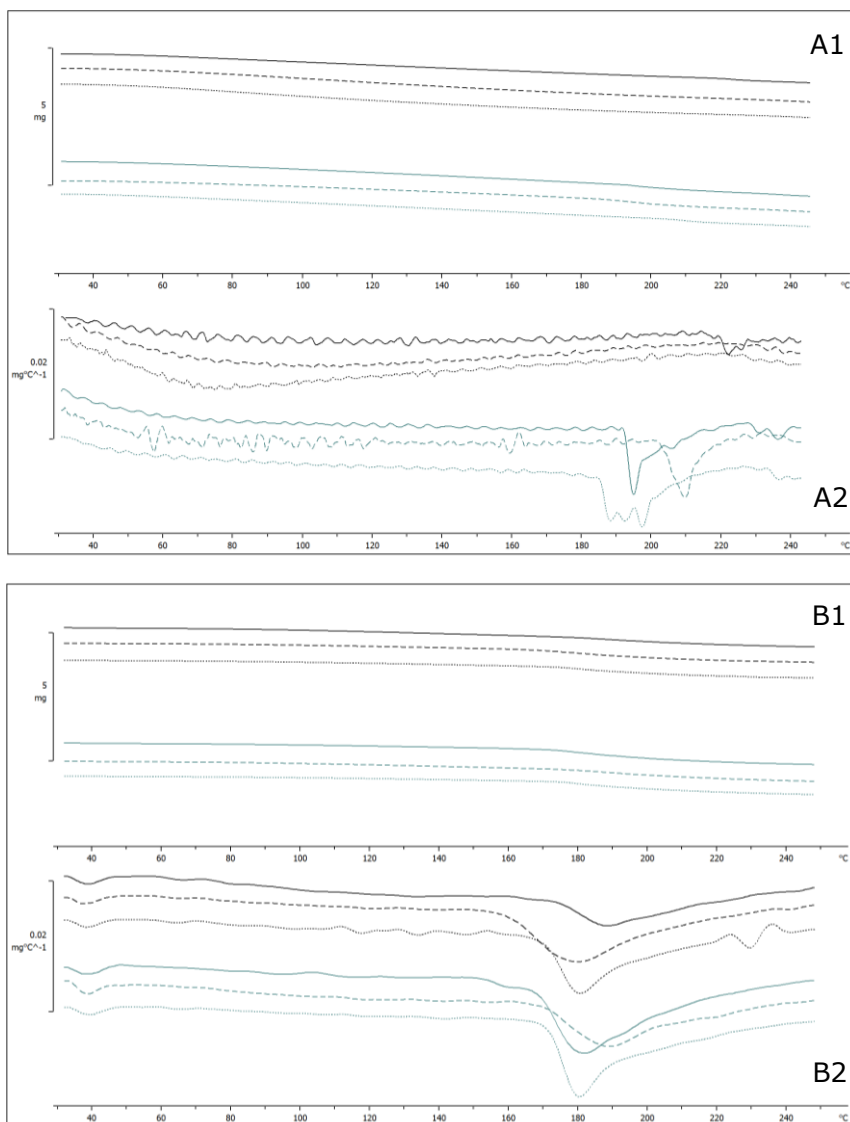


Figure 38. (A) Slow rate (5 °C/min) thermo-gravimetric analysis (TGA) of ground intermediates from 30 °C to 250 °C. (A1) Black = IP4 weight loss, green= IP2 40 weight loss. (A2) 1<sup>st</sup> derivative of IP4 (black) and IP2 40 (green). (B) Fast rate (40 °C/min) TGA of intermediates (B1) weight loss (%) (B2) 1<sup>st</sup> derivative.

When carrying out TGA at higher heating rates no statistically significant differences were found between water losses of IP2 40 and IP4 during heating (Table 11). All samples, irrespective of amorphicity, were found to have the greatest rate of change of water release between the temperatures of 160 °C and 230 °C (Figure 38 B2). This finding suggests that differences in water loss between samples are unlikely to be apparent during frying and therefore are less likely to influence the viscoelastic properties of the matrix. It is more realistic to assume the heating rate is so quick that events happen within a very short time frame; preventing differentiation between samples. As a result, the differences in  $E'$ , thought to be partly driven by water loss differences, is likely to partly be an artefact of the measurement itself.

**Table 11. Average % water loss  $\pm$  standard deviation of IP2 40 and IP4 between different temperature ranges. \* represent statistically significant differences in each data set ( $P < 0.05$ ).**

Water Loss (%)	IP2 40	IP4
30- °C-130 °C (@5 °C/min)	4.78 $\pm$ 0.77	6.27 $\pm$ 0.77
130 °C-250 °C (@5 °C/min)	8.37 $\pm$ 0.35	6.57 $\pm$ 0.55*
190 °C-230 °C (@5 °C/min)	3.39 $\pm$ 0.20	2.03 $\pm$ 0.51*
30 °C-130 °C (@40 °C/min)	1.91 $\pm$ 0.28	2.25 $\pm$ 0.23
130 °C-250 °C (@40 °C/min)	8.59 $\pm$ 0.51	7.95 $\pm$ 0.50
160 °C-230 °C (@40 °C/min)	7.11 $\pm$ 0.65	6.47 $\pm$ 0.65

To build on the effectiveness of the TGA methodology, it was observed that the higher the heating rate the lower the temperature at which sudden water loss occurs. Relating this back to van der Sman's state diagram (Figure 12), it was suggested intermediates lose the greatest water between

the temperatures of 120 and 140 °C. When taking into account the negative correlation between heating rate and temperature of greatest point of water loss, this data supports van der Sman (2016) hypothesis with vaporisation likely to occur between 100 and 160 °C. However, one thing important to consider is the dominating factor  $T_g$  will have on water release. Such that, intermediates with a lower  $T_g$  will have a reduction in internal pressure at a lower temperature and consequently vaporisation will occur sooner.

### 5.3.6 Product microstructure and textural attributes

#### *5.3.6.1 Microstructure of final products*

With the molecular, viscoelastic and microstructure properties of IP2 40 and IP4 in mind, differences in microstructure of final products were characterised qualitatively using SEM. Figure 39 displays micrographs of FP2 40 and FP4 cross-sections; demonstrating significant differences in both bubble cell size and wall thickness. FP4, which has a higher proportion of semi-crystalline material and consequently a greater DP, was found to have smaller cell diameters and thicker cell walls in the centre of the final product. However, on the product surface, differences between cell wall thickness of FP2 40 and FP4 were negligible.

On observation, the largest difference was associated with the continuous matrix, whereby FP2 40 appeared to be dominated by a smooth CP compared with FP4 which had a large proportion of dispersed starch granules within the continuous matrix, making it appear somewhat rough (Figure 39 E and F). This observation corresponds to the function of the DP in altering the rheological

properties of the matrix, with particle-matrix adhesion being reported as a key contributor to increasing storage modulus in the rubber phase. If particle-matrix adhesion was a key driver in altering measured rheological properties, thermographs of FP4 would suggest this to be predominately governed by the native starch granules to matrix adhesion rather than the zein or fibre within the intermediate.

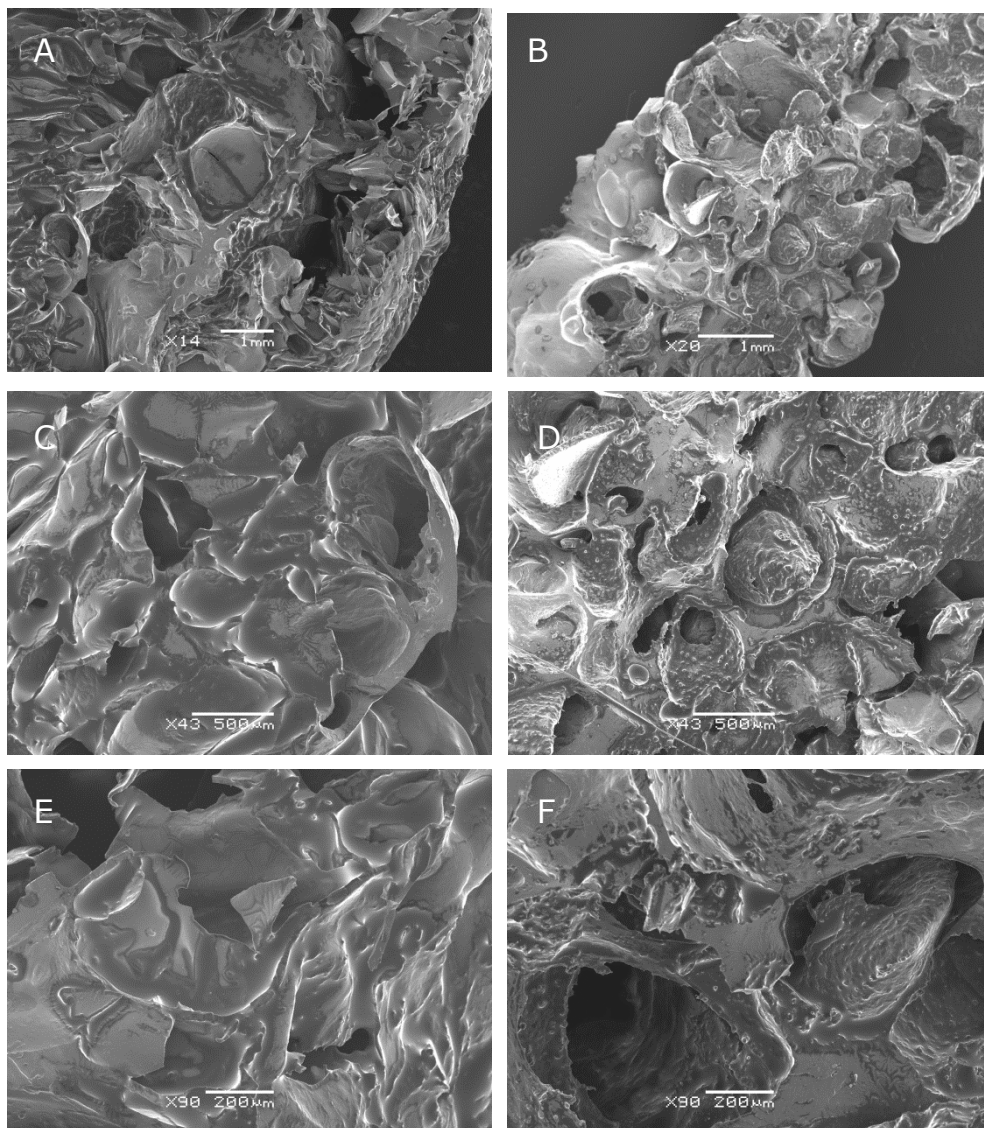


**Figure 39. Scanning electron micrographs of final products (A, C, E) FP2 40 cross section, (B, D, F) FP4 cross section.**

### 5.3.6.2 Textural attributes of final products

From a sensory perspective, it was unnecessary for detailed analysis by a trained panel, as basic sensory analysis was sufficient to identify differences in first bite, breakdown and clearance. Due to the thickness of the intermediates prior to expansion, final products were in excess of a size suitable for eating in one bite and therefore had to be broken first. The key output from sensory analysis identified that IP2 40 had a soft initial bite, short breakdown in the mouth (2 - 3 bites) and tooth packing upon clearance. IP4 had a hard initial bite, extended breakdown in the mouth but upon clearance had a gritty texture.

With it being a well-established theory that mechanical strength of 'brittle foams' is related to density, it is hardly surprising there is an inverse relationship between hardness and ER (density) (Lillford, 2001). Similarly, lower porosity and thicker cell walls are often negatively correlated with water absorption (Yao *et al.*, 2011). Therefore, it is likely with a greater expanded final product, saliva uptake within FP2 40 was promoted, resulting in a quick breakdown within the mouth; thought to be further promoted by the increase in solubility of the starch. As a result of the highly processed amorphous starch, a gummy paste formed at the end of the breakdown with significant tooth packing after swallow.

It is thought for FP4 that the remaining intact starch granules present at the surface and centre of the final product (Figure 39 F) acted to prevent hydration in the mouth. However, following breakdown of the continuous amorphous starch matrix these starch granules could have then promoted the perceived gritty texture. It is likely this attribute is a result of a combination of the

particle size and  $T_g$  of maize granules with an average particle size of 30 to 50  $\mu\text{m}$  and a  $T_g$  in excess of mouth temperature (37 °C) (Imai *et al.*, 1995).

## 5.4 Conclusion

From a processing perspective, twin-screw extrusion was successful at creating uniform intermediates. However, due to the elasticity of the pre-gelatinised material, limitations in the processing window for twin-screw extrusion were apparent. At barrel water contents below 40 %, undesirable direct expansion occurred and case hardening of intermediates was induced at high water contents (>50 % dwb). Therefore, to further optimise processing, a milder process should be used which would not only widen the processing window but prevent further molecular breakdown of the materials.

Similarly, as a result of combination of a larger die diameter and extrudate die swell, intermediate thicknesses were driven in excess of commercialised products (<1.5 mm). This had a direct effect on size of the final product which was undesirable for 'ease of eat'.

Following the manufacture of intermediates from native maize grits (IP4) and fully gelatinised grits (IP2 40), analytical characterisation supported significant differences in molecular properties that have primarily governed significant differences in expansion, with much of the work presented being supported by published literature (Kristiawan *et al.*, 2016; van der Sman, 2016; Dos Santos *et al.*, 2013; van der Sman and Broeze, 2013; Norton *et al.*, 2011). The key difference of IP4 and IP55 was found to be the ratio of semi-crystalline to amorphous starch, with IP4 retaining native starch into both intermediate and final products. In this case, the semi-crystalline to amorphous ratio directly influenced the CP:DP; where micrographs confirmed a larger proportion of DP in IP4.

However IP2 40 and IP2 55, which appeared to have an identical CP:DP, had significant differences in expansion. This was attributed to the physical properties of high water content intermediates which induced case-hardening; enabling differences in expansion from the centre to the surface of IP2 55. As a result, it is considered important to use a multitude of methods when characterising starch intermediates, as micrographs missed to identify the differences IP2 40 and IP2 55.

DMTA of IP2 40 and IP4 demonstrated significant differences in  $E'$  of intermediates following  $T_g$ . Although a combination of factors was likely to drive differences in  $E'$ , it is thought that the CP:DP is the primary driver of differences in both DMTA measurements and frying. Interestingly however,  $T_g$  onset and peak  $\tan \delta$  (mid- $T_g$ ) were not statistically significantly different between IP2 40 and IP4; suggesting the viscoelastic properties of the matrix govern the degree of expansion of intermediates more than that of  $T_g$ .

Method development using TGA enabled differences in water loss of intermediates to be characterised at both slow (5 °C/min) and fast heating rates (40°C/min), whereby semi-crystalline intermediates lost a greater proportion of water at lower temperatures  $T < T_g$  and amorphous intermediates lost a greater proportion at  $T > 130$  °C. These differences were found to be insignificant at higher heating rates; more similar to that of frying (40 °C/min) and therefore suggest differences in  $E'$  to be partly driven by method artefacts. As a result, it is advised DMTA should also be carried out within sealed aluminium pockets to understand the direct impact loss of water on  $E'$  and  $E''$ .

For pocket DMTA, results suggest smaller particles sizes (<1 mm) prevent spaces between larger particles influencing perceived  $E'$ . Similarly, it is advised in future development that faster heating rates should be used for TGA measurements; identifying differences between intermediate compositions in conditions more similar to that of frying.

## **Chapter 6 Single-screw extrusion of IP1 with intermediate and final product characterisation**

### **6.1 Introduction**

The main findings from intermediate and final product development presented in Chapter 5 were used to optimise processing conditions and consequently deliver final products with expansion and sensory properties more similar to that of commercialised products.

As a result, the secondary process was exchanged to single-screw extrusion whereby milder processing conditions enabled a wider processing window. Barrel temperatures and shear forces generated were minimised in an attempt to prevent further molecular breakdown of IP1.

To deliver proof of principle that the degree of semi-crystallinity is a key driver in changing both molecular and microstructural properties of final products; native potato starch, microcrystalline cellulose and rice flour were incorporated into IP1 recipes at a 10 % weight basis. These semi-crystalline materials were chosen to understand the impact of both A-type (rice) and B-type (potato) starches on expansion, with B-type expected to melt out during the frying stage and A-type to retain native. Additionally, to build an understanding of the impact of further protein (within rice flour) and fibre (MCC) in intermediates on the expansion and cellular structure of final products.

In this chapter, characterisation of intermediates and final products are presented following single-screw extrusion of IP1 at 40 % water content (IP3) and with the addition to the IP1 dry mix on a weight basis of 10 % potato starch (IP3 + PS), rice flour (IP3 + RF) or microcrystalline cellulose (IP3 + MCC). Consequently, the effects of addition of semi-crystalline materials on the molecular and

microstructure properties of intermediates and final products have been assessed, in addition to preliminary characterisation of differences in final product attributes.

## 6.2 Materials and Methods

### 6.2.1 Materials

IP1 manufactured from Yellow YG560 Maize grits was utilised as the bulk ingredient for all processing in Chapter 6. For details on the ingredient and processing conditions see Chapter 2.

Superior Native Potato Starch (KMC, Charleroi) at an average water content of 17.13 % (dwb) was incorporated into intermediates as a semi-crystalline DP ingredient. The potato starch had a mean particle size diameter of  $543.1 \pm 331.6 \mu\text{m}$  as demonstrated in Figure 40 A. Figure 40 B depicts the semi-crystalline nature of the material with clear Maltese crosses within the granules.

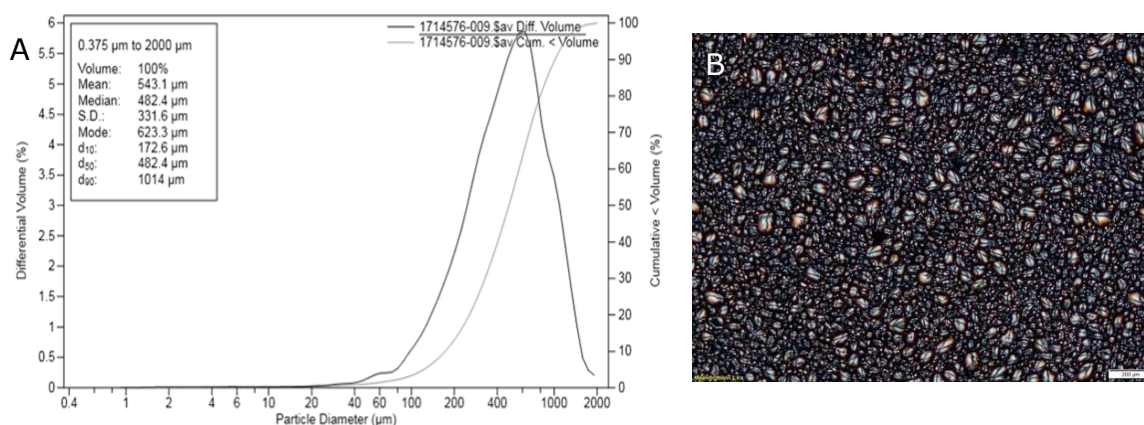


**Figure 40. (A) Particle size distribution of Superior Native Potato Starch and (B) Cross polarised light microscopy**

Rice flour (FL4097) (Whitworth Bros Ltd., Worksop) with an average water content of 11.52 % and nutritional profile of a maximum oil content of 1.5 % in addition to ~ 78 % starch, 3 % Fibre and 7 % protein was also incorporated with the IP1 bulk ingredient. Semi-crystalline starch in combination with fibre and protein is demonstrated in Figure 41 in addition to the particle size distribution which on average was  $203.2 \pm 132 \mu\text{m}$ .

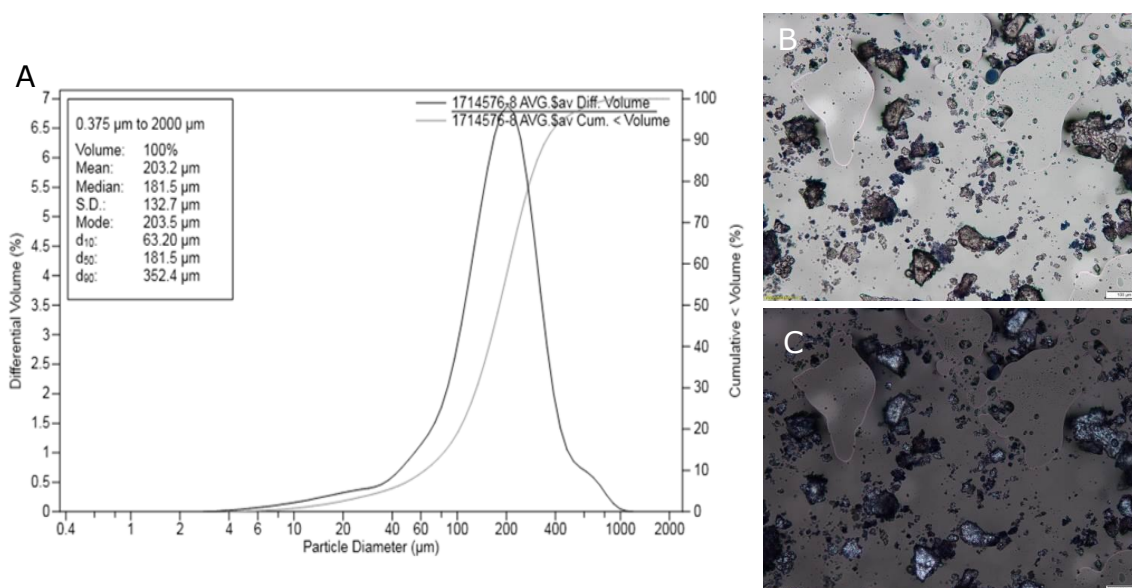


**Figure 41. (A) Particle size distribution of Rice Flour, (B) Hydrated Light microscopy and (C) hydrated cross polarised light microscopy**

Grindsted Micro-crystalline cellulose (MCC) 01ND (Danisco, Kettering) with an average water content of 4.8 % (dwb) and 0.25 % of water soluble substances was also utilised in intermediate manufacture. Bulk density was specified in the range of 0.26 - 0.36 g/ml with a particle size of no more than 35 % greater than 200  $\mu\text{m}$ . As a result of the geometry (elongated needle), particle size analysis was deemed inappropriate (Figure 42).

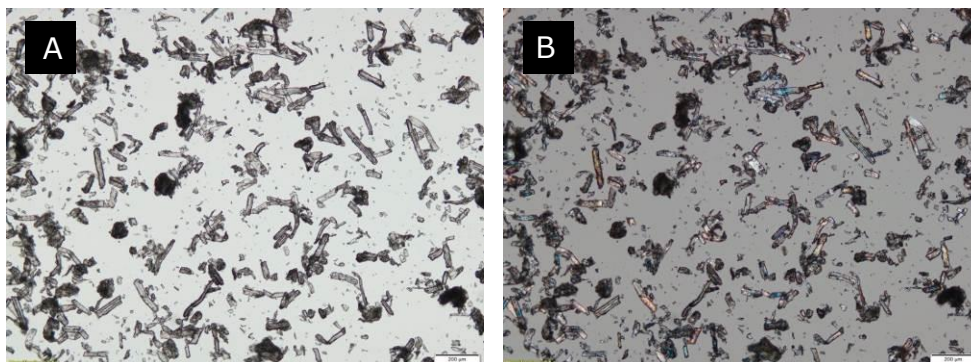


**Figure 42. (A) Light microscopy and (B) cross polarised light microscopy of micro-crystalline cellulose.**

## 6.2.2 Processing Methods

### 6.2.2.1 Pre-mixing

Prior to extrusion, 400 g of the dry mix was pre-mixed with water in a ThermoFisher Hyperforma single-use mixing unit at 600 rpm, 25 °C for 2.5 minutes; rendering a homogenous dough to be fed into the extruder directly. Calculated water added to the dry ingredients was based on the average raw material water content to reach a final water content from 30 to 40 % (wwb). Addition of water was carried out prior to extrusion rather than within the barrel since single-screw extruders do not have a water unit attached to the barrel.

### 6.2.2.2 Extrusion

Intermediate products were manufactured on a ThermoFisher single-screw HAAKE RHEOMEX OS extruder with a 1:1 conveying screw at a speed of 30 rpm. In an attempt to reduce the viscosity of the dough, minimising shear and retaining the molecular order within native ingredients; the

extruder barrel zones were heated from 1 to 4 at 20 °C, 30 °C, 40 °C and 40 °C ( $\pm 2$  °C) respectively. Due to the limited shear and temperature generation in the extruder, temperatures were consistent throughout manufacture. For variable process conditions see Table 12.

The pre-mixed dough was fed by hand into the extruder through a feeding port and as a result, throughput was unable to be controlled throughout the process. To over-come this, the feeding port was 'choke' fed in an attempt to control throughput through screw speed (rpm). The dough sheet on exit of the extruder was put through a ThermoFisher stretching unit to thin prior to cutting, which was carried out using hand scissors (Figure 43).

**Table 12. Processing conditions for single-screw extruder intermediate manufacture**

Material	Dough preparation				Process Conditions		Temperature of Extruder (°C)				
	Average moisture dry mix (%)	Dry mix weight (g)	Water added (ml)	Dough moisture (wwb) (%)	Torque (Nm)	Die Pressure (bar)	Temp Z1	Temp Z2	Temp Z3	Temp Z4	Temp Die
IP3 40 %	9.1	400	206	40	15 $\pm$ 0.65	62 $\pm$ 2.3	20	30	40	40	38 $\pm$ 0.17
IP3 + 10 % PS	9.9	400	200	40	17 $\pm$ 0.98	66.5 $\pm$ 3.3	20	30	40	40	38 $\pm$ 0.31
IP3 + 10 % RF	9.4	360	184	40	14.3 $\pm$ 0.34	56 $\pm$ 1.8	20	30	40	40	38 $\pm$ 0.16
IP3 + 10 % MCC	8.9	400	207	40	13.3 $\pm$ 1.2	55 $\pm$ 5.6	20	30	40	40	37.5 $\pm$ 0.20



**Figure 43. Pictures demonstrating stretching device attached to extruder to thin the dough sheet achieving thinner intermediates following cutting and drying.**

### 6.2.2.3 *Drying*

Intermediates following cutting were air dried over night at 26 °C to a water content of 10 - 12 % (dwb). Following drying, samples were sealed in plastic bags for a minimum of 3 days before frying to achieve a water distribution at equilibrium.

### 6.2.2.4 *Frying*

Samples were fried in a 3 litre Magimix 350 fryer with sunflower oil at 195 °C until intermediate products were fully expanded. As a result of sheet stretching prior to drying, intermediates had an average thickness of  $0.83 \pm 0.25$  mm and therefore frying times to full expansion were significantly reduced from Chapter 5 (Table 13).

**Table 13. Frying conditions for intermediates**

Sample Name	Temperature (°C)	Time (secs)
IP3	195	10
IP3 + PS	195	10
IP3 + RF	195	10
IP3 + MCC	195	10

### 6.2.3 Analytical Methods

To characterise intermediate and final products, samples were subjected to a range of analytical methods. Information on the analytical methods used in Chapter 6 are detailed in Chapter 3. The following methods were used to characterise intermediate and final product properties:

- Expansion Ratio (ER)
- Differential Scanning Calorimeter (Hydrated) (DSC)
- Thermogravimetric Analysis (TGA)
- X-Ray Powder Diffraction (XRPD)
- Rapid Visco Analyser (RVA)
- Light Microscopy
- Scanning Electron Microscopy (SEM)
- Confocal Light Microscopy
- Statistical Analysis (two-factor ANOVA with a Tukey Post Hoc Multiple Comparison test)

## 6.3 Results and Discussion

### 6.3.1 Processing Observations

The key changes in processing were made as a result of the processing and characterisation observations described in Chapter 5. Consequently, single-screw extrusion was adopted into the secondary intermediate process to prevent further depolymerisation of IP1 and to retain semi-crystallinity of additional ingredients into intermediates. Similarly, a stretcher was incorporated into the process at the end of the extruder which successfully reduced intermediate thicknesses to <1.5 mm following drying.

When comparing single-screw extrusion processing observations to twin-screw extrusion, the processing window was widened and water contents could go to below 30 % (wwb) without inducing expansion on exit of the die. This was thought to be dominated by the reduced temperature within the extruder barrel which prevented vaporisation of water on exit of the die (<T of boiling point of water at atmospheric pressure). Due to the wider processing window, a range of dough water contents could be extruded to understand the influence of water on additional processing parameters.

Figure 44 displays the average pressure, die temperature and torque of the extruder at three different dough water contents; 30 %, 35 % and 40 % (wwb). The reduction in temperature, pressure and torque with an increase in dough water content is attributed to a reduction in dough viscosity. Thus, the dough reduces resistance to flow through the extruder reducing the mechanical energy required to process the dough and consequently driving a reduction in torque and temperature.

To retain the semi-crystalline order within intermediates it was concluded all dry mixes should be pre-hydrated to a dough water content of 40 % to limit increases in pressure, temperature and torque. Therefore, the following characterisations of intermediates and final products are based on dough water contents at 40 % only (wwb).

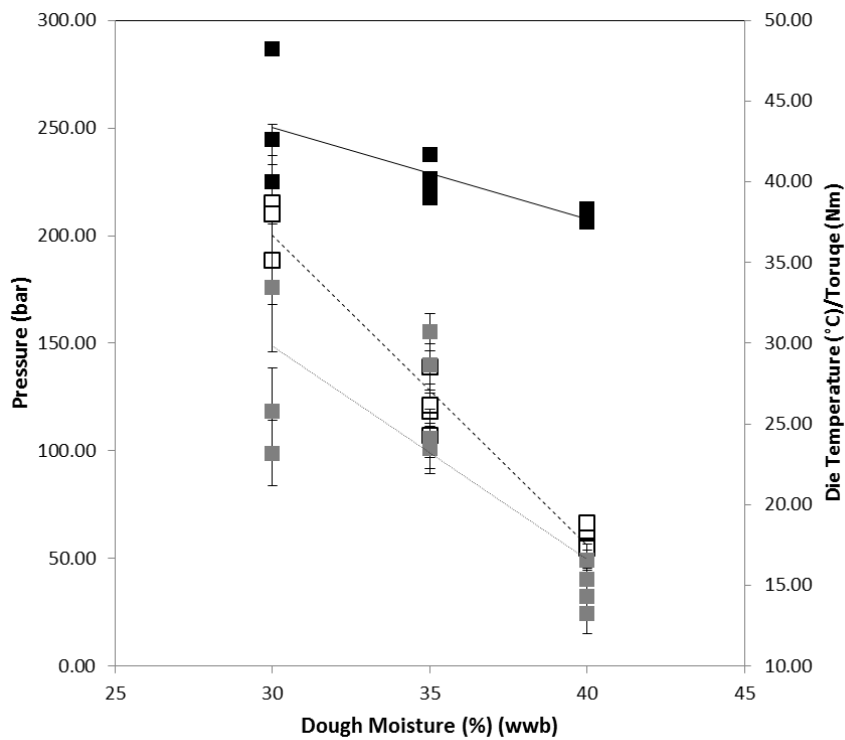


Figure 44. Graph demonstrating the impact of dough water content from 30 % to 40 % (wwb) on  $\square$  average pressure,  $\blacksquare$  die temperature and  $\blacksquare$  torque within a single-screw extruder based on 3 recipes. Error bars are based on standard deviation of 3 replicates.

### 6.3.2 Characterisation of the differences in single-screw and twin-screw extrusion intermediates

To understand the impact of differences in the secondary manufacturing process, intermediates and final products manufactured from IP1 using single- and twin-screw extrusion were compared. Figure 45 displays the viscosity traces of ground intermediates in excess water with respect to temperature and time. Here IP3, manufactured from single-screw extrusion, displays a viscosity trace most similar to that of IP2 55 presented in Chapter 5. Previous conclusions defined retrogradation during air drying to be responsible for the peak viscosity to appear at higher temperatures, occurring after disruption of the re-crystallised regions.

In literature, the final viscosity is negatively correlated with the degree to which starch is processed and is therefore assumed to be an in-direct measure of the  $M_w$  of solubilised polymers (packing density) (Majzoobi, 2004). Consequently, results suggest that single-screw extrusion has prevented further depolymerisation of starch in the secondary process more than twin-screw extrusion, even at when the dough water content of IP3 was lower than IP2 55; which often promotes depolymerisation (Majzoobi, 2004). It is likely this is a result of the reduction in mechanical energy during the extrusion process with one forward rotating screw rather than two intermeshing screws. However, contrary to what is observed, it would be expected for IP1, with no secondary processing, to display the highest final viscosity. The decrease in final viscosity of IP1 can be partly explained by the instruments inability to reduce the viscometer to the final temperature of 22 °C. As a result, the final temperature was on average 1 °C higher than that of other measured samples, which would directly influence the viscosity of the paste. Additionally, due to direct expansion and sudden loss of water transitioning the snack into a glassy state, no re-association of amorphous starch has been

able to occur. For IP2 and IP3 intermediates, slow air drying in the rubber state was likely to promote re-association of chains and therefore a greater final viscosity upon cooling.

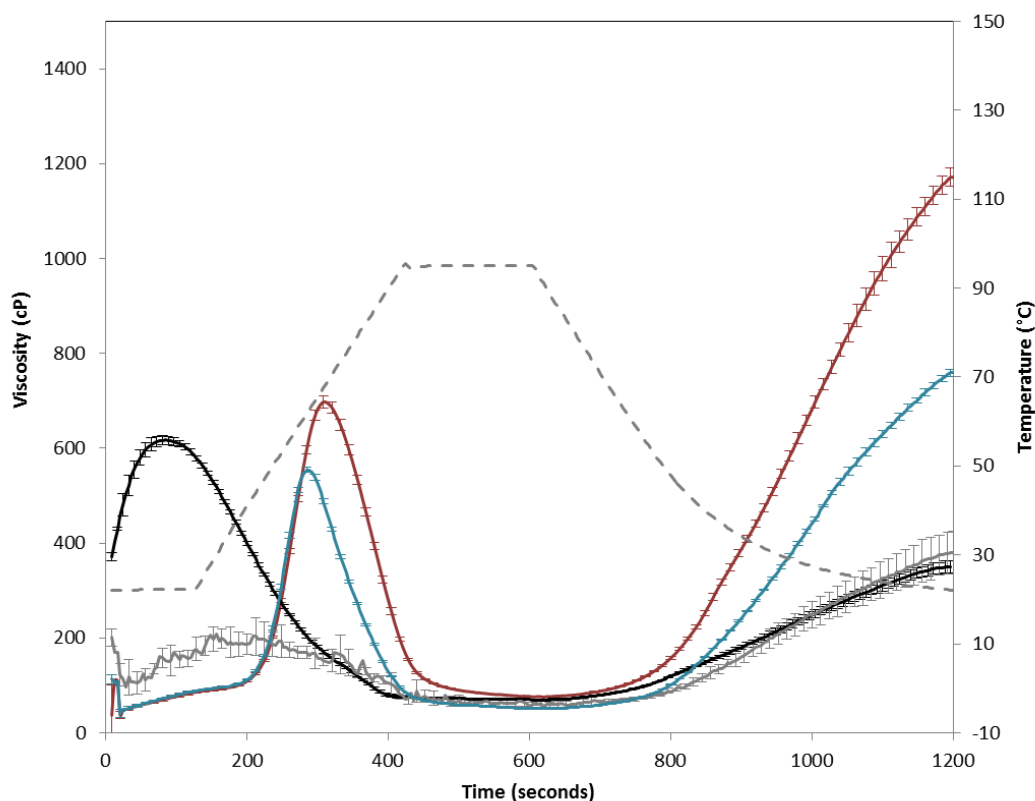


**Figure 45. Average viscosity (cP)  $\pm$  standard deviation with respect to time and temperature of intermediates. — IP1, — IP2 40, — IP2 55 and — IP3, - - - Temperature Standard deviation is based on 5 replicates for each sample.**

XRPD supports findings from RVA with defined peaks at the  $12.95^\circ$ ,  $18^\circ$  and  $19.75^\circ$   $2\theta$  positions (Figure 46). As discussed in previous chapters, the  $12.95^\circ$  peak is attributed to amylose-lipid complex formation and  $19.75^\circ$  is associated with B-type amylopectin crystal formation, supporting the suggestion of retrograded starch within intermediates from RVA. Peaks for IP2 and IP3 intermediates appear to be very similar suggesting little to no native A-type crystalline starch prevalent. Due to the

XRPD only characterising crystalline polymorphs and the highly processed IP1 prior to secondary extrusion being amorphous, XRPD is less effective at differentiating between the molecular properties of the starch following two different secondary processes.

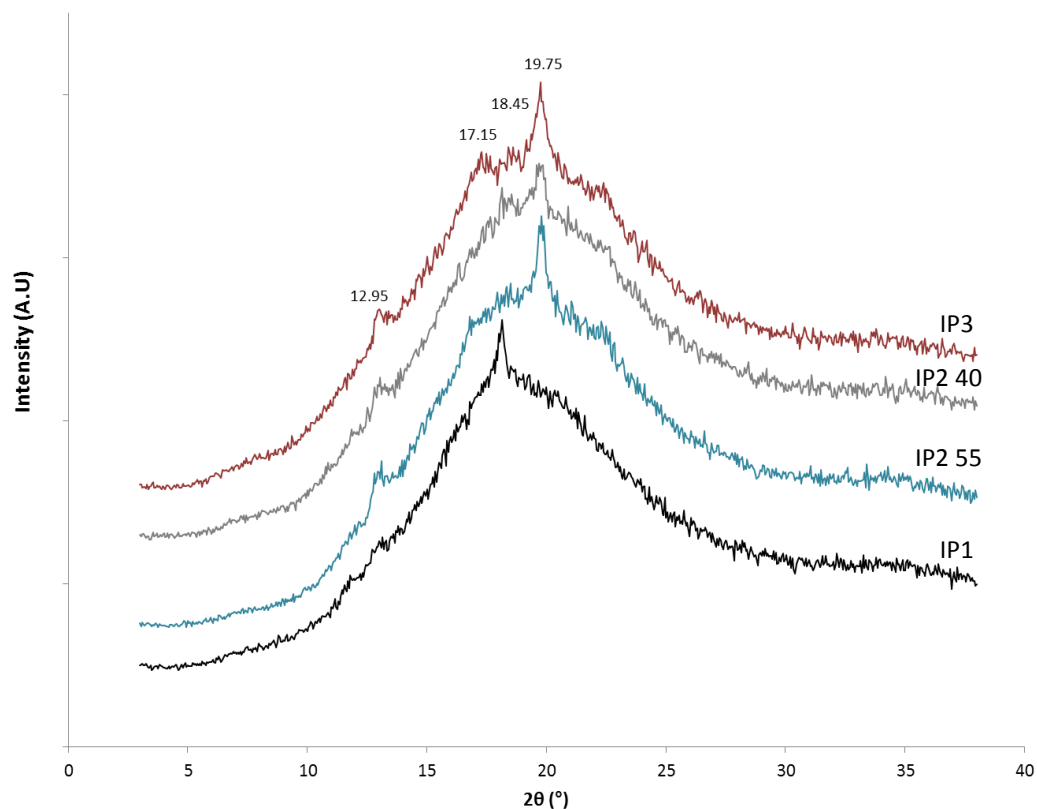
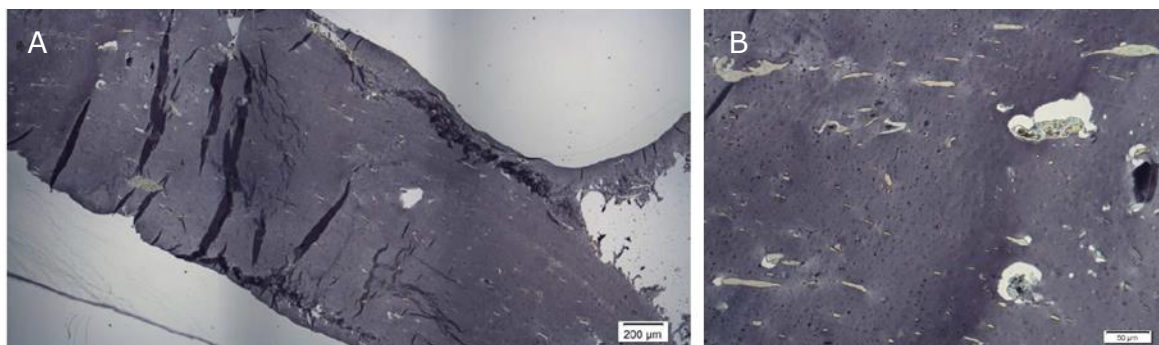


Figure 46. XRPD of — IP1, — IP2 55, — IP2 40 and — IP3. Numbers correspond to peak  $2\theta$  ( $^\circ$ ) positions of extruded intermediate-products.

When comparing IP2 and IP3 intermediate microstructures, very similar micrographs were prevalent with distributed protein and fibre throughout a continuous amorphous matrix (Figure 28 and 47).



**Figure 47. Light microscopy of IP3 following microtoming and iodine staining (A) Micrograph with scale bar 200 µm and (B) Scale bar 50 µm**

As a result, one can assume the physical properties of the intermediates, such as a reduction in case hardening and changes in intermediate thickness (mass per sample) primarily governed the differences in expansion of IP2 and IP3 (Figure 48).

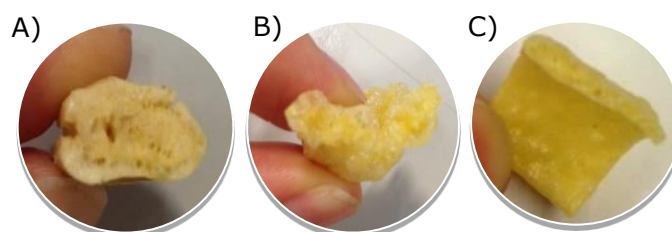


**Figure 48. Final products following expansion of intermediates (A) FP2 55, (B) FP2 40 (C) FP3.**

In an attempt to determine if water loss during slow and fast heating rates was similar for that of twin-screw and single-screw intermediates, TGA of IP3 was compared against previous

characterisations displayed in Figure 38. Figure 49 shows the water loss and 1<sup>st</sup> derivatives for IP3 with the greatest difference observed in the temperature at which water loss occurs. For slower heating rates, IP3 had its greatest water loss at 230 °C rather than 190 °C; as seen for IP2 40. At higher heating rates, these differences were less apparent, with the greatest water loss increased by ca. 20 °C; suggesting during frying that these differences are likely to be insignificant.

To interpret results in more detail, the water loss (%) between the temperature ranges of 30-130 °C (*a*) and 130-250 °C (*b*) are presented for IP2 40, IP3 and IP4, including the ratio of *a* to *b* (Table 14). The water loss mechanisms of the single-screw extruded IP1 seem more similar to that of IP4 with no statistical significant difference in the ratio of *a/b* of IP3 and IP4 at both heating rates. The ratio of *a* to *b* continues to highlight the inverse relationship between the level to which the material is processed and the proportion of water lost at milder temperatures.

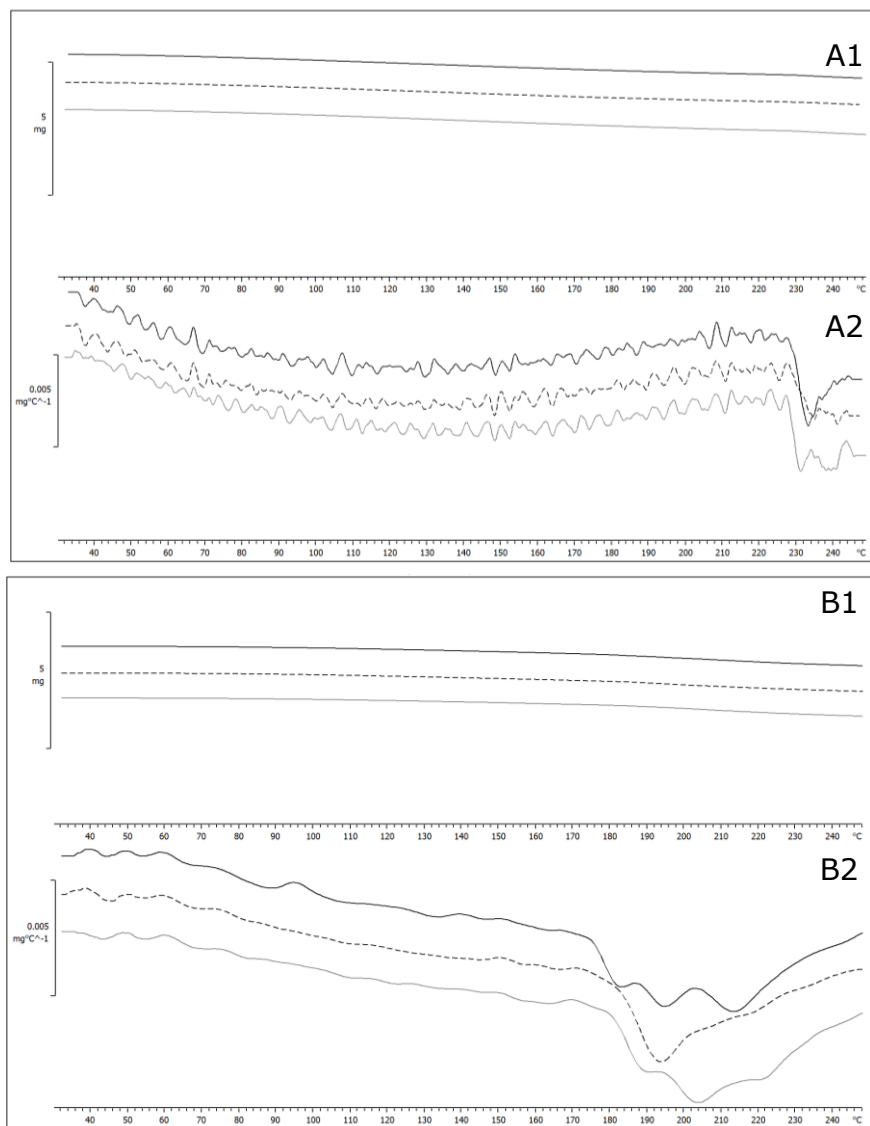


**Figure 49. Thermo-gravimetric analysis of ground intermediates to 1 mm in diameter at (A) slow rate (5 °C/min) and (B) fast heating rates (40 °C/min). (1) IP3 weight loss and (2) IP3 1st derivative. 3 replicates per sample.**

**Table 14. Average % water loss  $\pm$  standard deviation of IP2, IP3 and IP4 between the temperature ranges of 30-130 °C (a) and 130-250 °C (b). The average ratio of a/b  $\pm$  standard deviation is also presented. All figures are based on three replicates.**

Water Loss (%)	IP2 40	IP3	IP4
30 °C-130 °C (a) (@5 °C/min)	4.78 $\pm$ 0.77	4.58 $\pm$ 0.23	6.27 $\pm$ 0.77
130 °C-250 °C (b) (@5 °C/min)	8.37 $\pm$ 0.35	6.71 $\pm$ 0.24	6.57 $\pm$ 0.55
a/b @5 °C/min	0.57 $\pm$ 0.11	0.68 $\pm$ 0.05	0.97 $\pm$ 0.20
30 °C-130 °C (@40 °C/min)	1.91 $\pm$ 0.28	1.77 $\pm$ 0.13	2.25 $\pm$ 0.23
130 °C-250 °C (@40 °C/min)	8.59 $\pm$ 0.51	7.57 $\pm$ 0.14	7.95 $\pm$ 0.50
a/b @40 °C/min	0.22 $\pm$ 0.05	0.24 $\pm$ 0.02	0.28 $\pm$ 0.05

### 6.3.3 Characterisation of IP3 intermediates with additional semi-crystalline material

Intermediate and final products were analysed using DSC and XRPD to characterise the state of the different crystalline materials: rice flour (RF), potato starch (PS) and micro-crystalline cellulose (MCC) throughout the manufacturing process.

Due to the mild processing conditions it was expected for all semi-crystalline materials to retain their order into the intermediates. However during frying, as a result of the differences in temperatures that A- and B-type native starches melt, it was thought crystalline PS would melt but RF would remain semi-crystalline. Consequently, the impact of starch melting on the expansion of intermediates could be addressed since current published articles in this area are not in agreement.

Definitive results are limited due to the associated changes that could be argued to both promote and prevent expansion; addressed in detail by van der Sman (2016).

Figure 50 displays the hydrated DSC thermographs of native materials, intermediates and final products; where endothermic peaks are related to the loss of crystalline order. Since semi-crystalline materials were added in at 10 % weight basis of the total recipe, a 10 % reduction in enthalpy is expected from the native material to intermediate; as demonstrated in Table 15. As hypothesised, crystallinity within PS, RF and MCC retained into intermediates with average melting enthalpies between 1.06 and 3.31 J/g.

During frying, the semi-crystalline PS within the amorphous matrix melted and therefore the endothermic peak attributed to melting during DSC measurements was not prevalent in final products (Figure 50 A). Conversely, native RF as predicted retained crystalline structure, in both intermediates and final products, due to of A-type packing of amylopectin that is associated with cereals. The differences in melting temperatures of the polymorphs are demonstrated in the thermographs of PS and RF native materials, since this measurement was carried out in excess water peaks appear at 60 °C and 70 °C, respectively. During frying of intermediates, as the available water is reduced, the temperature at which the crystalline amylopectin loses order is expected to increase. Similarly, peaks are weak since starch is only part of the component associated with rice flour, reducing the concentration of the polymer that is melting.

MCC is typically reported to have a melting temperature in excess of 160 °C (Picker and Hoag, 2002; Szcześniak *et al.*, 2008). Therefore, no melting occurs in the thermograph of the raw material between the temperatures of 20 and 100 °C (Figure 50 C). However, within intermediates of combined MCC and amorphous maize starch (IP1) a small endothermic peak is prevalent between 50

and 70 °C which corresponds to an increase in enthalpy of 2.8 J/g based on 10 % of MCC in the amorphous matrix. The crystalline material driving the endothermic response does not appear in thermographs of final products following frying. To identify the driver of the endothermic peak, intermediates manufactured from IP1 alone were analysed; which were expected to be completely amorphous. Figure 50 D displays thermographs of IP3 which were manufactured without the addition of crystalline material, where the same endothermic peak between 50 - 70 °C appears. These results confirm that the peak in the IP3 + MCC thermograph is driven by the CP of the intermediate, not the MCC. As seen previously within air drying of twin-screw extruded intermediates, retrogradation is promoted when intermediates exist within the rubber state during air drying (Figure 31) and as a result retrogradation is considered responsible.

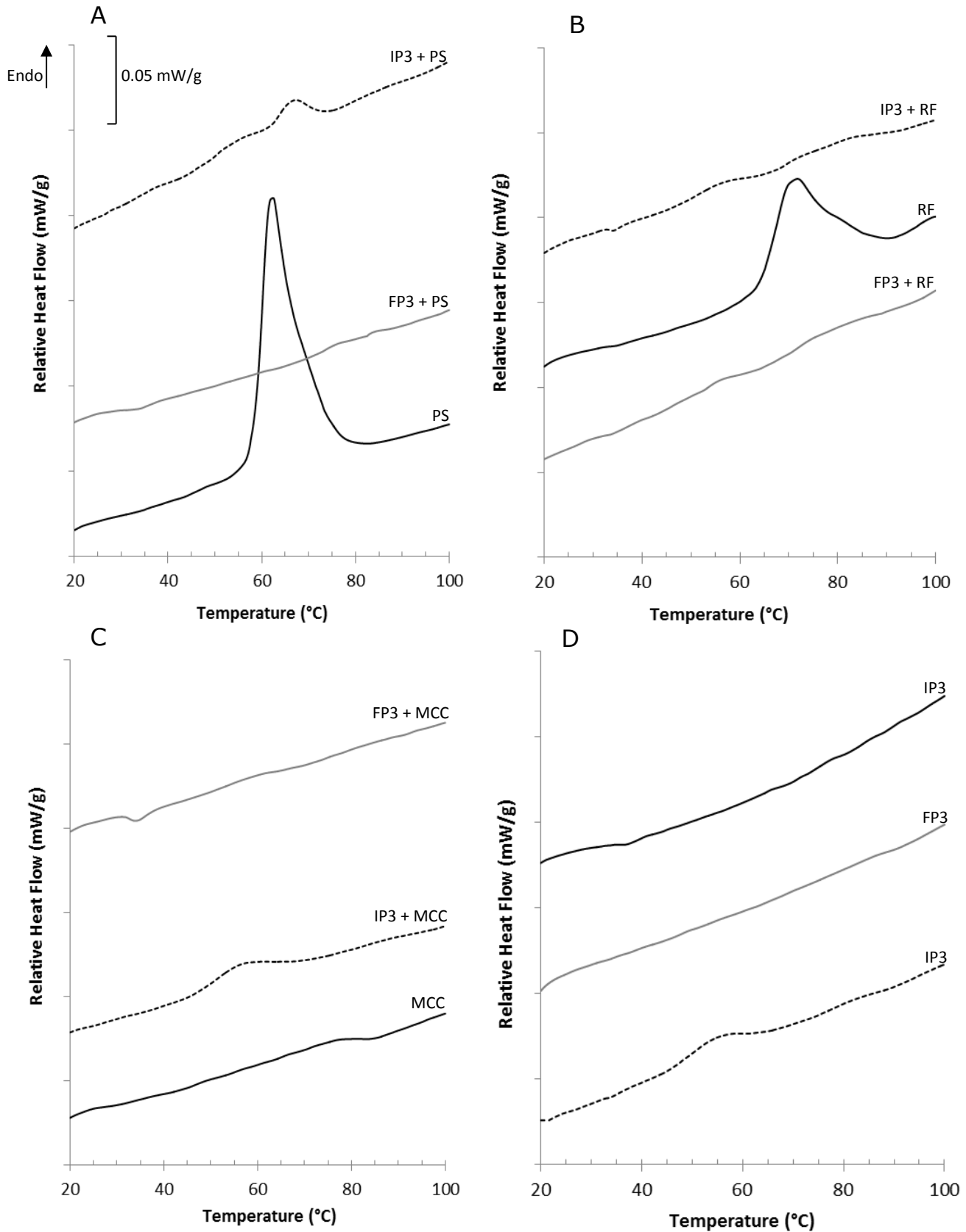


Figure 50. DSC thermographs of — native material, ..... intermediate (IP3) and — final product (FP3) of (A) + 10 % Potato Starch (PS), (B) + 10 % Rice Flour (RF), (C) + 10 % Microcrystalline cellulose (MCC) and (D) IP3 with no additional crystalline material. IP3 + MCC, IP3 + RF, FP3 + MCC and FP3 + RF have been offset by -0.05 mW/g for ease of interpretation. Heating rate 5 °C/min and >50 % water content.

**Table 15. Average enthalpy (J/g)  $\pm$  standard deviation of raw materials, intermediates and final products. Raw material refers to the crystalline material alone and not dry mixes.**

Recipe Code	Raw Material Enthalpy (J/g)	Intermediate Enthalpy (J/g)	Final Product Enthalpy (J/g)
IP3 + 10 % Potato Starch	18.67 $\pm$ 0.29	3.31 $\pm$ 0.19	0.41 $\pm$ 0.11
IP3 + 10 % Rice Flour	9.48 $\pm$ 0.24	2.06 $\pm$ 0.02	1.43 $\pm$ 0.05
IP3 + 10 % Microcrystalline Cellulose	1.20 $\pm$ 0.61	2.80 $\pm$ 1.04	0.2 $\pm$ 0.31
IP3	0.23 $\pm$ 0.13	1.42 $\pm$ 0.21	0.18 $\pm$ 0.09

By identifying retrogradation of the CP of intermediates, more detailed interpretation of PS and RF intermediates can be achieved. It is thought that the double peak formation for both PS and RF is from differences in melting temperatures of native and retrograded starch. Such that retrograded amylopectin melts at  $\sim 5$  °C lower than native starch, corresponding to thermographs presented in Figure 50 A, B and D. Similarly, it can be concluded that for IP3, IP3 + PS, IP3 + MCC and IP3 + RF that the enthalpy in intermediates as a result of melting retrograded starch are on average 1.4, 3.2, 2.8 and 1.0 J/g respectively.

XRPD was carried out on raw materials and intermediates to support the previously presented DSC and RVA data. Figure 51 displays defined peaks within the materials at the 17.25°, 18.35°, 19.7° and 22.35° 2 $\theta$  positions, where the 17.25° and 19.70° peaks are associated with B-type crystal formation. XRPD of final products continues to support this with melting of B-type crystalline polymorphs and loss of the 17.25° and 19.75° 2 $\theta$  peaks (Figure 51). Additionally, as seen in IP1, FP3 has a more definitive peak at the 18.35° 2 $\theta$  position supporting the original hypothesis of amylose-lipid complex formation in the presence of free amylose and excess oil.

Raw material MCC was shown to have defined peaks at the  $14.70^\circ$ ,  $16.25^\circ$ ,  $22.35^\circ$  and  $34.5^\circ$   $2\theta$  positions, as echoed in literature; corresponding to Type I Cellulose (Terinte *et al.*, 2011; Yue, 2011). The peak at the  $22.35^\circ$  position is prevalent amongst IP3 + MCC but corresponds to the same peak found in B-type crystal amylopectin polymorphs. Therefore, suggesting the interplanar distance ( $d$ ) between the two polymorphs is similar (Equation 2.1). The differentiation between the 3 intermediates (PS, MCC and RF) is with the peak at the  $17.25$  position, not as defined for IP3 + RF. It is suggested that this is a result of native A-type starch rather than B-type starch and as previously mentioned as a result of the lower proportion of total starch since it is rice flour not pure starch.

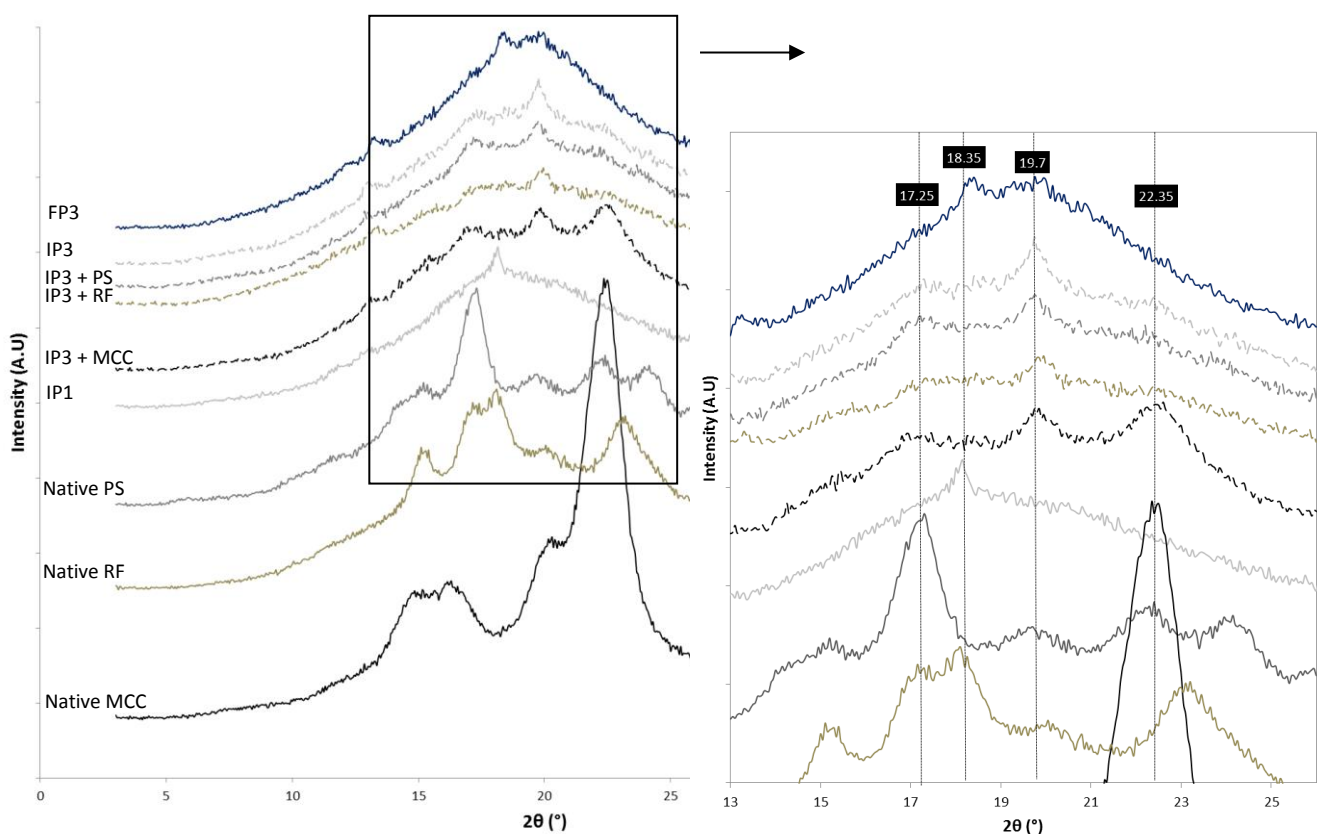


**Figure 51. X-Ray Diffraction patterns of raw materials, intermediates and final product.** — Native Micro-crystalline cellulose (MCC), — Native Rice Flour (RF), — Native Potato Starch (PS), — IP1, ..... IP3 + 10 % MCC, ..... IP3+10 % RF, ..... IP3+10 % PS, ..... IP3, — FP3.

### 6.3.4 The microstructural properties of semi-crystalline materials before and after expansion

To build on the findings from molecular characterisation of intermediate and final products, confocal light microscopy and light microscopy were used to characterise the microstructural properties of semi-crystalline materials before and after expansion (Figure 52 and 53). Figure 52 highlights the aggregation of semi-crystalline materials, particularly for PS and MCC within intermediates (refer to arrows). It is likely this is a result of the conveying screw, used in an attempt to prevent loss of crystallinity, which would appear to be insufficient at homogeneously distributing the semi-crystalline materials throughout the amorphous matrix of IP1.

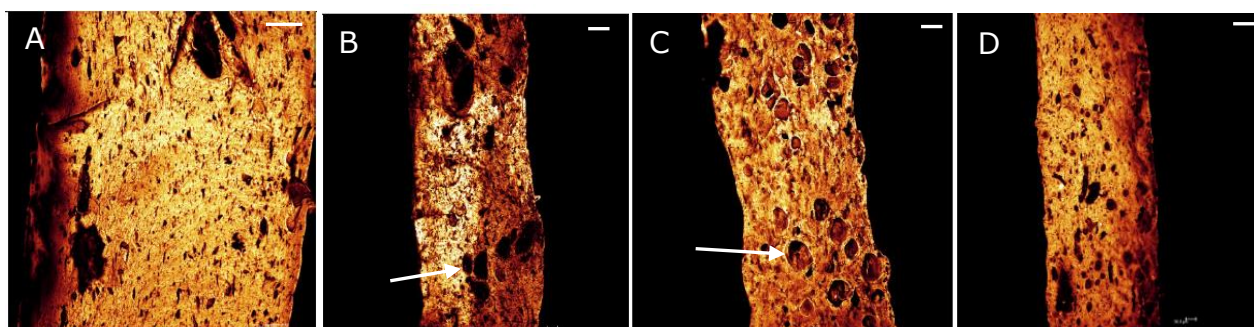


**Figure 52. Confocal light micrograph of intermediate cross-sections. (A) IP3, (B) IP3 + 10% PS, (C) IP3 + 10% MCC and (D) IP3 + 10% RF. White lines in top right corner relate to 100 µm scale bar.**

In Figure 53, intermediates following microtoming display, in more detail, the structure of both the CP and DP microstructure with staining at higher magnifications. The starch granules appear swollen in both IP3 + PS and FP3 + PS unlike rice starch granules in IP3 + RF and FP3 + RF. This observation supports the DSC thermographs in Figure 50, since no endothermic peak was apparent in FP3 + PS unlike FP3 + RF.

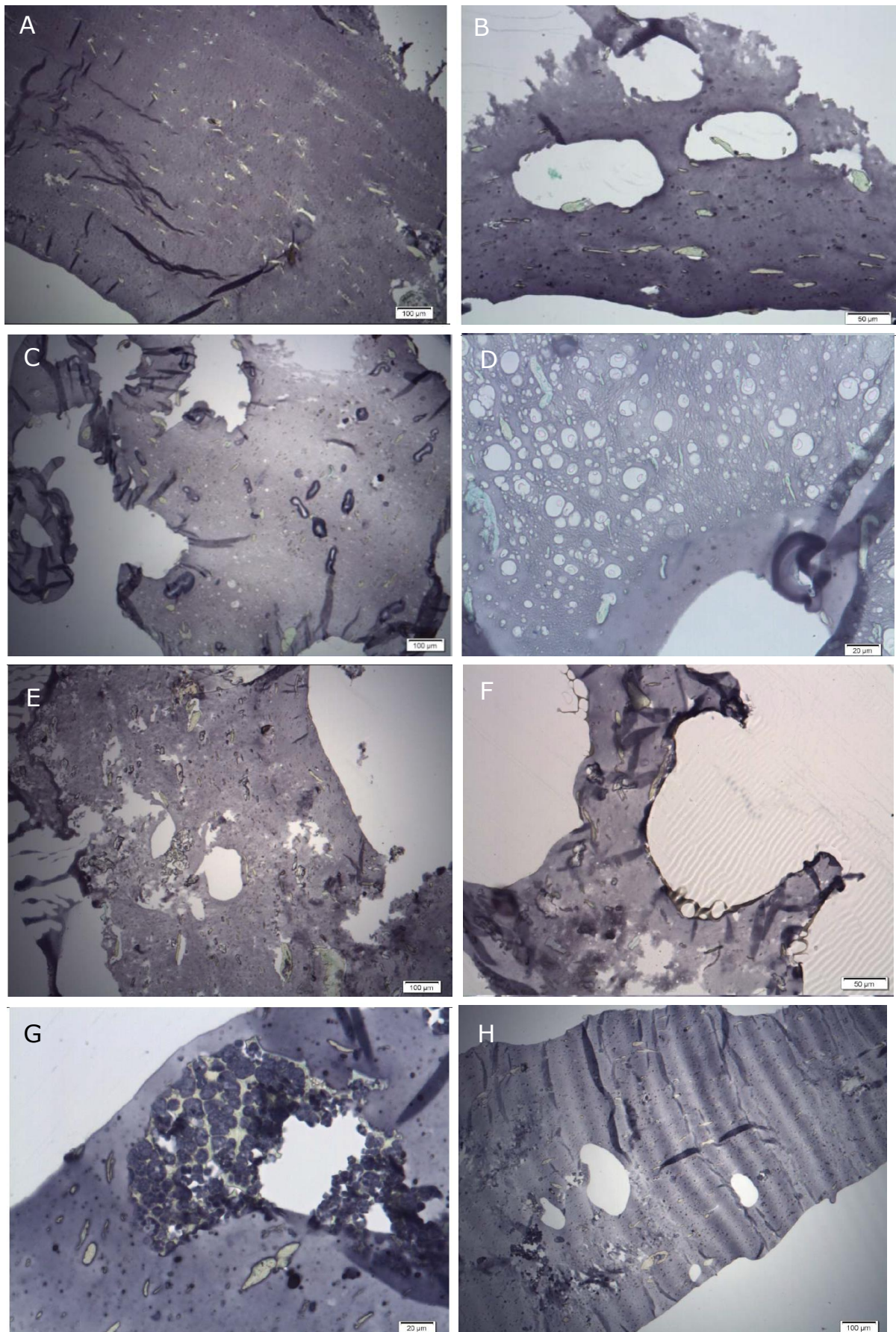


**Figure 53.** Light microscopy of intermediates and final products following microtoming and iodine staining. (A) IP3, (B) FP3, (C) IP3 + 10 % PS, (D) FP3 + PS, (E) IP3 + 10 % MCC (F) FP3 + 10 % MCC (G) IP3 + 10 % RF and (H) FP3 + 10 % RF.

Although hard to observe within micrographs, swelling of granules from intermediate to final product was in fact common amongst potato granules. However, swelling capacity was not exceeded prior to melting, leaving the granular structure still intact, even with the loss of crystalline order. Additionally the centre of the granules, thought to contain amorphous amylose, have leached out leaving just an amylose wall at the surface of the granule.

Particle size distribution of PS prior to addition into intermediates presented a mean diameter value of 543  $\mu\text{m}$  (Figure 40). When comparing this to the micrograph of singular starch granules, where diameters appear no greater than 100  $\mu\text{m}$  it would suggest that the extrusion process has had some effect on separating out aggregated granules.

Another interesting observation to highlight is the formation of spherical white spots with diameters between 5  $\mu\text{m}$  and 20  $\mu\text{m}$ , only present in final products containing PS, as displayed in Figure 53 D. It is thought this may be a result of phase separation of high and low  $M_w$  starch within the CP. Since the amylose and amylopectin in IP1 has gone through a significantly more violent cooking process, it is expected for the chains to be partially depolymerised; promoting phase separation. A similar phenomenon has been demonstrated by Tedeschi *et al.* (2016) in amorphous high  $M_w$  starch and sucrose blends, where spherical phase formation was observed at concentration ratios of 90:10 and 60:40 starch: sucrose (weight % on anhydrous basis). However, when comparing sizes of spheres, they appear much smaller in Figure 53 (<20  $\mu\text{m}$  vs. 500  $\mu\text{m}$ ).

Similarly, it could be argued that phase separation of single helices of amylose should not reveal differences in colour as iodine should still complex. Consequently, it could be suggested these spots are a result of amylose-lipid complex formation as the lipid being associated with the internal helices prevents iodine from complexing. However, an increase in amylose-lipid complexes was not

apparent in XRPD of FP3 + PS; suggesting this phenomenon should be apparent in all intermediate and final product micrographs. Similarly, morphology of amylose-lipid complexes observed in literature does not align with observations in micrographs which typically present a more elongated fibrous structure (Marinopoulou *et al.*, 2016; Perez and Bertoft, 2010; Zabar *et al.*, 2010).

Finally, double helical amylose formation into a crystalline form is considered highly resistant to temperature and therefore if prevalent within intermediates, would be unlikely to melt out in the frying stage. In addition, amylose retrogradation is considered a far quicker phenomenon than retrograded amylopectin, which has previously been characterised in hydrated DSC measurements (endothermic peak at ~60 °C). As these spherical white spots are only prevalent amongst potato starch final products it would suggest the PS amylose is retrograded. Interestingly, scanning electron micrographs of retrograded amylose from PS and maize starch, induced by leaving high water starch based systems at 25 °C for 4 days, show similar morphology to Figure 53 D with spherical or oval microstructures 10-20 µm in diameter (Utrilla-Coello *et al.*, 2013). To draw final conclusions, further work characterising intermediates and final products with known amylose-lipid complexation and retrogradation is required.

### 6.3.5 The impact of semi-crystalline material on the expansion and texture of final products

The influence of semi-crystalline material on the expansion ratio (ER) of intermediates is demonstrated in Figure 54 where IP3 is compared with the addition of 10 % PS, RF and MCC. ER of IP3 + PS was found to be statistically significantly greater than both IP3 + RF and IP3 + MCC ( $P < 0.05$ ), where it was the only semi-crystalline material to increase average ER of intermediates.

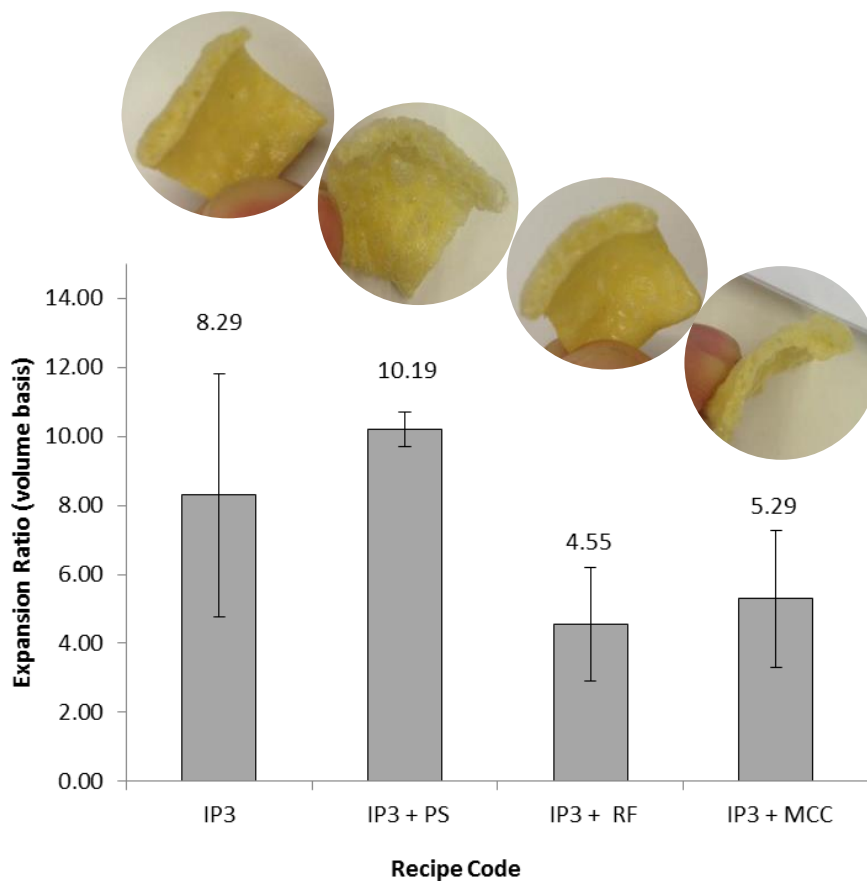


**Figure 54. Average expansion ratio (volume basis) ± standard deviation of IP3, IP3 + PS, IP3 + RF and IP3 + MCC.**

It is thought that the driver for differences in expansion of IP3 + PS intermediates may be associated with the amount and distribution of water prior to expansion. For the PS raw material, the water content was greater (18 %) than both MCC (5 %) and RF (13 %); since the less dense crystal packing allows a greater number of water molecules to be associated with the starch. To compensate for this, a smaller amount of additional water was added to the dry material during the manufacture of dough (Table 12). However, as melting of PS is apparent during frying (confirmed by DSC, XRPD and micrographs) the water associated with the crystalline regions could become available for plasticisation, which could decrease the  $T_g$  and viscosity of the matrix. If this is the case, one would expect bubble cells to appear in a similar region to where the potato starch granules appear in the matrix (as demonstrated in Figure 53 D). Similarly, melting of potato starch granules during frying is thought to alter the CP:DP with continued leaching of amylose forming part of the CP (van der Sman, 2016). As Chapter 5 concluded, the CP:DP has a significant effect on the rheological properties of the matrix which could partly contribute to enhanced expansion. However, due to the geometry of intermediates preventing successful mounting into the clamp, they were unable to be mechanically tested using DMTA. In addition, DMTA measured within pockets was found to lose the sensitivity of the machine with particle size being a greater factor for driving differences in storage and loss modulus than the composition of the sample itself. Therefore, viscoelastic properties of intermediates were unable to be characterised effectively.

Finally, it is stated in literature that nucleation is thought to occur in the centre of starch granules (van der Sman, 2016; Kokini and Moraru, 2003). Therefore, an increase in nucleation in addition to an increase in available water on melting of the granule coupled with a greater proportion of CP to stimulate bubble growth; it is unsurprising FP3 + PS is more expanded.

For FP3 + RF and FP3 + MCC, micrographs support that the semi-crystalline materials act as filler particles sitting aggregated within the CP with minimal change in morphology after frying (confirmed by DSC and XRPD). The function of filler particles in limiting expansion of the CP has previously been described in Section 2.5.1 with more detail recently published by van der Sman (2016). It is also likely that the low initial water content of both RF and MCC, combined with preferential absorption of water into the CP, reduced the availability of local water to lower the  $T_m$ ; promoting retention of crystalline order.

To build on the influence of MCC and RF on preventing expansion, SEM micrographs are presented of cross-sections (Figure 55). Figure 55 A demonstrates the heterogeneous microstructure of IP3 with a large central voids combined with smaller cells. In more detail it can be observed that smaller cell sizes are found at the product surface and larger cells in the centre of the product. It is thought this is a result of differences in the temperature gradient and water escape throughout intermediates since the surface will reach  $T_g$  sooner than the centre of the intermediate and escape of water from the surface will be easier; transitioning the expanded surface into a glass prior to the matrix reaching full expansion capacity. Following what is thought to be the glass transition of the intermediate surface, the central cavity will still be in the rubbery state, restricted by the glassy surface. As a result, pressure could increase and water loss will be limited. This is likely to promote bubble growth and cell coalescence of the central bubbles, driving large voids to appear in the centre of the product as often seen within literature (Nor *et al.*, 2013). Similarly, the inhomogeneity of intermediates prior to expansion, highlighted in Figure 52, is likely to promote inhomogeneity amongst all final products, as seen in Figure 55.

For FP3 + PS, the final product has a microstructure composing of a large proportion of small cell sizes (150  $\mu\text{m}$ ) and a small number of central voids with diameters in excess of 1 mm. The reduction in average cell size, when compared with IP3 is apparent in all samples containing PS. The smaller bubble cells could be suggested to support the hypothesis that nucleation occurs in the hilum of native starch granules, as cell diameters are a similar size to swollen potato starch granules (200 - 400  $\mu\text{m}$ ).

FP3 + RS and FP3 + MCC microstructures, on observation, appear to be most similar with a greater number of medium cell diameters (500 - 800  $\mu\text{m}$ ), opposed to a range of large (>1 mm) and small cells (<400  $\mu\text{m}$ ). At higher magnifications, aggregation of both RF and MCC were apparent sitting within cell walls (micrographs not show).

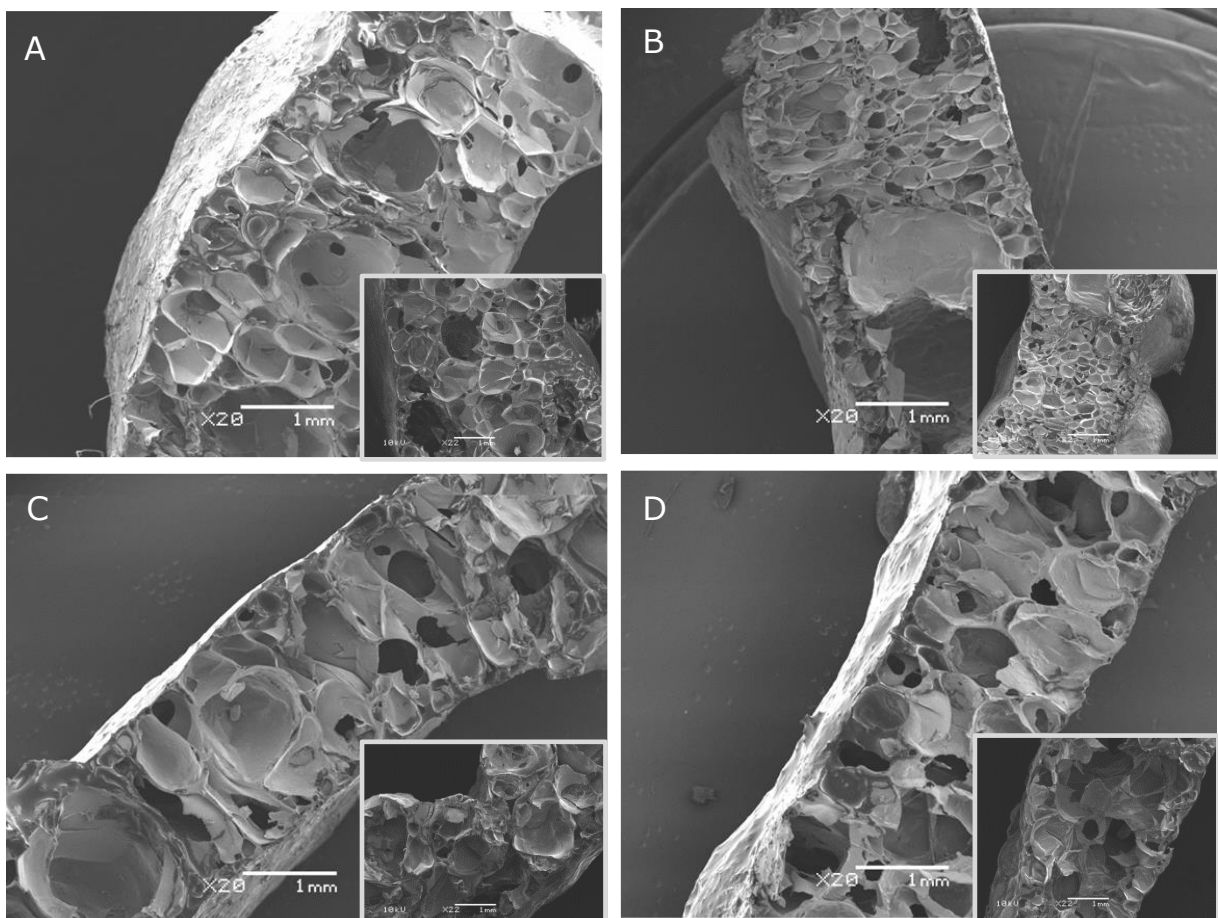


**Figure 55. Scanning electron micrographs of final products (A) FP3, (B) FP3 + PS, (C) FP3 + RF and (D) FP3 + MCC. Small micrographs show final product microstructures of trial repeats at x22 objective, Scale bar = 1 mm.**

In an attempt to characterise the differences in intermediates during expansion and couple this with the differences in final product microstructures, fast rate (40 °C/min) TGA was carried out. Figure 56 displays the loss of weight (%) and 1<sup>st</sup> derivative of intermediates with respect to temperature where results aligned with Chapter 5 (a sudden loss of water at ~ 180 °C). Results also appear to support that semi-crystalline material incorporated into an amorphous matrix promotes loss of water at lower temperatures (30 to 160 °C), with an average loss of  $5.43 \pm 0.55$  % water compared with IP3 with no semi-crystalline material which had an average loss of  $2.97 \pm 0.19$  %. It is hypothesised this is a result of the semi-crystalline material weakening the internal structure to facilitate water loss; however the change in the concentration of water in the amorphous region could play some role.

IP3 + MCC and IP3 + RF appear to have very similar 1<sup>st</sup> derivative traces whereby the greatest rate of water loss is broad between 170 to 240 °C. This is interesting as microstructures of final products appear most similar for IP3 + MCC and IP3 + RF. Conversely, IP3 + PS appears to have a sharper rate of loss of water at 180 °C with loss of water at lower temperatures more similar to that of 100 % amorphous intermediates (IP3). Since melting of amylopectin order in native PS during heating is apparent in intermediates it could be suggested that this enables the intermediates to function as amorphous composites, more similar to that of IP3. If the observation for retention of water to higher temperatures of IP3 and IP3 + PS were to translate to frying conditions, it could be suggested that retention of water is partly responsible for the increase in expansion by reducing the viscosity of the matrix and extending the time in the rubber state prior to  $T_g$ .

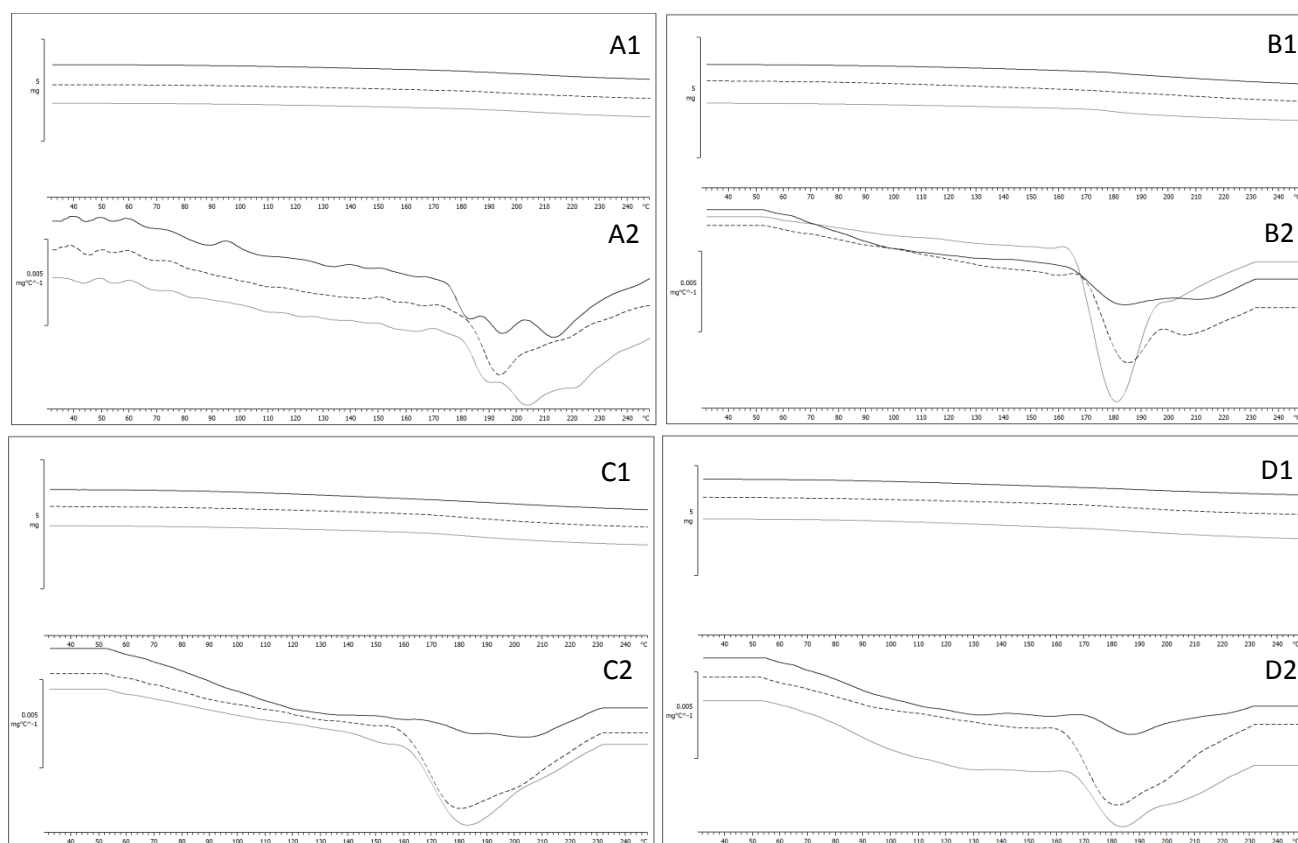


Figure 56. Thermo-gravimetric analysis (TGA) of intermediates at 40 °C/min. 1) Weight loss (%) and 2) 1<sup>st</sup> derivative. (A) IP3, (B) IP3 + PS, (C) IP3 + RF, (D) IP3 + MCC. 3 replicates per sample code.

### 6.3.5.1 Texture attributes of final products

Since SEM identified the addition of semi-crystalline material to successfully alter the microstructure of final products, preliminary sensory analysis was carried out to determine if the changes in microstructure and composition change the perceived attributes upon consumption. The attributes assessed were: hardness, rate of breakdown, melting and tooth packing as these properties were considered the key that limit the final product when compared with commercialised products.

Figure 57 displays the average degree of difference scores from an un-trained consumer panel where FP3 is reference (0) and the other final products (FP3 + RF, FP3 + MCC and FP3 + PS) are displayed relative to reference (*refer to Chapter 3 for scoring definitions*).

In general, it can be observed that the addition of semi-crystalline material at a 10 % weight basis can alter the attributes of final products, demonstrating how a design led approach to the development of snacks can be achieved. However, as expected, an un-trained panel increased the degree of error in the results; hence differences detected were not statistically significantly different. Similarly, the inhomogeneous distribution of the semi-crystalline material throughout the CP, highlighted in Figure 52, was likely to promote variability within sample batches driving further discrepancies throughout panel scores. Finally, 90 % of final products were manufactured from the same material, and following breakdown of the initial microstructure, it is clear from Figure 57 that the DP has less impact on the textural attributes, with differences between all final products reducing following melting.

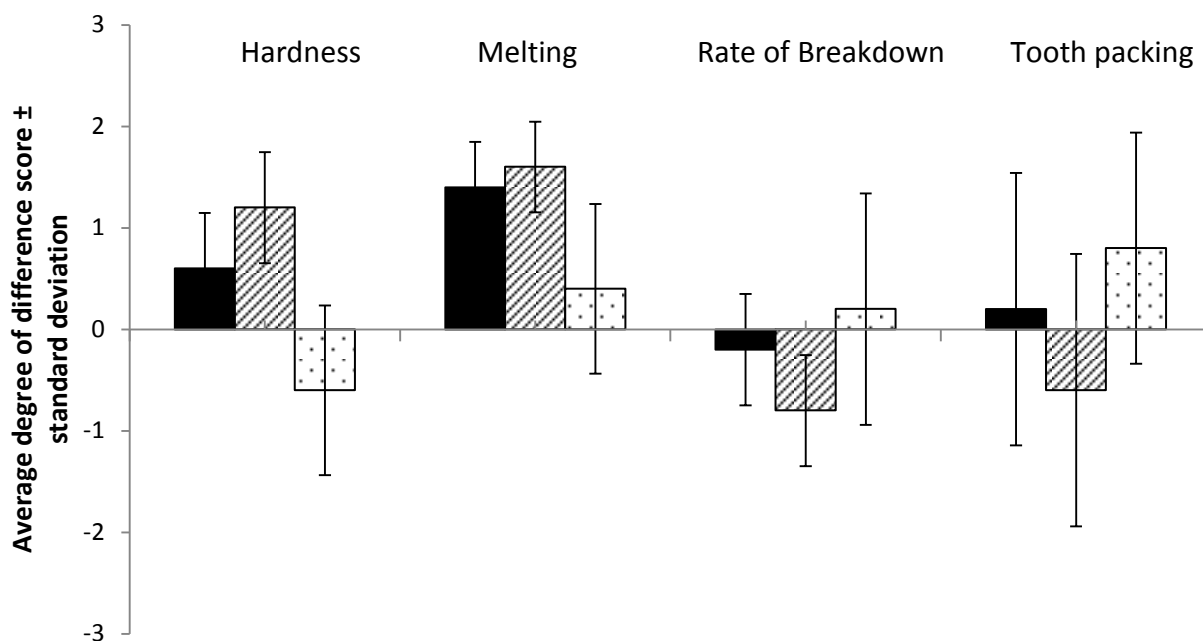


**Figure 57. Average degree of difference score ± standard deviation based on an un-trained sensory panel of 5 people. FP3 is 0 across all attributes as a reference, ■ FP3 + RF, ▨ FP3 + MCC and □ FP3 + PS.**

The addition of 10 % RF or MCC seems to alter final product attributes similarly with an increase in average hardness, perceived melting and a decrease in average rate of breakdown (Figure 57). With both FP3 + MCC and FP3 + RF resulting in a reduction in the ER ratio (density of the final product), it is unsurprising hardness is perceived greater; supporting the inverse relationship between hardness and ER, as demonstrated in both Chapter 5 and literature (Nor *et al.*, 2013; Lillford, 2001). Similarly, FP3 + PS, which had a statistically significant ( $P < 0.05$ ) increase in ER was perceived on average to be softer than IP3.

Melting, defined as 'the ease with which the product disappear to a liquid / pulp without chewing' was facilitated by the addition MCC, RF and PS, however MCC and RF were found on average to increase melting considerably more. With the melting attribute removing the impact of chewing, the initial microstructure of the final product is likely to dominate the attribute later into the eating experience. As a result, the reduction in melting of FP3 + PS, when compared with FP3+ MCC and MCC + RF, could be explained by the differences in microstructure characterised by SEM. The reduction in cell diameters, with a greater number of smaller cells, could limit the access of saliva to the central cavity of the snack which could slow hydration. Similarly, the hypothesised phase separation only observed in the CP of final products with the addition of PS, could play some role in affecting the melting attribute, particularly if this phase separation was a result of re-crystallised amylose.

Interestingly rate of breakdown, which takes into consideration the impact of chewing, was only found to be significantly changed by the addition of MCC. It could be suggested that following the breakdown of the aerated structure into a bolus, the retention of crystalline material seems to extend the rate of breakdown. It is thought this could be a consequence of preventing hydration as following the breakdown of the CP, the crystalline DP material will having less affinity for water. Conversely, when taking into consideration the impact of chewing, differences in initial microstructure are less dominating and therefore FP3 + PS, which had no crystalline structure in the DP following frying, had the most similar breakdown to FP3.

On average, the addition of MCC seems the most effective at reducing the attribute of tooth packing following clearance however differences between all final products are negligible. This could be a result of semi-crystalline DP reducing the solubility of the DP following the CP breakdown (Peksa *et*

*al.*, 2016). However, based on the results it would suggest the CP dominates the tooth packing attribute.

## 6.4 Conclusion

This chapter has attempted to test proof of principle in creating a homogenous CP prior to intermediate manufacture that can have 10 % semi-crystalline materials dispersed throughout; changing both intermediate and final product microstructure. In an attempt to reduce further starch damage and retain crystallinity of the DP, single-screw low shear extrusion was chosen as the process for combining the pre-gelatinised CP (IP3) and additional materials (PS, RF and MCC). This method of manufacture resulted in inhomogeneous intermediates since mixing was not vigorous enough to distribute the semi-crystalline materials throughout the continuous matrix. It is expected that a similar result would be apparent for the distribution of water throughout intermediates since water will preferentially be picked up by the pre-gelatinised CP than the semi-crystalline DP. Therefore, in future development it would be advised to input mixing elements into the screw profile and to consider pre-hydration of the semi-crystalline material prior to extrusion, depending on the desired functionality of that phase.

As concluded in Chapter 5, intermediates manufactured from melts as low as 30 - 40 % water content (wwb) retrograde upon air drying. However, the impact of retrogradation on the expansion and textural attributes of intermediates is still to be determined and it is unknown whether this is a desirable factor.

When concluding the impact of semi-crystalline materials on the expansion and textural attributes of final products, it is clear PS has unique properties. PS functions primarily as the DP but is thought to also enhance the CP properties following melting, with PS being the only additional ingredient that increased average ER. Additionally, the formation of spherical white spots throughout final products was unique to PS with no apparent formation in FP3, FP3 + RF or FP3 + MCC. Primarily thought to be phase separation that was promoted by the differences in the degree to which the two sources of amylose have been processed. However, further work needs to be conducted to test this.

RF and MCC seemed to function similarly in preventing expansion by acting as filler particles during frying and consequently both reduced average ER. The higher melting temperatures of these semi-crystalline materials coupled with reduced water contents enabled them to retain crystallinity into final products. As a result, FP3 + MCC and FP3 + RF were more effective at altering the textural attributes of final products than FP3 + PS, when compared against FP3. However, following the breakdown of the final products into a bolus, the semi-crystalline materials appeared to be less effective at altering attributes with negligible differences in rate of breakdown and tooth packing; assumed to be dominated by the 90 % IP3 (CP).

XRPD, DSC and microscopy have been extremely effective methods in characterising the state of both the CP and DP throughout the manufacturing process. Unfortunately, due to the fragility of very thin intermediates, DMTA was unable to be carried out 'as is' on intermediates to understand the influence of semi-crystalline materials on the bulk viscoelastic properties of intermediates to build on Chapter 5. However, TGA was very effective in highlighting the differences in temperature events from using slow rates (typically associated with analytical methods) and faster rates that are more characteristic of frying. Similarly, TGA of intermediates following the addition semi-crystalline

materials characterised how semi-crystalline materials promote loss of water at lower temperatures. Interestingly, PS was less effective at promoting this, assumed to be as a result of the crystalline regions melting at the early stages of heating and therefore intermediates functioned more similar to that of amorphous intermediates (IP3).

## Chapter 7 Final conclusions and future work

To conclude, this work has built on the proposed idea of a design-led approach to the microstructure of intermediates and consequently the expansion properties of intermediates during frying. Since the manufacturing model tested was proprietary, much of the work presented focused on process optimisation where single-screw extrusion at 40 % barrel water content with a stretching element was considered most optimum. However, further work is required to understand the influence of homogenous distribution of the DP, which wasn't achieved with a single-screw conveying extruder. Future work should optimise the screw profile to have mixing elements that encourage homogenous mixing but do not breakdown the starch to the extent of twin-screw extrusion.

In addition, this work has acted as a screening tool for the various analytical methods used in characterising the key properties of intermediates to identify the dominant drivers in differences in expansion. Whilst many of the analytical tools used have been insightful, the limitations associated with these methodologies have been raised. Particularly, the universal limitation being that expansion of intermediates within industry is associated with very high heating rates, most often in hot oil, which cannot currently be replicated during analytical measurements. To over-come this, fast rate TGA at 40 °C/min was adapted into intermediate characterisation and continued to build an understanding of the influence of heating rate on the properties of intermediates. In particular, highlighting the differences detected during DMTA measurements that can often be an artefact of slow heating rates (5 °C/min). By doing so, the importance of water in driving the properties of intermediates and final products was highlighted; where viscoelastic properties of intermediates measured by DMTA seemed to be partly governed by the water loss mechanisms during heating.

Water is critical in determining  $T_g$  at an appropriate temperature, effects the viscosity of the matrix and is the blowing agent that once vaporised, drives expansion. Therefore, upon the intension of altering the microstructure of final products, which is often achieved by changes in processing and ingredients (altering the CP:DP); water as a potential to drive these changes, should not be overlooked. Similarly, to build on method development and better characterise intermediates and final products, a focus should be put on developing a method to take measurements at faster heating rates and within hot oil.

With the addition of semi-crystalline materials altering both the microstructure of intermediates and final products; the proof of principle to a design led approach to microstructure has been demonstrated. However, this work has highlighted the complexity in biopolymer intermediates and that taking an over-simplified 'CP/DP' approach should be re-considered. Additional DP properties including the wetting/non-wetting and hard/soft interaction of fillers particles with the CP should also be considered.

Finally, this work has provided an effective screening tool for assessing the functionality of DP ingredients in an amorphous matrix. One key conclusion from Chapter 6 is that semi-crystalline material at only 10 % of the total recipe, limits the effectiveness of altering the textural attributes following bolus formation, as the amorphous matrix at 90 % seems to dominate the latter part of the texture journey. Similarly, this work was within the initial scoping of the project and as a result only 3 semi-crystalline DPs were assessed in addition to the sensory results presented being conducted using an un-trained panel as sensory attribute validation using a trained panel was not within the scope of this project.

As a result, future work should continue to understand the influence of alternative DPs on the microstructure and textural attributes of final products as well as looking into potential substrates that could change the properties of the CP, enabling the whole texture journey to be optimised. Finally, all future work should validate textural attributes using a trained sensory panel.

## Chapter 8 Appendices

Appendix 1. Material Safety Data Sheet (MSDS) of raw maize grits supplied by Whitworth Bros. Ltd.

**Whitworth Bros.Ltd.**  
FLOUR MILLERS

**Product Specification**  
YG600 MAIZE GRITS – WORKSOP

Head Office: Victoria Mills, Wellingborough, Northants. NN8 2DT

Tel: (01933) 441000 Email: [enquiries@whitworthbros.ltd.uk](mailto:enquiries@whitworthbros.ltd.uk) Fax: (01933) 222523

### Product Information

<b>Name:</b> YG600 – Maize Grits	<b>Code:</b> FL4131
----------------------------------	---------------------

<b>Product Description:</b>	A coarse yellow maize grit milled from French maize. Bland odour and taste – no taints. Relatively free flowing.
-----------------------------	--

Ingredient	% in Component	% in Flour	Supplier	Country of Origin
Maize	n/a	100.00	Approved Merchants	France
<b>Ingredients Declaration:</b>		Maize		
<i>No additives are used in the production of this material.</i>				

Analytical Specification		Minimum	Target	Maximum
<b>Moisture (%)</b>		12.5	-	15.0
<b>Oil Content (%)</b>		-	-	0.9
<b>Particle Size</b>	<b>&gt;1000µ (%)</b>	-	-	0.0
	<b>&gt;710µ (%)</b>	0.0	-	2.0
	<b>&gt;500µ (%)</b>	50.0	-	80.0
	<b>&gt;355µ (%)</b>	20.0	-	50.0
	<b>&gt;250µ (%)</b>	-	-	5.0
	<b>Through 250µ (%)</b>	-	-	2.0

**Whitworth Bros.Ltd.**  
FLOUR MILLERS

**Product Specification**  
YG600 MAIZE GRITS – WORKSOP

Head Office: Victoria Mills, Wellingborough, Northants. NN8 2DT

Tel: (01933) 441000

Email: [enquiries@whitworthbros.ltd.uk](mailto:enquiries@whitworthbros.ltd.uk)

Fax: (01933) 222523

<b>GMO</b>	
It is the policy of Whitworth Bros. Ltd. not to buy, manufacture or use any genetically modified products or ingredients, or any materials made using GM technology. All maize is sampled and PCR Tested prior to being accepted for intake at Whitworth Bros Ltd.	

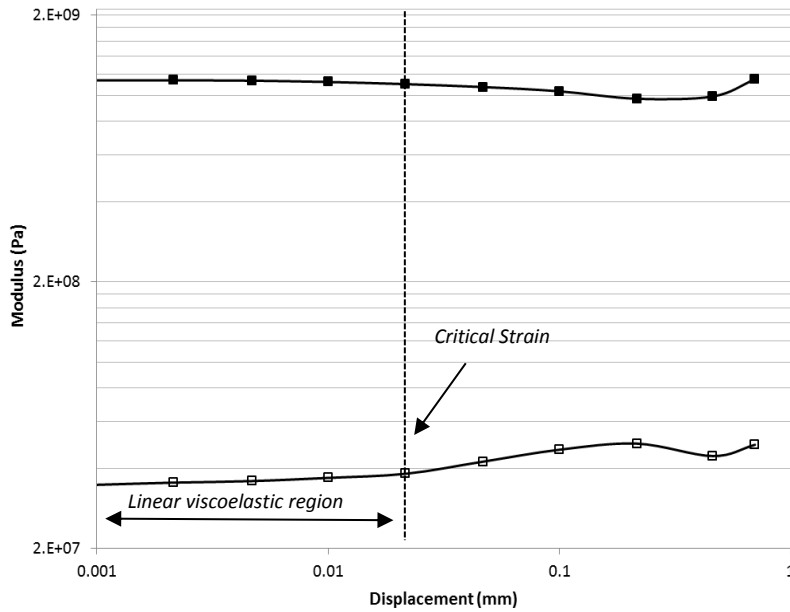
<b>Irradiated Material</b>	
Whitworth Bros. Ltd. do not use irradiated material in any products.	

<b>Nutritional Information (per 100g)</b>	
Energy (KJ)	1265
Energy (KCal)	300
Total Fat:	1.6g
- of which saturates:	0.2g
- of which mono-unsaturates:	0.4g
- of which poly-unsaturates:	0.8g
Carbohydrate:	56.7g
- of which sugars:	1.1g
- of which starch:	55.6g
Fibre(non-starch polysaccharides):	16.9g
Protein:	6.4g
Sodium:	0.04g
Total Salt	0.10g
Moisture:	13.1g
Information Source:	Analysis – Alcontrol Laboratories, UKAS Number 1349

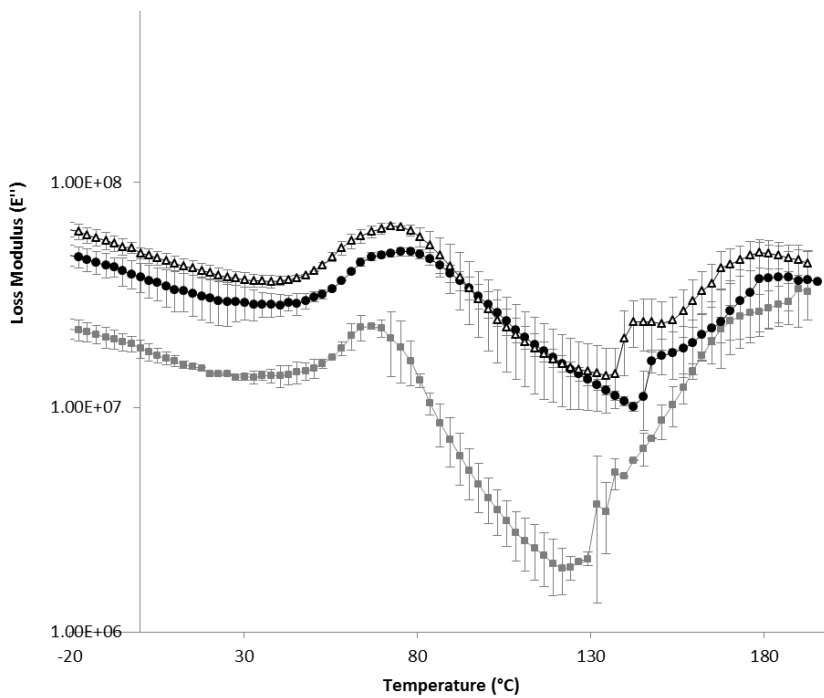
<b>Microbiological Testing</b>	
Not manufactured to microbiological specification, levels will reflect those naturally occurring in Maize which will vary from season to season.	
Product is intended for further thermal processing.	

<b>Contaminants Monitoring</b>	
Whitworth Brothers Ltd. operates a surveillance programme for potential contaminants of maize and maize products. The results of this testing demonstrates compliance with the legal limits. All Maize shipments are fully tested prior to acceptance by Whitworth Bros Ltd.	
Contaminant	Limit
DON (Deoxynivalenol)	750 µg/kg
ZON (Zearalenone)	200 µg/kg
OTA (Ochratoxin A)	3.0 µg/kg
Fumonisin	1400 µg/kg
Aflatoxins (Total)	4.0 µg/kg
Aflatoxin B1	2.0 µg/kg
Cadmium	0.1 mg/kg
Lead	0.2 mg/kg
Pesticide Residues	Not exceeding MRL

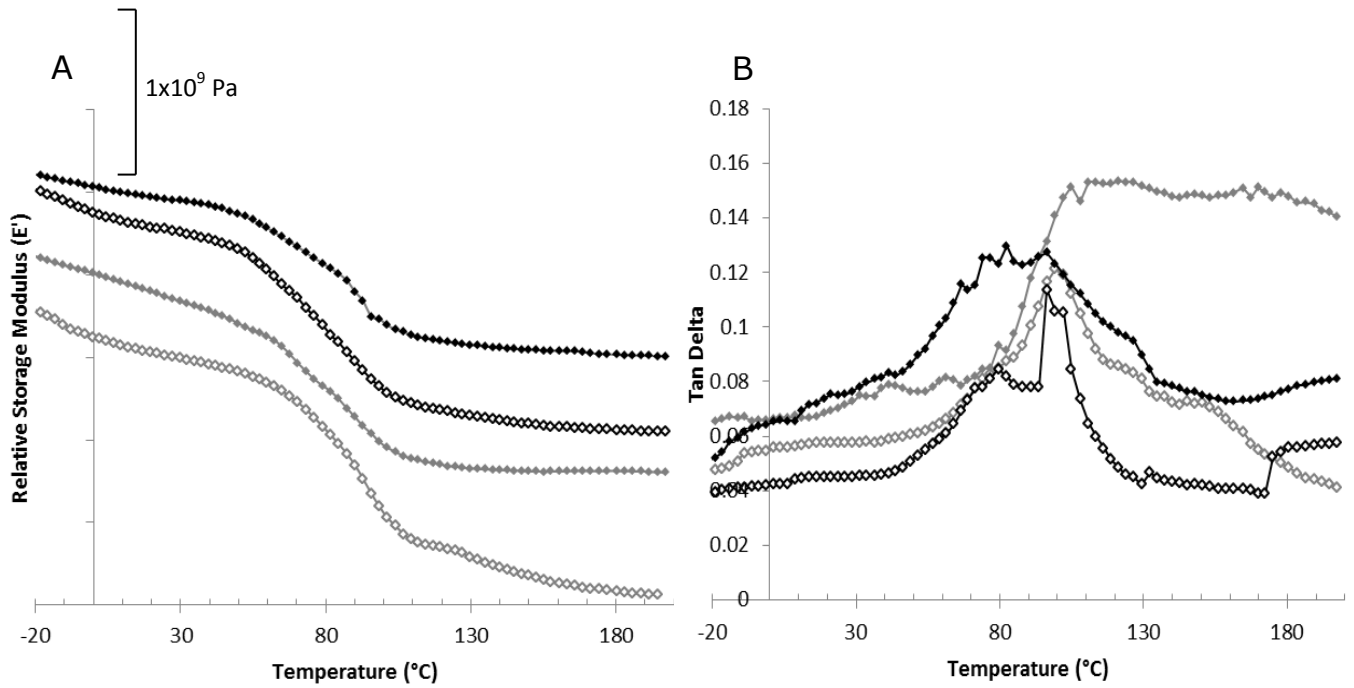
**Appendix 2.** —■—■— Storage modulus ( $E'$ ) and —□—□— Loss modulus ( $E''$ ) of IP3 strain sweep from 0.001 mm to 1 mm displacement whereby critical strain is in excess of 0.02 mm (>10 % difference in original  $E'$  and  $E''$ ).



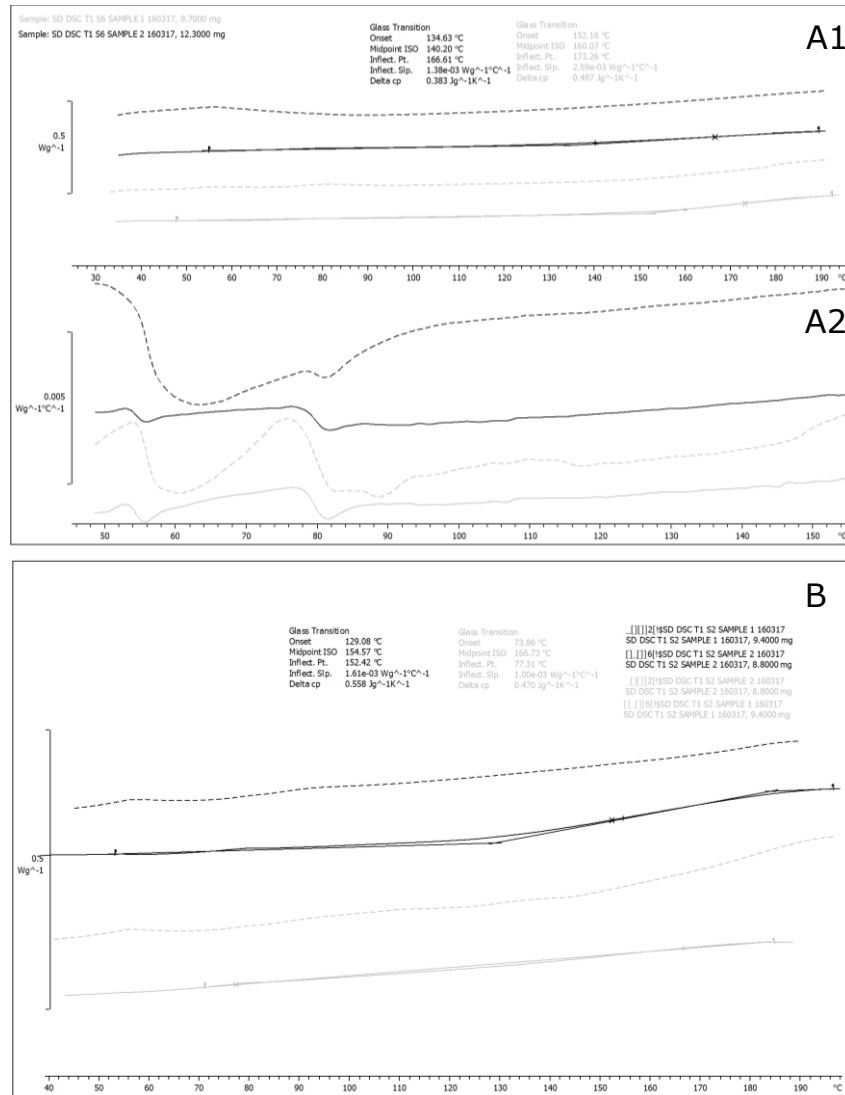
**Appendix 3.** Loss modulus ( $E''$ ) of —●—●— IP4, —△—△— IP4 + grease —■—■— IP2 40 with respect to temperature from -20 to 200 °C, measured by DMTA. Error bars based on 3 replicates.



**Appendix 4. (A) Relative storage modulus ( $E'$ ) and (B)  $\text{Tan } \delta$  ( $E''/E'$ ) of milled intermediates at particle sizes  $>1$  mm and  $<1$  mm within aluminium pockets from  $-20$  to  $200$  °C.  $\diamond$ - $\diamond$ - $\diamond$  IP2 40  $>1$ mm,  $\blacklozenge$ - $\blacklozenge$ - $\blacklozenge$  IP2 40  $<1$  mm,  $\diamond$ - $\diamond$ - $\diamond$  IP4  $>1$  mm and  $\blacklozenge$ - $\blacklozenge$ - $\blacklozenge$  IP4  $<1$  mm (repeats).**



**Appendix 5. DSC thermographs of (A) IP2 40 and (B) IP4 at a heating rate of 10 °C/min. (A1) Heat flow and (A2) 1<sup>st</sup> derivate.**



**Appendix 6. Raw data of un-trained sensory panel scores presented in Chapter 6 (degree of difference against IP3 which is reference).**

	<b>Hardness</b>	<b>Rate of Breakdown</b>	<b>Melting</b>	<b>Tooth Packing</b>
<b>Reference (IP3)</b>	0	0	0	0
<b>IP3 + RF</b>	0	0	0	0
	1	0	2	1
	1	-1	3	0
	1	0	2	0
	0	0	0	0
<b>Average</b>	0.6	-0.2	1.4	0.2
<b>Standard Deviation</b>	0.55	0.45	1.34	0.45
<b>IP3 + MCC</b>	1	0	3	0
	2	-2	2	-1
	0	-1	1	0
	2	-1	2	-1
	1	0	0	-1
<b>Average</b>	1.2	-0.8	1.6	-0.6
<b>Standard Deviation</b>	0.84	0.84	1.14	0.55
<b>IP3 + PS</b>	0	0	0	0
	0	0	0	1
	-2	0	0	2
	-1	0	0	0
	0	1	2	1
<b>Average</b>	-0.6	0.2	0.4	0.8
<b>Standard Deviation</b>	0.89	0.45	0.89	0.84

## Chapter 9 References

Addesso, K., Dzurenko, T.E., Moisey, M.J., Levine, H., Slade, L., Manns, J.M., Fazzolare, R.D., Ievolella, J. and Wang, M.Y. (1995) Production of chip-like starch based snacks. US Patent No. US5500240. Available from: <http://www.google.co.uk/patents/US5500240> [Accessed: March 5, 2017].

Ahmed, Z.S. (1999) Physico-chemical, structural and sensory quality of corn-based flax-snack. *Food Nahrung*. **43**(4), 253–258.

Alcázar-Alay, S.C. and Meireles, M.A.A. (2015) Physicochemical properties, modifications and applications of starches from different botanical sources. *Food Science and Technology (Campinas)*. **35**(2), 215–236.

Amin, S., Barnett, G. V, Pathak, J.A., Roberts, C.J. and Sarangapani, P.S. (2014) Protein aggregation, particle formation, characterization & rheology. *Current Opinion in Colloid & Interface Science*. **19**(5), 438–449.

Askadskii, A., Popova, M., Matseevich, T. and Afanasyev, E. (2014) The Influence of the Degree of Crystallinity on the Elasticity Modulus of Polymers. In *Environmental Engineering. Advanced Materials Research*. Trans Tech Publications, 640–643.

Aust, L.B., Gacula, M.C., Beard, S.A. and Washam, R. (1985) Degree of Difference Test Method in Sensory Evaluation of Heterogeneous Product Types. *Journal of Food Science*. **50**(2), 511–513.

Ayadi, F., Rosentrater, K.A., Muthukumarappan, K. and Kannadhasan, S. (2016) Effects of Amylose-To-Amylopectin Ratios on Binding Capacity of DDGS/Soy-Based Aquafeed Blends. *Journal of Food Research*. **5**(5), 42-43.

Babin, P., Della Valle, G., Dendievel, R., Lourdin, D. and Salvo, L. (2007) X-ray tomography study of the cellular structure of extruded starches and its relations with expansion phenomenon and foam mechanical properties. *Carbohydrate Polymers*. **68**(2), 329–340.

Badrie, N. and Mellowes, W.A. (1991) Effect of Extrusion Variables on Cassava Extrudates. *Journal of Food Science*. **56**(5), 1334–1337.

Bagnell, R. (2012) Polarized light microscopy. *UNC School of Medicine*. **73**(3), 206–208.

Balasubramanian, S., Singh, K.K., Patil, R.T. and Onkar, K.K. (2012) Quality evaluation of millet-soy blended extrudates formulated through linear programming. *Journal of Food Science and Technology*. **49**(4), 450–458.

Baud, B., Colonna, P., Della Valle, G. and Roger, P. (2001) Macromolecular degradation of extruded starches measured by HPSEC-MALLS. *Starch - Advances in Structure and Function*. **3**(1), 40–44.

Bhandari, B.R., Datta, N., Crooks, R., Howes, T. and Rigby, S. (1997) A semi-empirical approach to optimise the quantity of drying aids required to spray dry sugar-rich foods. *Drying Technology*. **15**(10), 2509–2525.

Bhandari, B.R. and Howes, T. (1999) Implication of glass transition for the drying and stability of dried foods. *Journal of Food Engineering*. **40**(1–2), 71–79.

Bhattacharya, S. (2017) Extrusion Technology and Glass Transition. In *Non-Equilibrium States and Glass Transitions in Foods*, Elsevier Ltd., 137-152.

Biliaderis, C.G. (2009) Structural Transitions and Related Physical Properties of Starch. *Starch*. **5**(2), 293–372.

Biliaderis, C.G. and Galloway, G. (1989) Crystallization behavior of amylose-V complexes: Structure-property relationships. *Carbohydrate Research*. **189**(1), 31–48.

Blennow, A., Bay-Smidt, A.M., Olsen, C.E. and Møller, B.L. (2000) The distribution of covalently bound phosphate in the starch granule in relation to starch crystallinity. *International Journal of Biological Macromolecules*. **27**(3), 211–218.

Bowen, S.E., Gray, D.A., Giraud, C., Majzoobi, M., Testa, C.E.M., Pérez, L.A.B. and Hill, S.E. (2006) Lipid oxidation and amylopectin molecular weight changes occurring during storage of extruded starch samples. *Journal of Cereal Science*. **43**(3), 275–283.

Brent, J.L., Mulvaney, S.J., Cohen, C. and Bartsch, J.A. (1997) Viscoelastic properties of extruded cereal melts. *Journal of Cereal Science*. **26**(1), 313–328.

Carvalho, C.W.P., Takeiti, C.Y., Onwulata, C.I. and Pordesimo, L.O. (2010) Relative effect of particle size on the physical properties of corn meal extrudates: Effect of particle size on the extrusion of corn meal. *Journal of Food Engineering*. **98**(1), 103–109.

Case, S.E., Hamann, D.D. and Schwartz, S.J. (1992) Effect of starch gelatinization on physical properties of extruded wheat- and corn-based products. *Cereal Chemistry (USA)*. **69**(3), 401-404.

Chanvrier, H., Appelqvist, I.A.M., Li, Z., Morell, M.K. and Lillford, P.J. (2013) Processing high amylose wheat varieties with a capillary rheometer: Structure and thermomechanical properties of products. *Food Research International*. **53**(1), 73–80.

Chanvrier, H., Chaunier, L., Della Valle, G. and Lourdin, D. (2015) Flow and foam properties of extruded maize flour and its biopolymer blends expanded by microwave. *Food Research International*. **76**(4), 567–575.

Chanvrier, H., Della Valle, G. and Lourdin, D. (2006) Mechanical behaviour of corn flour and starch-zein based materials in the glassy state: A matrix-particle interpretation. *Carbohydrate Polymers*. **65**(3), 346–356.

Chaudhary, D.P., Kumar, S. and Langyan, S. (2013) *Maize: Nutrition dynamics and novel uses*. London: Springer, 1–161.

Chinnaswamy, R. and Hanna, M.A. (1990) Macromolecular and Functional Properties of Native and Extrusion-Cooked Corn Starch. *Cereal and Feed Industry*. **67**(5), 490–499.

Chinnaswamy, R. and Hanna, M.A. (1987) Relationship between Amylose content and extrusion expansion properties of corn starches. *Cereal Chemistry*. **65**(2), 138–143.

Copeland, L., Blazek, J., Salman, H. and Tang, M.C. (2009) Form and functionality of starch [online]. University of Sydney. Available from: [https://www.researchgate.net/publication/223514163\\_Form\\_a\\_functionality\\_of\\_starch](https://www.researchgate.net/publication/223514163_Form_a_functionality_of_starch) [Accessed: 5 March 2017].

Chung, H.J. and Lim, S.T. (2006) Physical aging of amorphous starches (a review). *Starch/Staerke*. **58**(12), 599–610.

Cieśła, K. and Eliasson, A.C. (2007) DSC studies of retrogradation and amylose–lipid complex transition taking place in gamma irradiated wheat starch. *Nuclear Instruments and Methods in Physics Research Section B: Beam Interactions with Materials and Atoms*. **265**(1), 399–405.

Coral, D.F., Pineda-Gómez, P., Rosales-Rivera, A. and Rodriguez-Garcia, M.E. (2009) Determination of the gelatinization temperature of starch presented in maize flours. *Journal of Physics: Conference Series*. **167**(4), 12057.

CPS Industry News (2015) Meal skippers, social Gatherers driving snack industry growth [online]. Available from: <http://www.cspdailynews.com/category-news/snacks-candy/articles/meal-skippers-social-gatherers-driving-snack-industry-growth>. [Accessed: November 2, 2016].

Davies, S.L. (2016) Re-design of snack pellet manufacture to address limitations in global production : a preliminary study. *Undergraduate Dissertation: The University of Nottingham*, 1–36.

Day, L. and Golding, M. (2016) Food Structure, Rheology, and Texture [online]. Available from: [http://www.sciencedirect.com/science/article/pii/B978008100596503\\_4120](http://www.sciencedirect.com/science/article/pii/B978008100596503_4120) [Accessed: September 2, 2017].

Ditudompo, S., Takhar, P.S., Ganjyal, G.M. and Hanna, M.A. (2013) The Effect of Temperature and Moisture on the Mechanical Properties of Extruded Cornstarch. *Journal of Texture Studies*. **44**(3), 225–237.

Dogan, H., Romero, P.A., Zheng, S., Cuitino, A.M. and Kokini, J.L. (2008) Chapter 17 - Characterization and Prediction of the Fracture Response of Solid Food Foams. In Campbell, G.M., Scanlon, M.G. and Pyle, D.L. eds. *Bubbles in Food 2*, 163–174.

Donovan, J.W. (1979) Phase transitions of the starch–water system. *Biopolymers*. **18**(2), 263–275.

Doyle, M.J. (2000) On the effect of crystallinity on the elastic properties of semicrystalline polyethylene. *Polymer Engineering & Science*. **40**(2), 330–335

Duizer, L.M. (2003) Physiological measures related to crispness perception of extruded snacks [online]. *PhD Thesis: Massey University*. Available from: <https://mro.massey.ac.nz/handle/10179/2017> [Accessed: May 4, 2017].

Ehrenstein, G.W., Riedel, G. and Trawiel, P. (2004) Chapter 6: Dynamic Mechanical Analysis. In *Thermal Analysis of Plastics: Theory and Practice*, 236–299.

Emerson, D.B., Russell, K.M.K. and Trezza, T.A. (2011) Pellet drying process [online]. US Patent No: US20090258113. Available from: <http://www.google.com/patents/US20090258113> [Accessed: December 3, 2016].

Enrione, J.I., Díaz, C.P., Matiacevich, S.B.E. and Hill, S. (2012) Mechanical and Structural Stability of an Extruded Starch-protein-polyol Food System. *Journal of Food Research*. **1**(2), 224–232.

Fallahi, P., Muthukumarappan, K. and Rosentrater, K.A. (2016) Functional and Structural Properties of Corn, Potato, and Cassava Starches as Affected by a Single-Screw Extruder. *International Journal of Food Properties*. **19**(4), 768–788.

Fan, J.T. (1994) Bubble growth and starch conversion in extruded and baked cereal systems. *PhD Thesis: University of Nottingham*.

Finkenstadt, V.L., Felker, F.C., Fanta, G.F., Kenar, J.A., Selling, G.W., Hornback, K.J. and Fisk, D.L. (2016) Extruded foams prepared from high amylose starch with sodium stearate to form amylose inclusion complexes. *Journal of Applied Polymer Science*. **133**(13), 136-142.

Fredriksson, H., Silverio, J., Andersson, R., Eliasson, A.C. and Aman, P. (1998) The influence of amylose and amylopectin characteristics on gelatinization and retrogradation properties of different starches. *Carbohydrate Polymers*. **35**(3-4), 119-134.

Frost, K., Kaminski, D., Kirwan, G., Lascaris, E. and Shanks, R. (2009) Crystallinity and structure of starch using wide angle X-ray scattering. *Carbohydrate Polymers*. **78**(3), 543-548.

Fu, Z.Q., Wang, L.J., Li, D., Zhou, Y.G. and Adhikari, B. (2013) The effect of partial gelatinization of corn starch on its retrogradation. *Carbohydrate Polymers*. **97**(2), 512-517.

Gaudin, A.M. (1926) An investigation of crushing phenomenon [online]. The American Institute of Mining, Metallurgical, and Petroleum Engineers. Available from: <http://www.onemine.org/document/abstract.cfm?docid=164880&title=An-Investigation-Of-Crushing-Phenomena> [Accessed: March 7, 2017].

Gomez, M.H. and Aguilera, J.M. (1984) A Physicochemical Model for Extrusion of Corn Starch. *Journal of Food Science*. **49**(1), 40-43.

González, R.J., Cavada, E.P., Peña, J.V., Torres, R.L., Greef, D.M. and Drago, S.R. (2013) Extrusion Conditions and Amylose Content Affect Physicochemical Properties of Extrudates Obtained from Brown Rice Grains. *International Journal of Food Science*. **51**(3) 407-415.

Gudipati, V., Chouksey, M.K. and Thachil, M.T. (2013) Amylose-lipid complex formation during extrusion cooking: Effect of added lipid type and amylose level on corn-based puffed snacks. *International Journal of Food Science & Technology*. **49**(2), 309-316.

Gwartz, J.A. and Garcia-Casal, M.N. (2014) Processing maize flour and corn meal food products. *Annals of the New York Academy of Sciences*. **1312**(1), 66-75.

Habeych, E., Dekkers, B., van der Goot, A.J. and Boom, R. (2008) Starch-zein blends formed by shear flow. *Chemical Engineering Science*. **63**(21), 5229-5238.

Hanna, M.A. and Bhatnagar, S. (1994) Amylose-Lipid complex formation during single-screw extrusion of various corn starches. *Cereal Chemistry*. **71**(6), 582-587.

Harper, J.M. (1992) A comparative analysis of single-screw and twin-screw extruders. In H. C. T. and K. M. V Kokini, J L, eds. *Food Extrusion Science and Technology*. New York: Marcel Dekker, Inc.

Hellman, N., Fairchild, B. and Senti, F. (1954) The bread staling problem. Molecular organization of starch upon aging of concentrated starch gels at various. *Cereal Chemistry*. **31**(2), 495–505.

Hoover, R., Hughes, T., Chung, H.J. and Liu, Q. (2010) Composition, molecular structure, properties, and modification of pulse starches: A review. *Food Research International*. **43**(2), 399–413.

Ida, T. (2012) Characterisation methods for nanostructure of materials. In T. Hosokawa, M., Nogi, K., Naito, M. and Yokoyama, ed. *Nanoparticle Technology Handbook*. Amsterdam: The Netherlands: Elsevier Ltd, 270–274.

Imai, E., Hatae, K. and Shimada, A. (1995) Oral perception of grittiness: Effect of particle size and concentration of the dispersed particles and the dispersion medium. *Journal of Texture Studies*. **26**(5), 561–576.

Imberty, A., Chanzy, H., Pérez, S., Buléon, A. and Tran, V. (1988) The double-helical nature of the crystalline part of A-starch. *Journal of Molecular Biology*. **201**(2), 365–378.

Imberty, A. and Perez, S. (1988) A revisit to the three-dimensional structure of B-type starch. *Biopolymers*. **27**(8), 1205–1221.

Jane, J. (2009) Structural Features of Starch Granules. In BeMiller, J.N. and Whistler, R.L. eds. *Starch: Chemistry and Technology*. London: Elsevier Ltd, 193–230.

Jane, J., Chen, Y.Y., Lee, L.F., McPherson, A.E., Wong, K.S., Radosavljevic, M. and Kasemsuwan, T. (1999) Effects of Amylopectin Branch Chain Length and Amylose Content on the Gelatinization and Pasting Properties of Starch. *Cereal Chemistry*. **76**(5), 629–637.

Jenkins, P.J. and Donald, A.M. (1995) The influence of amylose on starch granule structure. *International Journal of Biological Macromolecules*. **17**(6), 315–321.

Kang, N., Zuo, Y.J., Hilliou, L., Ashokkumar, M. and Hemar, Y. (2016) Viscosity and hydrodynamic radius relationship of high-power ultrasound depolymerised starch pastes with different amylose content. *Food Hydrocolloids*. **52**(3), 183–191.

Kawada, J. and Marchessault, R.H. (2004) Solid State NMR and X-ray Studies on Amylose Complexes with Small Organic Molecules. *Starch - Stärke*. **56**(1), 13–19.

- Kaya, E., Hogg, R. and Kumar, S.R. (2002) Particle shape modification in comminution. *KONA Powder and Particle Journal*. **20**(3), 188–195.
- Kibar, E.A.A., Gönenc, I. and Us, F. (2010) Gelatinization of waxy, normal and high amylose corn starches. *Gida*. **35**(4), 237–244.
- Kirby, A.R., Ollett, A.L., Parker, R. and Smith, A.C. (1988) An experimental study of screw configuration effects in the twin-screw extrusion-cooking of maize grits. *Journal of Food Engineering*. **8**(4), 247–272.
- Kloker, M., Kenig, E., Gorak, A., Franczek, K., Salacki, W. and Orlikowski, W. (2003) Experimental and theoretical studies of the TAME synthesis by reactive distillation. In Kraslawski, A and Turunen, I. eds. *Proceedings of 13th European Symposium on Computer Aided Process Engineering*. Amsterdam: The Netherlands: Elsevier Ltd, 713–718.
- Kokini, J. L., Chang, C.N. and Lai, L.S. (1992) The role of rheological properties on extrudate expansion. In M. V. Kokini, J. L., Ho, C.T. and Karwe, ed. *Food Extrusion Science and Technology*. New York: Marcel Dekker, Inc.
- Kokini, J.L. and Moraru, C.I. (2003) Nucleation and expansion during extrusion and microwave heating of cereal foods. *Comprehensive Reviews in Food Science and Food Safety*. **2**(4), 147–165.
- Kokini, J.L., Park, T.S., Martinez-Bustos, F. and Chang, Y.K. (1999) The influence of specific mechanical energy on cornmeal viscosity measured by an on-line system during twin-screw extrusion. *Brazilian Journal of Chemical Engineering*. **16**(3), 285–295.
- Kraus, S., Enke, N., Schuchmann, H.P. and Gaukel, V. (2014) Influence of sucrose content on expansion of extruded, starch-based pellets during microwave vacuum processing. *Journal of Food Process Engineering*. **37**(6), 628–634.
- Kristiawan, M., Chaunier, L., Della Valle, G., Lourdin, D. and Guessasma, S. (2016) Linear viscoelastic properties of extruded amorphous potato starch as a function of temperature and moisture content. *Rheologica Acta*. **55**(7), 597–611.
- Lai, L.S. and Kokini, J.L. (1991) Physicochemical Changes and Rheological Properties of Starch during Extrusion (A Review). *Biotechnology Progress*. **7**(3), 251–266.
- Lattuada, M., Yates, A. and Morbidelli, M. (2015) Impact of aggregate formation on the viscosity of protein solutions. *Soft Matter*. **11**(1), 9–11.

Lillford, P.J. (2001) Review Paper: Mechanisms of fracture in foods. *Journal of Texture Studies*. **32**(5), 397–417.

Lilyestrom, W.G., Yadav, S., Shire, S.J. and Scherer, T.M. (2013) Monoclonal Antibody Self-Association, Cluster Formation, and Rheology at High Concentrations. *The Journal of Physical Chemistry*. **117**(21), 6373–6384.

Liu, P., Yu, L., Liu, H., Chen, L. and Li, L. (2009) Glass transition temperature of starch studied by a high-speed DSC. *Carbohydrate Polymers*. **77**(2), 250–253.

Louis Alexandre, A., Mestres, C. and Faure, J. (1991) Measurement of endosperm vitreousness of corn: a quantitative method and its application to African cultivars. *Cereal Chemistry*. **68**(6), 614–617.

Majzoobi, M. (2004) The effect of processing on the molecular structure of wheat starch. *PhD Thesis: The University of Nottingham*.

Majzoobi, M., Radi, M., Farahnaky, A., Jamalian, J., Tongdang, T. and Mesbahi, G. (2011) Physicochemical properties of pre-gelatinized wheat starch produced by a twin drum drier. *Journal of Agricultural Science and Technology*. **13**(2), 193–202.

Manners, D.J. (1989) Recent developments in our understanding of Amylopectin structure. *Carbohydrate Polymers*. **11**(2), 112–187.

Marinopoulou, A., Papastergiadis, E., Raphaelides, S.N. and Kontominas, M.G. (2016) Morphological characteristics, oxidative stability and enzymic hydrolysis of amylose-fatty acid complexes. *Carbohydrate Polymers*. **141**(5), 106–115.

Matignon, A. and Tecante, A. (2017) Starch retrogradation: From starch components to cereal products. *Food Hydrocolloids*. **68**(3), 43–52.

Menard, H.P. (2008) *Dynamic Mechanical Analysis: A Practical Introduction*, 2nd Ed. *Taylor & Francis*. New York: CRC Press, 269–74.

Messaâdi, A., Dhouibi, N., Hamda, H., Belgacem, F.B.M., Abdelkader, Y.H., Ouerfelli, N. and Hamzaoui, A.H. (2015) A New Equation Relating the Viscosity Arrhenius Temperature and the Activation Energy for Some Newtonian Classical Solvents. *Journal of Chemistry*. **5**(2), 7–10.

Meuser, F., van Lengerich, B. and Reimers, H. (1984) Kochextrusion von Stärken. Vergleich experimenteller Ergebnisse zwischen Laborextrudern und Produktionsextrudern mittels Systemanalyse. *Starch - Stärke*. **36**(6), 194–199.

Mihhalevski, A., Heinmaa, I., Traksmäa, R., Pehk, T., Mere, A. and Paalme, T. (2012) Structural changes of starch during baking and staling of rye bread. *Journal of Agricultural and Food Chemistry*. **60**(34), 8492–8500.

Mishra, S. and Rai, T. (2006) Morphology and functional properties of corn, potato and tapioca starches. *Food Hydrocolloids*. **20**(5), 557–566.

Mohammadi Moghaddam, T., BahramParvar, M. and Razavi, S.M.A. (2015) Effect of frying temperature and time on image characterizations of pellet snacks. *Journal of Food Science and Technology*. **52**(5), 2958–2965.

Moisio, T., Forssell, P., Partanen, R., Damerou, A. and Hill, S.E. (2015) Reorganisation of starch, proteins and lipids in extrusion of oats. *Journal of Cereal Science*. **64**(3), 48–55.

Morrison, W.R., Milligan, T.P. and Azudin, M.N. (1984) A relationship between the amylose and lipid contents of starches from diploid cereals. *Journal of Cereal Science*. **2**(4), 257–271.

Neher, M.B., Pheil, R.W. and Watson, C.A. (1973) Thermoanalytical Study of Moisture in Grain. *American Association of Cereal Chemists*. **50**(9), 617–628.

Nor, N., Carr, A., Hardacre, A. and Brennan, C. (2013) The Development of Expanded Snack Product Made from Pumpkin Flour-Corn Grits: Effect of Extrusion Conditions and Formulations on Physical Characteristics and Microstructure. *Foods*. **2**(2), 160–169.

Norton, A.D., Greenwood, R.W., Noble, I. and Cox, P.W. (2011) Hot air expansion of potato starch pellets with different water contents and salt concentrations. *Journal of Food Engineering*. **105**(1), 119–127.

Ofoli, R.Y., Morgan, R.G. and Steffe, J.F. (1993) Characterization of the swelling of starch doughs during extrusion. *Journal of Food Engineering*. **18**(3), 297–312.

Oikonomou, N.A. and Krokida, M.K. (2012) Water Absorption Index and Water Solubility Index Prediction for Extruded Food Products. *International Journal of Food Properties*. **15**(1), 157–168.

Ozcan, S. and Jackson, D.S. (2005) Functionality behavior of raw and extruded corn starch mixtures. *Cereal Chemistry*. **82**(2), 223–227.

Padmanabhan, M. and Bhattacharya, M. (1991) Flow behavior and exit pressures of corn meal under high-shear–high-temperature extrusion conditions using a slit die. *Journal of Rheology*. **35**(3), 315–343.

Patel, B., Lillford, P. and Linter, B. (2016) The Material Science of Quavers. *Food Structure and Ingredient Science White Paper (internal resource)*.

Peksa, A., Kita, A., Carbonell-Barrachina, A.A., Miedzianka, J., Kolniak-Ostek, J., Tajner-Czopek, A., Rytel, E., Siwek, A., Miarka, D. and Drozd, W. (2016) Sensory attributes and physicochemical features of corn snacks as affected by different flour types and extrusion conditions. *LWT - Food Science and Technology*. **72**(4), 26–36.

Peplinski, A.J., Anderson, R.A. and Alaksiewicz, F.B. (1984) Corn Dry-Milling Studies: Shortened Mill Flow and Reduced Temper Time and Moisture. *Cereal Chemistry*. **61**(1), 60–62.

Perez, S. and Bertoft, E. (2010) The molecular structures of starch components and their contribution to the architecture of starch granules: A comprehensive review. *Starch*. **62**(8), 389–420.

Picker, K.M. and Hoag, S.W. (2002) Characterization of the thermal properties of microcrystalline cellulose by modulated temperature differential scanning calorimetry. *Journal of Pharmaceutical Sciences*. **91**(2), 342–349.

Pineda-Gómez, P., Acosta-Osorio, A., Coral, D.F., Rosales-Rivera, A., Sanchez-Echeverri, L., Rojas-Molina, I. and Rodríguez-García, M.E. (2012) Physicochemical characterization of traditional and commercial instant corn flours prepared with threshed white corn. *Journal of Food*. **10**(4), 287–295.

Pushpadassa, H.A., Kumara, A., Jackson, D.S., Wehling, R.L., Dumais, J.J. and Hanna, M.A. (2009) Macromolecular changes in extruded starch-films plasticized with glycerol, water and stearic acid. *Starch/Stärke*. **61**(5), 256–266.

Putseys, J. (2010) Structural and functional properties of amylose-lipid complexes and their applications [online]. *Laboratorium voor Levensmiddelenchemie en -biochemie*. Available from: <https://www.biw.kuleuven.be/m2s/clmt/lmcb/publications/docs/jputseys> [Accessed: 12 June, 2017].

Ratnayake, W.S., Otani, C. and Jackson, D.S. (2009) DSC enthalpic transitions during starch gelatinisation in excess water, dilute sodium chloride and dilute sucrose solutions. *Journal of the Science of Food and Agriculture*. **89**(12), 2156–2164.

Reddy, M.K., Kuna, A., Devi, N.L., Krishnaiah, N., Kaur, C. and Nagamalleswari, Y. (2014) Development of extruded Ready-To-Eat (RTE) snacks using corn, black gram, roots and tuber flour blends. *Journal of Food Science and Technology*. **51**(9), 1929–1937.

Riaz, M.N. (2002) Benefits of pre-conditioning. In *Extruders in Food Applications*. New York: CRC Press. 116–118.

Ring, S.G., Anson, K. and Morris, V.J. (1985) Static and dynamic light scattering studies of amylose solutions. *Macromolecules*. **18**(2), 182–188.

Robin, F., Dattinger, S., Boire, A., Forny, L., Horvat, M., Schuchmann, H.P. and Palzer, S. (2012) Elastic properties of extruded starchy melts containing wheat bran using on-line rheology and dynamic mechanical thermal analysis. *Journal of Food Engineering*. **109**(3), 414–423.

Sahai, D. and Jackson, D. (1996) Structural and chemical properties of native corn starch granules. *Starch - Stärke*. **48**(8), 249–255.

Dos Santos, W.N., De Sousa, J.A. and Gregorio, R. (2013) Thermal conductivity behaviour of polymers around glass transition and crystalline melting temperatures. *Polymer Testing*. **32**(5), 987–994.

Sarifudin, A. and Assiry, A.M. (2014) Some physicochemical properties of dextrin produced by extrusion process. *Journal of the Saudi Society of Agricultural Sciences*. **13**(2), 100–106.

Saunders, J., Izydorczyk, M. and Levin, D.B. (2011) Limitations and Challenges for Wheat-Based Bioethanol Production. In Dos, M.A. and Bernardes, S. eds. *Economic Effects of Biofuel Production*. Rijeka: InTech.

Shamai, K., Shimoni, E. and Bianco-Peled, H. (2004) Small Angle X-ray Scattering of Resistant Starch Type III. *Biomacromolecules*. **5**(1), 219–223.

Shogren, R.L., Fanta, G.F. and Felker, F.C. (2006) X-ray diffraction study of crystal transformations in spherulitic amylose/lipid complexes from jet-cooked starch. *Carbohydrate Polymers*. **64**(3), 444–451.

Shukla, R. and Cheryan, M. (2001) Zein: the industrial protein from corn. *Industrial Crops and Products*. **13**(3), 171–192.

Sievert, D. and Pomeranz, Y. (1989) Enzyme-resistant starch. I. Characterization and evaluation by enzymatic, thermoanalytical, and microscopic methods. *Cereal Chemistry*. **66**(4), 342–347.

Simmons, M.J.H., Jayaraman, P. and Fryer, P.J. (2007) The effect of temperature and shear rate upon the aggregation of whey protein and its implications for milk fouling. *Journal of Food Engineering*. **79**(2), 517–528.

Van der Sman, R.G.M. (2016) Filler functionality in edible solid foams. *Advances in Colloid and Interface Science*. **231**(3), 23–35.

Van der Sman, R.G.M. and Broeze, J. (2013) Structuring of indirectly expanded snacks based on potato ingredients: A review. *Journal of Food Engineering*. **114**(4), 413–425.

Szcześniak, L., Rachocki, A. and Tritt-Goc, J. (2008) Glass transition temperature and thermal decomposition of cellulose powder. *Cellulose*. **15**(3), 445–451.

Tang, J. and Ding, X.-L. (1994) Relationship between functional properties and macromolecular modifications of extruded corn starch. *Cereal Chemistry*. **71**, 364–369.

Tang, M.C., Salman, H., Blazek, J. and Copeland, L. (2016) Form and functionality of starch. *Food Hydrocolloids*. **23**(6), 1527-1534.

Tangram Technology (2014) Extrusion Definitions [online]. Available from: [http://www.tangram.co.uk/TI-Polymer-Extrusion\\_Definitions.html](http://www.tangram.co.uk/TI-Polymer-Extrusion_Definitions.html) [Accessed: November 6, 2016].

Tedeschi, C., Leuenberger, B. and Ubbink, J. (2016) Amorphous-amorphous phase separation in hydrophobically-modified starch-sucrose blends I. Phase behavior and thermodynamic characterization. *Food Hydrocolloids*. **58**(2), 75–88.

Terinte, N., Ibbett, R. and Schuster, K.C. (2011) Overview on Native Cellulose and Microcrystalline Cellulose I Structure Studied By X-Ray Diffraction ( Waxd ): Comparison Between Measurement Techniques. *Lenzinger Berichte*. **89**(4), 118–131.

Tester, R.F.F. (1997) Properties of damaged starch granules: composition and swelling properties of maize, rice, pea and potato starch fractions in water at various temperatures. *Food Hydrocolloids*. **11**(3), 293–301.

- Tomasik, P. (2003) *Chemical and Functional Properties of Food Saccharides*. New York: CRC Press.
- Tuorila, H., Jouppila, K., Roininen, K. and Roos, Y.H. (1998) Glass transition and water plasticization effects on crispness of a snack food extrudate. *International Journal of Food Properties*. **1**(2), 163–180.
- Ubwa, S.T., Abah, J., Asemave, K. and Shambe, T. (2012) Studies on the Gelatinization Temperature of Some Cereal Starches. *International Journal of Chemistry*. **4**(6), 22–28.
- Utrilla-Coello, R.G., Bello-Pérez, L.A., Vernon-Carter, E.J., Rodriguez, E. and Alvarez-Ramirez, J. (2013) Microstructure of retrograded starch: Quantification from lacunarity analysis of SEM micrographs. *Journal of Food Engineering*. **116**(4), 775–781.
- Vesterinen, E., Suortti, T. and Autio, K. (2001) Effects of preparation temperature on gelation properties and molecular structure of high-amylose maize starch. *Cereal Chemistry*. **78**(4), 442–446.
- Walton, G. (2015) Soaring snack sales spell the death of the crisp [online]. Available from: <http://www.telegraph.co.uk/finance/newsbysector/retailandconsumer/11581694/Soaring-snack-sales-spell-the-death-of-the-crisp.html>. [Accessed: December 7, 2016].
- Wang, K., Wang, W., Ye, R., Liu, A., Xiao, J., Liu, Y. and Zhao, Y. (2017) Mechanical properties and solubility in water of corn starch-collagen composite films: Effect of starch type and concentrations. *Food Chemistry*. **216**(2), 209–216.
- Wang, S., Li, C., Copeland, L., Niu, Q. and Wang, S. (2015) Starch Retrogradation: A Comprehensive Review. *Comprehensive Reviews in Food Science and Food Safety*. **14**(5), 568–585.
- Wang, T.L., Hedley, C.L. and Bogracheva, Ya, T. (1998) Starch: As simple as A, B, C? *Journal of Experimental Botany*. **49**(320), 481–502.
- Whittam, M.A., Noel, T.R. and Ring, S.G. (1990) Melting behaviour of A- and B-type crystalline starch. *International Journal of Biological Macromolecules*. **12**(6), 359–362.
- Xu, X., Huang, X.F., Visser, R.G.F. and Trindade, L.M. (2017) Engineering potato starch with a higher phosphate content. *PLoS ONE*. **12**(1), 1–21.
- Yao, N., White, P.J. and Alavi, S. (2011) Impact of  $\beta$ -glucan and other oat flour components on physico-chemical and sensory properties of extruded oat cereals. *Journal of Food Science*, **65**(7), 651–660.

Yue, Y. (2011) A Comparative Study of Cellulose I and II Fibers and Nanocrystals [online]. *Masters Thesis: Louisiana State University*. Available from: [http://digitalcommons.lsu.edu/cgi/viewcontent.cgi?article=1763&context=gradschool\\_theses](http://digitalcommons.lsu.edu/cgi/viewcontent.cgi?article=1763&context=gradschool_theses). [Accessed: June 8, 2017].

Zabar, S., Lesmes, U., Katz, I., Shimoni, E. and Bianco-Peled, H. (2010) Structural characterization of amylose-long chain fatty acid complexes produced via the acidification method. *Food Hydrocolloids*. **24**(4), 347–357.

Zeleznek, K.J. and Hosney, R.C. (1987) The glass transition in starch. *Cereal Chemistry*. **64**(4), 121–124.

Zobel, H.F. (1988) Molecules to Granules: A Comprehensive Starch Review. *Starch - Stärke*. **40**(2), 44–50.

Zobel, H.F., Young, S.N. and Rocca, L.A. (1988) Starch Gelatinization: An X-ray Diffraction Study. *Cereal Chemistry*. **65**(6), 443–446.